

Mining the Human Microbiome for Novel Nonribosomal Peptides

Exploring the Role of Nonribosomal Peptides in the Human Microbiome Through the Oral Commensal *Streptococcus mutans*, the Probiotic *Lactobacillus plantarum*, and Crohn's Disease Associated *Faecalibacterium prausnitzii*

By

Nikola Lukenda

A thesis submitted to the faculty of graduate studies in partial fulfillment of the requirements for the degree of Master of Sciences.

McMaster University

© Copyright by Nikola Lukenda, July 2012

Title: Exploring the Role of Nonribosomal Peptides in the Human Microbiome Using the Oral Commensal *Streptococcus mutans*, the Probiotic *Lactobacillus plantarum*, and the Crohn's Disease Associated *Faecalibacterium prausnitzii*

Author: Nikola Lukenda HBS (McMaster University, Ontario, Canada)

Supervisor: Dr. Nathan A. Magarvey

Committee Members: Dr. Michael G. Surette
Dr. Paul H. M. Harrison

Thesis Statement and Goals

Nonribosomal peptides, polyketides, and fatty acids comprise a distinct subset of microbial secondary metabolites produced by similar biosynthetic methods and exhibit broad structural diversity with a high propensity for biological activity. Dedicated studies of these specific microbial small molecules have identified numerous potent actions towards human cells with many clinical translations. Interestingly, most therapeutically used nonribosomal peptides and polyketides were discovered from soil bacteria, meanwhile, bacteria that have co-evolved within a human context, the human microbiota, have barely been explored for secondary metabolites. The central goal of this thesis is to explore the secondary metabolome of human microbiota for nonribosomal peptides and polyketides, which are hypothesized to possess biological activities significant within the human host context. Candidate organisms were chosen for their established connections to human health and evidence suggestive of secondary metabolite production. Specifically, questions about gene to molecule prediction capability, metabolite production, structural diversity, and biological activity were explored from studies of the dental caries linked *Streptococcus mutans* UA159, from the probiotic *Lactobacillus plantarum* WCFS1, and the Crohn's disease associated *Faecalibacterium prausnitzii*.

Acknowledgments

Firstly, I'd like to thank Dr. Magarvey for giving me the opportunity to work on the projects described in this thesis. As each project was made possible through collaborative efforts I've had the pleasure of working with a number of influential individuals and groups who are to be thanked: Dr. Dennis Cvitkovitch and his group at the University of Toronto, Dr. Waliul Khan and his students at McMaster University, and Dr. Philippe Langella and his team from the French National Institute for Agricultural Research (INRA). I'd also like to thank Dr. Wenliang Wang and Dr. Xiang Li for their expertise in NMR and roles in solving novel chemical structures. Finally, I'd like to thank my father Tono (Tut), my mother Ozana, and my sister Angela for their unending support, words of wisdom, and encouragement.

Table of Contents

	Thesis statement and goals.....	iv
	Acknowledgments.....	v
	Table of contents.....	vi
	List of figures.....	vii
	Abbreviations.....	viii
1	Introduction.....	10
	1.1 The human microbiome.....	10
	1.2 Chemical signalling in the human microbiome.....	11
	1.3 Biosynthesis of nonribosomal peptide and polyketide secondary metabolites.....	15
	1.4 New developments in the discovery of secondary metabolites.....	19
2	Chapter 1: Discovery and Study of the Nonribosomal Peptide-Polyketide Mutanobactins, and the Modified Fatty Acid Mutanamide from <i>Streptococcus mutans</i> UA159.....	22
	2.1 Chapter forward.....	23
	2.2 Abstract.....	24
	2.3 Introduction.....	26
	2.4 Results and discussion.....	31
	2.5 Materials and methods.....	58
3	Chapter 2: Development of a LC-MS Selected Reaction Monitoring (SRM) Method for the Detection and Quantification of a <i>S. mutans</i> Pheromone.....	65
	3.1 Chapter forward.....	66
	3.2 Abstract.....	67
	3.3 Introduction.....	68
	3.4 Results and discussion.....	71
	3.5 Materials and methods.....	75
4	Chapter 3: Expanding the Catalogue of Immunomodulatory Effector Molecules from the Probiotic <i>Lactobacillus plantarum</i> WCFS1.....	78
	4.1 Chapter forward.....	79
	4.2 Abstract.....	80
	4.3 Introduction.....	82
	4.4 Results and discussion.....	87
	4.5 Materials and methods.....	106

5	Chapter 4: Faecalienes are Anti-Inflammatory Metabolites from Crohn's Disease Associated <i>Faecalibacterium Prausnitzii</i>	111
5.1	Chapter foreward.....	112
5.2	Abstract.....	113
5.3	Introduction.....	114
5.4	Results and discussion.....	118
5.5	Materials and methods.....	128
6	Conclusions	132
7	References.....	135

List of Figures

Figure 1. Major Classes of Bacterial Secondary Metabolites.....	14
Figure 2. Fundamental Steps in NRP Biosynthesis by NRPS Enzymes.....	18
Figure 3. Application of Principle Component Analysis (PCA) in Aiding Natural Product Discovery Efforts.....	20
Figure 4. The <i>S.mutans</i> Hybrid NRPS-PKS Biosynthetic Operon TnSmu2 with its Predicted Product.	28
Figure 5. Mutanobactin A HRESIMS and 1D - (¹³ C DEPTq), and 2D - NMR (¹ H- ¹ H COSY and ¹ H- ¹³ C HMBC) Correlations.	29
Figure 6. Untargeted Metabolomic Investigation of <i>S. mutans</i> TnSmu2 Biosynthetic Capacity Using Principal Component Analysis (PCA) of LC-MS Data.....	33
Figure 7. O _{2(g)} Levels Affect Mutanamide Production in <i>S. mutans</i>	37
Figure 8. Expression of Selected Genes Within the TnSmu2 Locus in the VicRK Mutant Versus UA159 Parent Strains.....	39
Figure 9. Proposed Mutanamide Structure Based on Partial Structures From Acid Hydrolysis, MS/MS Studies and NMR Experiments.....	41
Figure 10. LC-MS Analysis of TnSmu2 Mutant Strains.....	43
Figure 11. Aspartic Acid is Not Incorporated by Smu_1345 into Mutanobactin A.....	46
Figure 12. Supplementing <i>S. mutans</i> Cultures with Decanoic Acid Analogues Results in Novel Mutanobactin Analogues.....	48
Figure 13. MS/MS Fragmentation Data of Mutanamide Analogues from Fatty Acid Feeding Studies Suggests Single Monomer Incorporation.....	49
Figure 14. Comparison of TnSmu2 Products Ability to Inhibit the Hyphal Transformation of <i>Candida albicans</i>	52
Figure 15. TnSmu2 Biosynthetic Products Elicit an Immune Response in Mouse Dendritic Cells.....	54

Figure 16. Proposed Biosynthetic Pathway for the Mutanobactins and Mutanamide.....	57
Figure 17. Loss of Transformation Frequency Correlates with Decreased XIP Levels in Culture Supernatant as Measured by SRM LC-MS.....	73
Figure 18. Development of a Selected Reaction Monitoring (SRM) LC-MS Experiment for <i>S. mutans</i> XIP.....	74
Figure 19. Cellular Pathways Significantly Modulated After Consumption of <i>L. plantarum</i> Cultures and NRPS Operon with Predicted Metabolite.....	84
Figure 20. Differential Induction of Immune Response in DCs by <i>L. plantarum</i> Metabolite Extracts.....	88
Figure 21. Multivariate Analysis of LC-MS Data from Wildtype and NRPS Mutant <i>L. plantarum</i> Metabolite Extracts.....	90
Figure 22. Multivariate Analysis of LC-MS Data from Stationary and Mid-Log <i>L. plantarum</i> Metabolite Extracts.....	92
Figure 23. Extracted Ion Chromatograms for Stationary Growth Phase Unique Metabolites Identified by Multivariate Analysis.....	93
Figure 24. Structural Elucidation of PyroGlu-Leu by MS/MS Fragmentation Mapping and 1D-NMR Correlations.....	95
Figure 25. Structural Elucidation of PyroGlu-Phe by MS/MS Fragmentation Mapping and 1D-NMR Correlations.....	96
Figure 26. <i>L. plantarum</i> Produces Multiple Analogues of PyroGlu-X Dipeptides.....	98
Figure 27. <i>L. plantarum</i> PyroGlu-X Dipeptides Modestly Induce IL-6 Expression in Mouse Dendritic Cells.....	101
Figure 28. <i>L. plantarum</i> PyroGlu-X Dipeptides Strongly Induce IL-12 Expression in Mouse Dendritic Cells.....	102
Figure 29. Supplementing Mice with PyroGlu-Phe Decreases IFN-Gamma Secretion by Splenocytes in Response to LPS.....	105

Figure 30. <i>Faecalibacterium prausnitzii</i> Supernatant Exhibit's Anti-Inflammatory Activity on Caco-2 Cells and Provides Protective Effects on Mice After TNBS Challenge.....	117
Figure 31. Anti-Inflammatory Guided Fractionation of <i>F. prausnitzii</i> Metabolites.....	120
Figure 32. Identification of Structurally Related <i>F. prausnitzii</i> Metabolites in Anti-Inflammatory Pool P1.....	121
Figure 33. Structural Elucidation of the Faecalienes by 1D and 2D NMR.....	124
Figure 34. Faecalienes are Anti-Inflammatory Metabolites Secreted by <i>F. prausnitzii</i>	127

Abbreviations

ACP – Acyl carrier protein
AT – Acyltransferase
BHI – Brain heart infusion
BPC – Base peak chromatogram
CD – Crohn's Disease
CDM – Chemically defined media
CFS – Cell free supernatant
COSY – Correlation spectroscopy
CSP – Competence stimulating peptide
DC – Dendritic cell
DMEM – Dulbecco's modified Eagle's minimal essential medium
DMSO – Dimethyl sulfoxide
EDTA – Ethylenediaminetetraacetic acid
EIC – Extracted ion chromatogram
ELISA – Enzyme-linked immunosorbent assay
FACL – Fatty acid (acyl-carrier protein) ligase
FBS – Fetal bovine serum
FISH – Fluorescence in situ hybridization
HMBC – Heteronuclear multiple-bond correlation spectroscopy
HSQC – Heteronuclear single-bond correlation spectroscopy
HPLC-MS(/MS) – High performance liquid chromatography-mass spectrometry
HRESIMS – High resolution – electrospray ionization mass spectrometry
IBD – Inflammatory bowel disease
IBS – Irritable Bowel Syndrome
IFN- γ – Interferon-gamma
IL – Interleukin
KS – Ketosynthase

LAB – Lactic acid bacteria
LC-MS/MS – Liquid chromatography-tandem mass spectrometry
LPS - lipopolysaccharide
MPLC – Medium pressure liquid chromatography
MRS – de Man, Rogosa and Sharpe
MS – Mass spectrometry
NF- κ B – Nuclear factor- kappaB
NMR – nuclear magnetic resonance (spectroscopy)
NRPS – Nonribosomal peptide synthetase
NRP – Nonribosomal peptide
PBS – Phosphate buffered saline
PCA – Principle component analysis
PDTC – Pyrrolidine dithiocarbamate
PKS – Polyketide synthase
PK – Polyketide
SRM – Selected Reaction Monitoring
sXIP – synthetic XIP
TACE – TNF-alpha converting enzyme
TE – Thioesterase
THYE – Todd Hewitt Yeast Extract
TNF- α – Tumor necrosis factor-alpha
UC – Ulcerative colitis
XIP – SigX-inducing peptide

1 Introduction

1.1 The Human Microbiome

From birth we are colonized by an extraordinary number of diverse microbes, establishing the foundation of our own personal microbial environment. Complex chemical crosstalk begins immediately between the signalling pathways of our immune system and our newly acquired commensals, with a mutually beneficial relationship quickly developing. Our first explorations into the human microbiome revealed colonizing microbes in the gut had genetically adapted to thrive in the human environment hinting at the close-knit relationship between commensals and host (1). When these evolutionary conserved symbiotic relationships become imbalanced, known as dysbiosis, disease pathologies can ensue. From inflammatory bowel disease (IBD) to depression, obesity to autoimmune disorders, numerous diseases have been traced to the microbiome (2, 3). As with many pioneering fields, the more we learn about the human microbiome, the more we realize we need to learn. The composition of bacteria from one body site to another varies on a single individual, let alone in a complex population. Numerous international collaborative efforts are attempting to delineate this complexity in order to extract therapeutically relevant connections between microbial composition and health. A recent study by the Human Microbiome Project Consortium sought to facilitate the discovery of these links by defining the structure, function and diversity of a normal, healthy, human microbiome (4). By recognizing the parameters to a healthy microbiome it is hoped that individual bacterial species, or families, which act as indicators or promoters of disease can be readily identified.

Currently, only a few specific bacterial species have been linked to disease states, as the majority of host-commensal relationships studied are on a community level. Using this more global perspective, shifts in families of bacteria have been linked to obesity, immune system development, host colonization, and other scenarios (5-7). Exceptions do exist, and in some instances, specific candidate species have been identified as factors in disease, including *Helicobacter pylori* to gastric cancer, *Streptococcus mutans* to dental caries, and *Bifidobacteria* and *Lactobacilli* to IBD (8-10). Identifying shifts in bacterial composition or even of individual species is just beginning to address the subject however. Only by understanding molecularly how microbiota interact with the human host, and each other, can the most thorough understanding of our relationship with our commensals be developed, and viewed opportunistically for therapeutic intervention

1.2 Chemical Signalling in the Human Microbiome

A foundation has been paved by the human microbiome project and reinforced by individual studies confirming the existence of chemical crosstalk between humans and our microbiota, and microbiota amongst themselves. From this growing body of knowledge, the prospect of mining specific candidate human microbiota for bioactive small molecules has emerged as an intriguing reality. Microbial metabolites, used by the producing organisms for communication or survival can exhibit antibacterial, anti-fungal, cytotoxic, anti-inflammatory, immunomodulatory, and other biological activities, in part towards human cells (11-14). Many of these compounds end up being clinically used, and surprisingly, many of these have been isolated from soil dwelling organisms which have

no evolutionary incentive to improve human fitness. Efforts have since been made to identify similarly bioactive compounds from human microbiota, spurred by increasingly frequent discoveries linking specific bacterial species to distinct human effects. Despite this new vigour in metabolic investigation, a disparity exists, where most of the methods used to identify the mechanism of action of a targeted bacterium have biased the discovery of specific classes of metabolites over others.

Due to their propensity for genetic studies, bacterial peptides are heavily focused on within current studies of effector molecules. Bacterial peptides, such as the antimicrobial bacteriocins, can alter the composition of a particular environment towards host favourable or unfavourable compositions (15). Peptidic pheromones, such as competence stimulating peptides (CSPs) are produced by human streptococci and regulate the uptake of environmental DNA, and therefore also species genetic heterogeneity, shaping their evolution within the human host (16).

Another class of bacterial metabolite implicated in an array of disorders are fatty acids. Short chain fatty acids, including acetate, propionate, and butyrate are produced in high amounts by clostridia that reside in the gut (17). While short chain fatty acids are an essential part of human metabolism, when produced by gut bacteria such acids are also absorbed by the human large intestine, providing excess energy to colonic epithelial cells, resulting in obesity, insulin resistance, and colorectal cancer (18, 19). More complex lipids including LPS, conjugated linoleic acid, and peptidoglycans on the other hand are staples in inflammatory pathways due to their ability to induce multiple immune signalling pathways in human epithelial and immune cells. Because of their potent

immune activity, and well founded implications in chronic systemic inflammation, and gut function, the activity of many probiotics is quickly attributed to their lipid and cell wall components (20). However, other, yet to be discovered factors are also believed to exist.

Other lesser characterized chemical classes are also now being viewed with increased significance. Phenolic compounds produced by *Bifidobacteria*, *Lactobacilli*, and *Clostridia* are currently being investigated as disease biomarkers and host immunomodulatory indole derivatives from *Bifidobacterium* may prove to be probiotic factors (21, 22). There exist still other microbial metabolite classes which are even less studied within the human microbiome, despite having one of the best precedents for biological activity in a human setting; these are secondary metabolites, namely nonribosomal peptides (NRPs) and polyketides (PKs) (Figure 1).

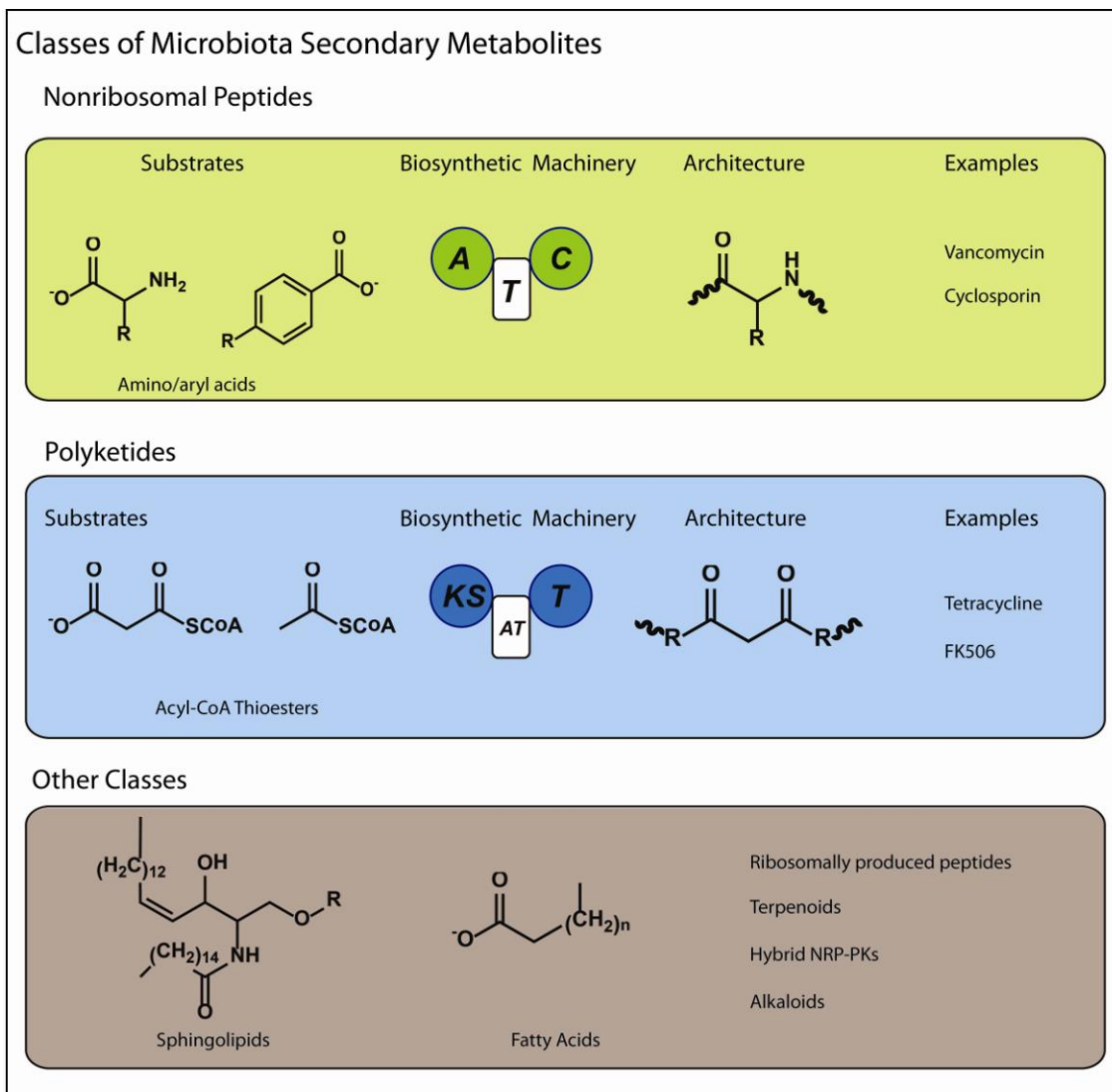


Figure 1. Major Classes of Bacterial Secondary Metabolites. Bacteria possess diverse metabolic potential including non-ribosomal peptides (NRPs) and polyketides (PKs) produced by modular non-ribosomal peptide synthetases (NRPS) and polyketide synthases (PKS). Other metabolite classes, including sphingolipids, and fatty acids are produced by independent biosynthetic mechanisms creating a diverse metabolic landscape.

1.3 Biosynthesis of Nonribosomal Peptide and Polyketide Secondary Metabolites

Human relevant NRPs include the antibiotics daptomycin, and vancomycin, the immunosuppressants cyclosporine and rapamycin, and the antitumor agents bleomycin and ech (23-28). By understanding how NRPs are produced, we gain insight into the methods used for their discovery and study. Multimodular enzymatic assembly lines, known as nonribosomal peptide synthetases (NRPSs) are employed, with one module corresponding to the stepwise addition of a single monomer. A minimal module consists of two catalytic domains (A and C domains) and a T domain, usually in the order of C-A-T (Figure 2) (29). The first step in NRP biosynthesis, catalyzed by adenylation (A) domains, involves the selection and activation of amino acid monomers by conversion to aminoacyl-AMP mixed anhydrides. A rich pool of monomers exist including the 20 proteinogenic amino acids and more than 500 non proteinogenic amino acids but also includes aryl acids and α -hydroxy acids, allowing for vast structural diversity (30, 31). These activated monomers are then transferred to the thiolate anion of a pantetheinyl-phospho-carrier protein domain (T domain). Condensation (C) domains catalyze peptide bond formation between the upstream peptide tethered to a T domain and a downstream aminoacyl monomer attached to a second T domain. Conversion of the peptidyl thioester to the amide bond of the peptidyl chain is thermodynamically favourable, and drives chain elongation. In polyketide synthases (PKSs), the minimal module consists of KS-AT-T domains, which are analogous to the C-A-T domains in NRPSs, however acyltransferase (AT) domains now select for acyl-CoA-thioesters as monomeric building blocks.

The first module of a NRPS, the initiation module, usually consists of two domains, A and T, with A selecting for the first monomeric unit in a peptide chain and again, catalyzing its covalent attachment to the T domain. Chain elongation continues through subsequent modules as described previously until chain completion, whereby a termination module is encountered, usually consisting of C-A-T-TE domains. Once the final amino acid monomer is added a thioesterase (TE) domain catalyzes chain release, either through hydrolysis or peptide cyclization, liberating the final metabolite (32).

The chemical logic described is retained in most NRPSs and makes possible the prediction of a final metabolite through investigation of its biosynthetic assembly line. Where ribosomes read genetic information in the form of mRNA to specify monomer addition, in NRPSs the identity and ordering of protein domains acts as the template. The number of A domains present, for example, can be viewed as a determinant of chain length. As the specificity of A domains has also been thoroughly studied, the nonribosomal code for monomer incorporation is well known, allowing for predictions of monomer incorporation based on key residues within the A domain examined (33-35). Facilitating this process are *in silico* programs for analyzing biosynthetic clusters including ClustScan, NRPS-PKS, NP. searcher, and most recently antiSMASH (36). These programs take advantage of the same biosynthetic principles described here, however do so in an automated fashion; rapidly screening an organism's entire genome for biosynthetic enzymes, and by applying the conserved chemical logic inherent in the assembly of NRPs and PKs, produce a putative structure for a predicted metabolite. This strategy of identifying biosynthetic clusters, and predicting biosynthetic products from

their genes is collectively known as genome mining, and has successfully aided the discovery of NRP siderophores from *Streptomyces coelicolor*, hybrid NRP-PK biosurfactants from *Pseudomonas fluorescens*, and PK antifungals and antimicrobials from different actinobacteria (37-39). As successful as the method is, only a few instances of its application to human microbiota exist. This is surprising as a major pillar of the human microbiome initiative is the mass sequencing and availability of human microbiome genomes. The number of genomes already available exceeds 3000 and is growing at a rapid pace, establishing an unexplored genomic pool ready to be mined for biosynthetic machinery. Identifying the genetic potential for secondary metabolite biosynthesis is just one half of the problem however, as ultimately the product metabolite needs to be isolated.

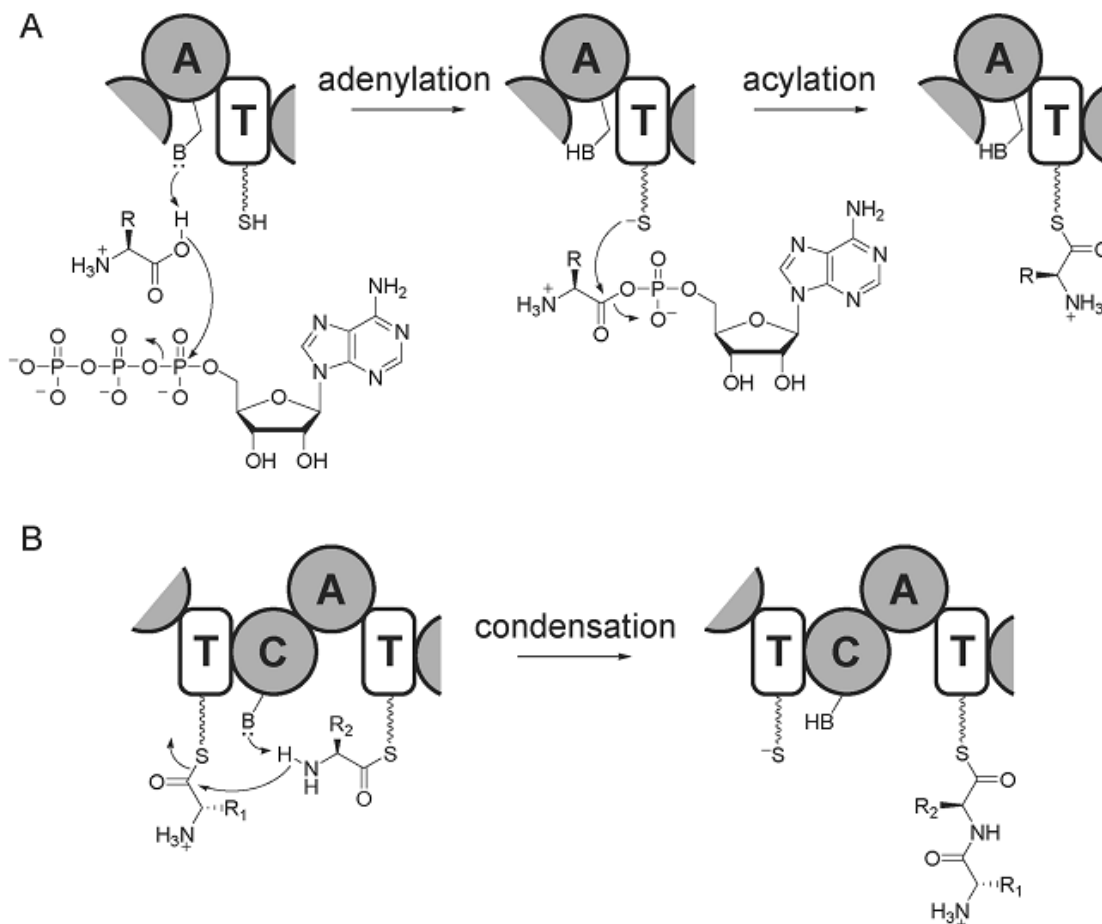


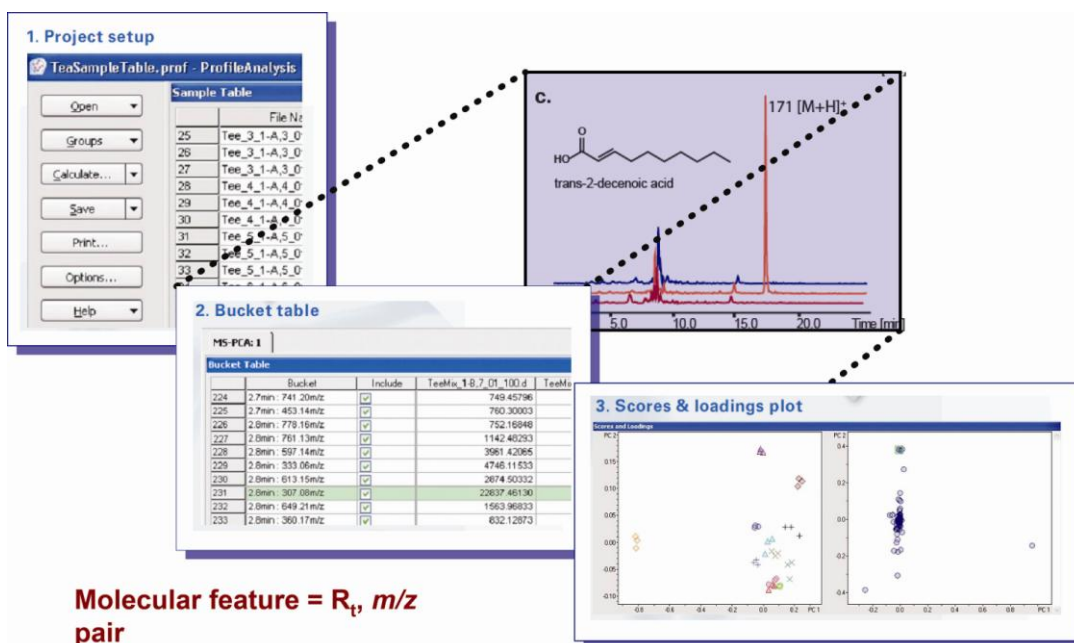
Figure 2. Fundamental Steps in NRP Biosynthesis by NRPS Enzymes. Replicated from Fischbach, M.A., and Walsh, C.T., 2006 **(A)** Adenylation (A) domains catalyze the activation of specific amino acid monomers (or aryl, or α -hydroxy acids) by adenylation and acylation to a downstream T domain. **(B)** C-N bond formation between the downstream aminoacyl-S-T and upstream peptidyl-S-T is catalyzed by condensation (C) domains, extending the growing peptide chain iteratively.

1.4 New Developments in the Discovery of Secondary Metabolites

The process of identifying and linking bacterial natural products to the biosynthetic genes predicted to produce them has relied heavily on techniques relatively unchanged since the advent of the field. Of these, the inactivation or deletion of biosynthetic genes through genetic techniques has remained a corner stone, facilitating the downstream detection, through their absence, of metabolites using LC-MS or other analytical processes. While these methods have successfully expanded the catalogue of bacterial secondary metabolites, an inherent flaw exists in their execution. These traditional methods heavily favour the discovery of “low hanging fruit” metabolites, those structurally biased to be identified by the particular analysis method employed, and/or that are produced in high abundance. However, highly biologically active metabolites are often found in significantly lower levels correlating to their potent biological activity. This occurrence is exemplified by *C. elegans* ascarosides, which exhibit femtomolar biological activity (40). Another example is the interkingdom signalling molecule *trans*-2-decenoic acid, secreted by *S. mutans*, which was only identified following large scale fermentation and bioactivity guided fractionation efforts (41). To this end, bacterial signalling molecules produced at low levels often prove elusive for traditional natural product based detection and isolation techniques.

To address this concern a trend has emerged within secondary metabolite studies whereby the traditional process of contrasting wild type and biosynthetic mutant strains has evolved through the application of metabolomic principles (Figure 3) (42-44). Multivariate analysis models, including principal component analysis and the students t-

test, facilitate more thorough pairwise comparisons between sample sets than manual means. By contrasting data sets (ex. LC-MS) for statistically significant deviations, even low abundance or poorly ionizing metabolites are readily extracted by computational programs.



Molecular feature = R_t , m/z pair

Figure 3. Application of Principle Component Analysis (PCA) in Aiding Natural Product Discovery Efforts. Using multivariate analysis methods like PCA, pairwise comparison of LC-MS data sets is relatively straightforward, requiring three main steps. First, in the project setup stage, retention time and m/z ranges are defined, allowing for preliminary filtering of LC-MS data. Using these parameters, molecular features, defined as a signal's retention time and m/z intensity, are identified within each LC-MS data set producing a bucket table. Molecular features within the bucket table of one sample set are compared to those of another, allowing discrimination. Molecular features significantly divergent from one sample set to another are identified, and represented as points on the loading plot. Overall differentiation of one sample set to another is judged by the separation of points, representative of a complete sample, in the scores plot, and is dependent on identifying statistically significant differences in sample sets.

Software packages, such as XCMS or Bruker Profile Analysis, identify changes in metabolite levels by first assigning peaks within LC-MS chromatograms as unique molecular features based on their retention time and m/z (45). These molecular features are then quantified by integrating the specific ion's peak area, allowing for a fold change to be measured across sample sets and differences to be ranked by statistical significance. By using this process, a number of new secondary metabolites have been identified which had remained undiscovered from previously well studied systems including myxoprincomide from *Myxococcus xanthus*, alkyl-dihydrothiazole-carboxylates (ATCs) from *Pseudomonas aeruginosa*, and gliotoxin intermediates and analogues from *Aspergillus fumigates* (46-48). In these cases, traditional natural product methods had in fact already yielded a number of secondary metabolites, however, by applying multivariate analysis the authors were able to expand the secondary metabolite catalogue, discovering new metabolites while gaining biosynthetic insight. By combining recent advances in natural product discovery based on metabolomics, and by focusing on new classes of secondary metabolites within key organisms identified through metagenomic efforts, a new era of natural product discovery within the human microbiota is proposed.

2 CHAPTER 1:

Discovery and Study of the Nonribosomal Peptide-Polyketide Mutanobactins, and the Modified Fatty Acid Mutanamide from *Streptococcus mutans* UA159

2.1 Chapter Forward

The first candidate organism chosen for probing the role of NRPS and PKS derived molecules from human microbiota was Streptococcus mutans UA159 due to its extensive study as a human oral microbiome member, a result of its contribution to tooth decay, and the presence of a NRPS-PKS operon within its genome. Since S.mutans was first linked to dental caries, it has become one of the best studied oral microorganisms, providing an important wealth of background knowledge useful in identifying, isolating, and testing its secondary metabolites. Genome sequencing of UA159 revealed the TnSmu2 NRPS-PKS operon, predictive of secondary metabolite production, with subsequent genome hybridization experiments detecting TnSmu2 in numerous other S. mutans strains. Interestingly, while in these other strains TnSmu2 retains NRPS and PKS genes, the number, order, and predicted amino acid incorporation differ. That different S. mutans strains have evolved to produce similar, although not identical NRP-PK metabolites, suggests the lipopeptide structural architecture to be a defining characteristic of TnSmu2 products, and not the individual chemical nuances between them.

2.2 Abstract

A hybrid non-ribosomal peptide synthetase, polyketide synthase (NRPS-PKS) operon, TnSmu2, was discovered in the human dental caries associated *Streptococcus mutans* and revealed to produce the lipopeptides mutanobactins A and C. Studies by the Cichewicz group confirmed the structures of mutanobactins A and C, and these authors also reported the structures of mutanobactins B and D. Cross-kingdom signalling capabilities of the mutanobactins were also reported through their ability to inhibit germ tube formation by the fungus *Candida albicans*. As a strong literature precedent exists for lipopeptide producing operons to assemble a number of analogous compounds, the full biosynthetic capacity of the TnSmu2 operon was catalogued by contrasting the metabolic extracts of wild-type and TnSmu2 mutant strains using multivariate analysis of LC-MS(/MS) data sets. A number of novel wild type specific compounds were identified and confirmed to be peptidic in nature using MS/MS analysis and the incorporation of isotopically labelled precursor amino acids. Unexpectedly, a non-peptidic metabolite was also identified as being unique to the wild type strain. Production optimization experiments revealed biosynthesis of this new molecule to be linked to environmental conditions, with highest production occurring when atmospheric conditions mimicking those of the oral microbiome were simulated. Isolation and structure elucidation experiments identified this compound, referred to as mutanamide, as possessing fatty acid derived, linked di-acyl moieties. Further mutational studies confirmed mutanamide's biosynthetic origins to PKS genes within TnSmu2 and revealed *trans*-2-decenoic acid as a

key building block in mutanobactin/mutanamide biosynthesis. Promiscuity of the TnSmu2 operon in incorporating other fatty acid building blocks was also producing novel bioengineered mutanobactins and mutanamides. Through bioactivity studies mutanamide was found to inhibit *C. albicans* hyphal formation at concentrations much lower than the mutanobactins. Together, these results suggest that within the context of its human environment *S. mutans* produces a series of potent defensive metabolites against *C. albicans*, as well as other compounds whose purposes remain to be discovered.

2.3 Introduction

In 2002 the first genome sequence of *Streptococcus mutans* UA159 was completed revealing several genetic islands with divergent G+C content, indicative of horizontal gene transfer (49). Of these islands, TnSmu2 stands out as it makes up 2.76% of *S. mutans*'s genome, and harbours the largest genes found in the genome (49). Using the BLAST algorithm, these genes were identified as enzymes for secondary metabolite biosynthesis, specifically, nonribosomal peptide synthetases (NRPSs) and polyketide synthases (PKSs). Similar clusters are known to produce an important class of secondary metabolite, known as lipopeptides, which exhibit broad activities as surfactants to antimicrobial agents (50-52). Interest in TnSmu2 is further extended by its conserved presence across multiple *S. mutans* strains, as determined by DNA hybridization and sequencing experiments (53-55). However, while present in other strains, the organization of TnSmu2 differs strain by strain, suggesting a preservation of lipopeptide production may be more important than absolute metabolite conservation.

Consisting of 14 genes from Smu.1334 to Smu.1348c, TnSmu2 contains a full repertoire of genes necessary for the biosynthesis and secretion of a hybrid NRP-PK secondary metabolite (Figure 4). An ATP dependent transporter is found at the start of the operon at Smu.1348c followed by a permease (Smu.1347c) both of which are believed to play roles in metabolite secretion. Following these, a standalone thioesterase domain is observed at Smu.1346, suggestive of a Type II thioesterase, an identity reinforced by BLAST analysis. At Smu.1345c, a potential acyl-coA synthetase/ligase is found based on

homology to MycA from *B. subtilis*. In *B. subtilis*, MycA is responsible for activating a fatty acid, which is subsequently incorporated in the biosynthesis of mycosubtilin, hinting at a possible similar lipoinitiation role for Smu.1345c (56, 57). Two polyketide synthase genes follow; a lone AT domain at Smu.1344c and a KS-ACP-C tri-domain module at Smu.1343c. Four nonribosomal synthetases genes are next encountered spanning from Smu.1342 to Smu.1339. In-silico analysis of these genes using online domain analysis software (<http://www.nii.res.in/nrps-pks.html>) revealed the presence of 6 A domains, suggesting the incorporation of 6 amino acid monomers in the following order: leucine, serine, proline, valine, cysteine, and glycine (58). A more detailed analysis also revealed an epimerization domain following the serine selecting domain, suggesting the final product may possess D-serine. Also of note is the inclusion of a reductase domain at the end of Smu.1339, possibly possessing a role in chain termination or cyclization. At the end of the operon a number of standalone biosynthetic enzymes are found including TE (Smu.1337c), AT (Smu.1336c), and ER domains. Also present in TnSmu2 is a phosphopantetheinyl transferase at Smu.1344c and a transporter gene at Smu.1338c, rounding out all of the necessary components for a functional biosynthetic assembly line to produce and secrete a NRP.

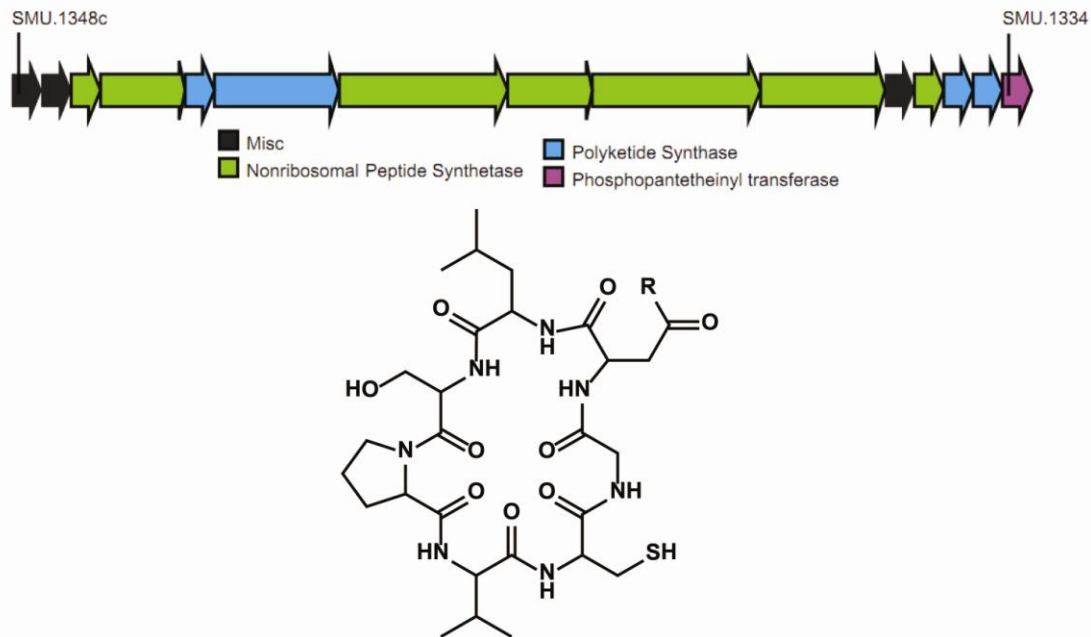


Figure 4. The *S.mutans* Hybrid NRPS-PKS Biosynthetic Operon TnSmu2 with its Predicted Product. Genome mining of *S. mutans* UA159 revealed a 14 gene operon, spanning SMU_1348-SMU_1334, containing 5 NRPS enzymes (green) and a single PKS module (blue). A phosphopantetheinyl transferase was identified at SMU_1334 (purple) and all other genes were non-biosynthetic in nature and are shown in black. Adenylation domain analysis by in silico analysis led to the putative mutanobactin macrocyclic structure shown, with a predicted mass range of 640-800 amu.

Previous efforts resulted in the successful isolation and structural elucidation of the TnSmu2 lipopeptide and its stereoisomer, however, studies by Joyner *et al.*, pre-empted the publication of these results for the molecule now referred to as mutanobactin (Figure 5) (59, 60). In those reports, only a single metabolite, mutanobactin A, was identified and revealed to participate in cross-kingdom signalling through its capacity to inhibit the hyphal transition of *Candida albicans*, a key factor in its pathogenesis. Subsequent analysis by Wu *et al.*, identified three additional closely related mutanobactin analogues, mutanobactins B-D, exhibiting slight structural deviations from the original

scaffold (60). Through structural experiments mutanobactin C was identified as a stereoisomer of mutanobactin A and mutanobactin B to possess a isoleucine monomer instead of valine. Mutanobactin D differed the most as it lacked the 1,4-thiazepan-5-one system found in the macrocycle core of the other mutanobactins.

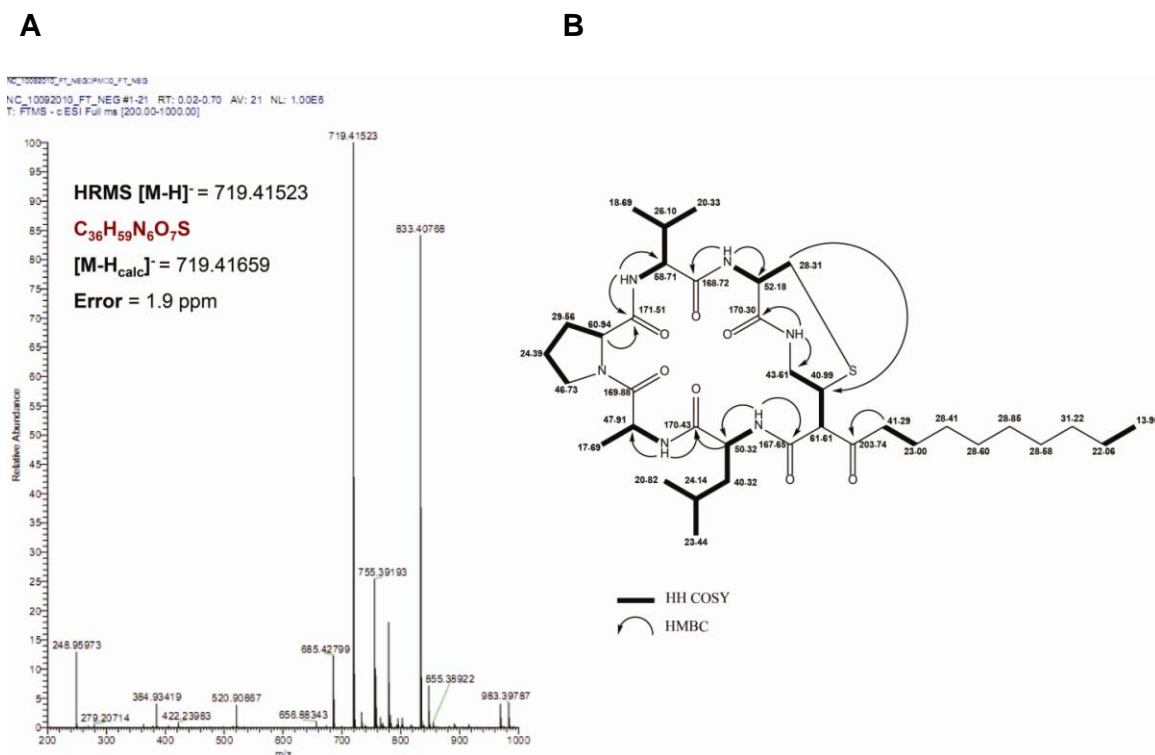


Figure 5. Mutanobactin A HRESIMS (A) and 1D- (¹³C DEPTq) and 2D- NMR (¹H-¹H COSY ¹H-¹³C HMBC) Correlations (B). High-resolution mass spectral data were obtained using a Thermo Scientific LTQ Orbitrap XL, generating a molecular formula of $C_{36}H_{60}N_6O_7S$. Full mutanobactin A characterization required 1D and 2D-NMR experiments performed on a Bruker 700 MHz spectrometer (in 100% CD_3OD). Amino acid composition and order were confirmed using ¹H-¹H COSY (bold lines) and long range ¹H-¹³C HMBC interactions (curly arrows). Identical spectral results were obtained for the stereoisomer mutanobactin C.

The discovery of other mutanobactins is not surprising as biosynthetic operons often generate a variety of analogues alongside the predominant species (61, 62). For lipopeptides, these analogues can differ in the acyl tail moiety or their macrocyclic peptide core, resulting in distinct and measurable differences in bioactivity (63-65). In the case of the mutanobactins, these significant differences were observed when contrasting their signalling ability. Mutanobactin C showed no apparent activity, while mutanobactin D far surpassed the other analogues in its ability to inhibit *C. albicans* biofilms.

As mutanobactin D was the least abundant of the mutanobactins isolated, we were intrigued by the possible existence of other analogues within this signalling family which may yet be present at even lower abundances due to their potent biological activity. Seeking to catalogue the full biosynthetic output of the TnSmu2 operon, we applied metabolomic techniques to thoroughly contrast the metabolomes of wild type and Δ TnSmu2 strains of *S. mutans*. In combination with MS/MS and isotopically labelled precursor feeding experiments we discovered a number of novel metabolites linked to TnSmu2, thereby expanding its biosynthetic catalogue. Of these, we focused our efforts on the only non-peptidic metabolite, and identified it as a divergent metabolite exhibiting exceptional ability in inhibiting the *C. albicans* hyphal transition. These results highlight the need for more thorough comparisons of wild type and biosynthetic mutant strains, especially within the context of signalling molecules which may achieve their activity at exceptionally low abundances.

2.4 Results and Discussion

Analysis of *S. mutans* TnSmu2 Biosynthetic Capacity.

To catalogue the full biosynthetic output of the TnSmu2 NRPS-PKS operon we first created a complete biosynthetic operon deletion strain (Δ TnSmu2) using in-frame allelic exchange, substituting genes Smu.1334c to Smu.1342 for a erythromycin resistance cassette. By performing a complete operon deletion, the possibility of detecting biosynthetic intermediates or mutational artefacts is excluded as no biosynthetic machinery is present. Wild type and mutant strains were grown for 48hr in a chemically defined medium (CDM) in 40 mL cultures (N=4) and subsequently freeze dried. Lyophilized extracts were reconstituted in methanol and analyzed by liquid-chromatography mass-spectrometry (LC-MS). Comparison of UV profiles readily identified two major peaks present in the wild type strain but absent in Δ TnSmu2, corresponding to mutanobactin A and C, however, to fully explore the metabolic output from TnSmu2 the LC-MS data sets were interrogated using principal component analysis (PCA).

A non-supervised statistical method, PCA is able to find and rank variances in the LC-MS data sets, providing a visual representation of metabolic differences. Concurrently, a supervised statistical method, student's t-test, was performed to determine the statistical significance of variances observed by PCA. Through multivariate analysis, all major ions in the chromatograms were extracted and defined as molecular features based on their specific retention time and m/z . Molecular features from both WT

and Δ TnSmu2 data sets were compared in MS signal intensity, providing fold changes representative of a metabolite's level in one sample relative to another. In this step, metabolites present in one sample, but absent in another are quickly identified as divergent features. This process requires statistical filtering, and only those molecular features with statistically significant p-values were pursued. As an added control, all metabolites of interest from PCA and t-test models were verified by creating individual extracted ion chromatograms for candidate m/z values and ensuring their absence or presence in the original chromatograms.

In contrasting WT and Δ TnSmu2 LC-MS data sets, a spatial distribution representative of discriminatory chemical information is generated by PCA (Figure 6). The scores plot gives a measure of similarity within sample sets, and differences to other sample sets. In contrasting intra-grouping variability, WT and Δ TnSmu2 samples represented by blue and red circles respectively, in the scores plot, being clustered closely together signify little deviation exists between replicate LC-MS data sets. While greater dispersion is noted between Δ TnSmu2 by reviewing the raw LC-MS data, only differences in the intensities of major ions were noted, suggesting this to be the cause of the divergence and not the absolute presence or absence of metabolites. (Data not shown).

In examining inter-grouping differences, a significant separation of WT and Δ TnSmu2 groupings in the scores plot is indicative of drastic metabolic variation between the two sample sets. Examining the distribution/identity of identified chemical entities, represented by blue circles in the loadings plot, chemical entities critically important to

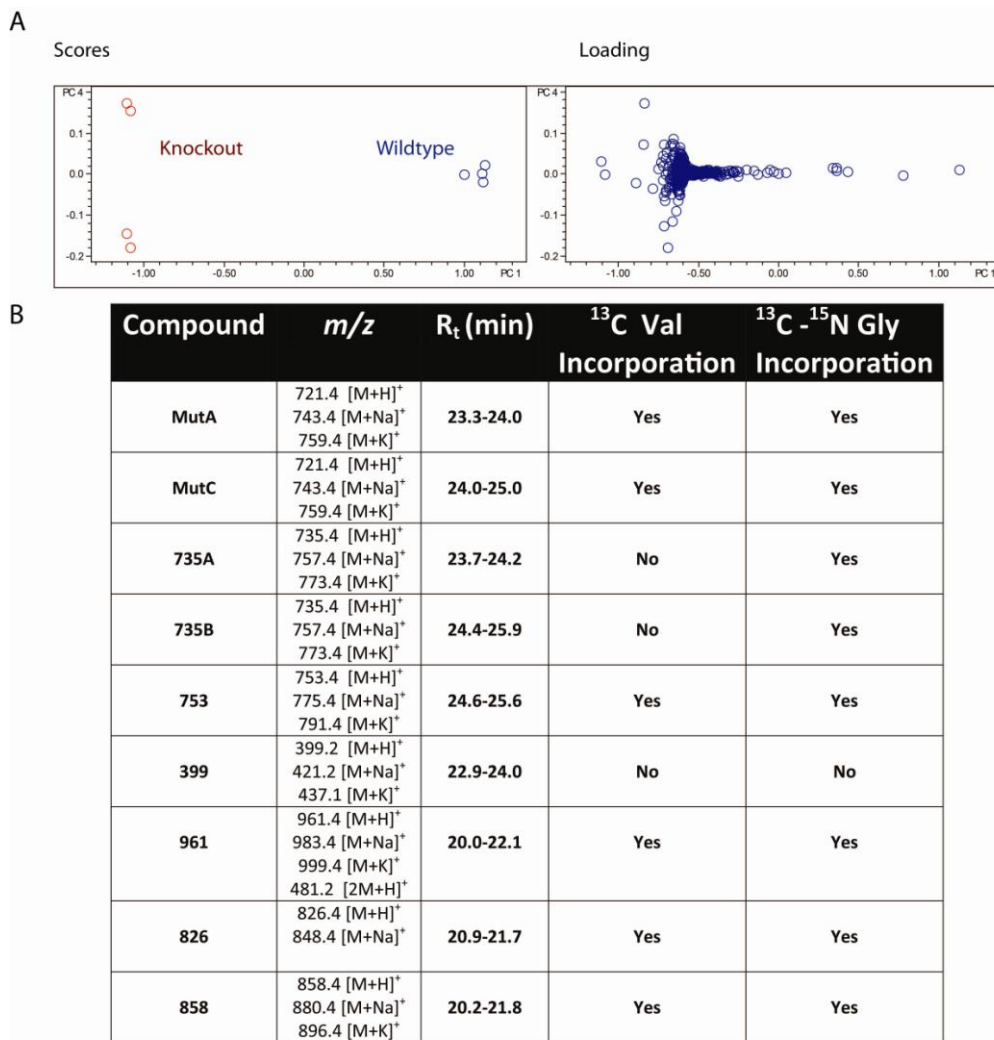


Figure 6. Untargeted metabolomic investigation of *S. mutans* TnSmu2 biosynthetic capacity using principal component analysis (PCA) of LC-MS data. A) Untargeted metabolomic comparison of wildtype and TnSmu2 knockout *S. mutans* strains using PCA. The Scores plot shows the grouping and differentiation of LC-MS data generated from wildtype (blue circles) and Δ Tnsmu2 (red circles) crude metabolic extracts (biological replicates, N=4). The loading plot shows critical ions in the LC-MS data as determined by PCA represented by blue circles. Ions clustered closely together are common to both strains while those with higher PC 1 values are unique to the wildtype strain. In analyzing the LC-MS data 100.5-1000.5 m/z and 8.0-17 min liquid chromatography retention time ranges were defined. **B)** Molecular features unique to wildtype samples are listed with their respective retention times, molecular ions and ability to incorporate isotopically labelled amino acids. Mutanobactin A and C were identified by their significant abundance over other compounds.

differentiating WT and Δ TnSmu2 groups were identified and are listed in a tabular format. Specifically, only those unique to the wild type strain are shown.

Each wild type unique compound was traced back to its original LC-MS (/MS) data file, allowing for the identification of mutanobactin A, its stereoisomer mutanobactin C and mutanobactin B, which again, has an isoleucine substituted for valine. The identification of previously known TnSmu2 products validates the use of PCA, and supports its use in the discovery of novel products. To probe the nature of molecular features identified as wild type specific, wild type *S. mutans* was grown with isotopically labelled amino acids, and its metabolic extract analyzed by LC-MS/MS. Two new closely related analogues with molecular ions $[M+H]^+$ of 735 *m/z* and 753 *m/z* noted in the PCA results were found to exhibit similar MS/MS fragmentation patterns to mutanobactin A, and also incorporated isotopically-labelled precursor amino acids in feeding experiments, supporting their identity as analogues.

To examine the relationship between these new analogues and TnSmu2, the MS/MS fragmentation patterns of mutanobactin A and the 735 *m/z* analogue were first contrasted revealing an identical fragmentation pattern with specific daughter ions maintaining the 14 *m/z* difference. Furthermore, as this new metabolite possessed a molecular ion identical to mutanobactin B, their fragmentation patterns were compared and revealed to be exactly identical. The lack of incorporation of isotopically labelled valine by both mutanobactin B and the new 735 *m/z* compound, creating the hypothesis of the new 735 *m/z* compound being a stereoisomer of mutanobactin B, just as mutanobactin C is to A.

Analysis of MS/MS fragmentation data and incorporation of isotopically labelled amino acids also strengthened the nonribosomal nature of the remaining wild type unique compounds. Fragmentation of the 753, 961, 826 and 858 m/z $[M+H]^+$ metabolites all resulted in peptide like fragmentation patterns, with partial amino acid mapping being possible. However, their fragmentation patterns were distinctly different from mutanobactins A, B, and C, indicative of drastic structural deviations. Coupled with unconventional mass differences not relating to any common post-translational modifications, the structural variations of the compounds could not be determined by tandem mass spectrometry alone.

Unexpectedly, a metabolite with a molecular weight noticeably lower from the mutanobactins, with a $[M+H]^+$ molecular ion at 399 m/z , was also identified by PCA as belonging to the wild type samples. Alongside its markedly lower molecular weight, MS/MS analysis further diverged the metabolite from the mutanobactins as it produced no peptide-like fragmentation and incorporated neither isotopically labelled glycine nor valine. The original LC-MS data was re-examined for the newly identified compound, and revealed a significant amount of co-elution with the mutanobactins, explaining its previous lack of detection by UV trace comparison. Focusing on this divergent metabolite, an HPLC method was developed for its isolation, however, it became apparent that due to the low level of compound present, growth conditions would need to be manipulated to generate enough of the 399 m/z metabolite for further study.

Environmental Conditions Regulate Metabolite Production.

It is well established that secondary metabolism can be affected by environmental factors leading to altered biosynthetic capacity in response to stresses or environmental conditions. For example, culturing the soil organism *Clostridium cellulolyticum* using typical laboratory conditions for clostridia yields no secondary metabolites, however, by adding soil to its fermentation media, production of the antimicrobial closthioamide is triggered (66). Several necrotrophic (host killing) *Penicillium* strains were also found to produce increased amounts of corymbiferone metabolites only when grown on macerated host tissue media, supporting the important role mimicking an organisms natural environment may have on metabolite production (67).

In an effort to increase production of the 399 m/z compound we set forth to alter commonly modified growth conditions including media composition, growth duration, and temperature. Wild type *S. mutans* grown in Brain Heart Infusion (BHI) broth had decreased 399 m/z production compared to THYE and changing temperature had no effect on production. Cultures grown for 24, 36, 48, 60 and 72 hours were also extracted and analyzed, showing 399 m/z levels peaking at 48 hrs of growth and decreasing afterwards. From these experiments, only when $\text{CO}_2(\text{g})$ levels were modified was a drastic change in production observed (Figure 7). While *S. mutans* is typically grown under anaerobic conditions, by switching to a 5% $\text{CO}_2(\text{g})/\text{air}$ environment, as is found in the oral cavity, a large increase in the UV peak corresponding to the 399 m/z compound was noted (68). Quantification of metabolite production showed that a 5-fold increase in production

occurred relative to anaerobic conditions, while only nominal changes in mutanobactin A and D production were observed (Figure 7).

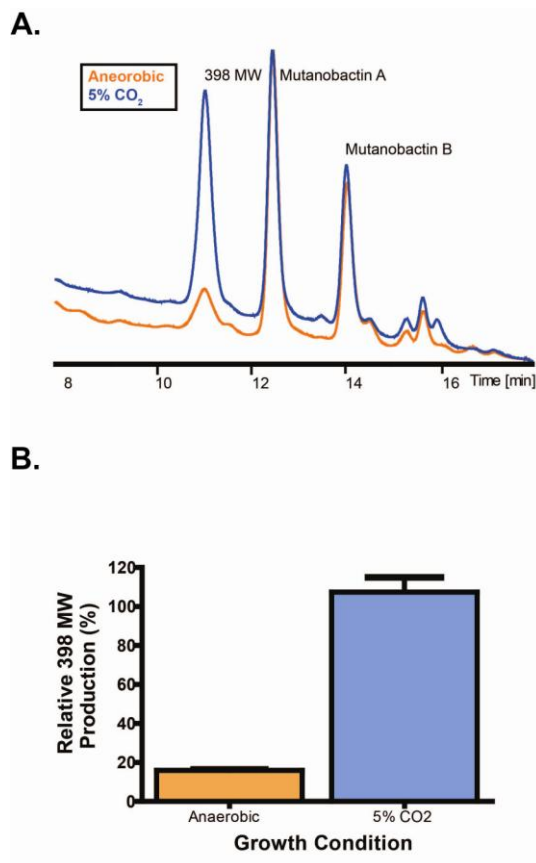


Figure 7. O₂ (g) Levels Affect Mutanamide Production in *S. mutans* . A. LC-MS UV profile shows differential production of TnSmu2 products based on O₂(g) level during culture growth. Cultures were grown as previously described for PCA analysis, with growth at 5% CO₂(g) achieved using a CO₂(g) cabinet. Anaerobic growth was achieved using an anaerobic chamber provided by Dr. Surette. Differences observed in Figure 2A. were quantified by integrating the UV peak specific for each compound as shown in **B.** Extracts were prepared as described previously, N=5.

A genetic link to metabolite production is hinted at through some RT-PCR data performed by Dr. Cvitkovitch's lab at the University of Toronto, when examining the VicRK two-component signal transduction system in *S. mutans*. The *vicRK* genes are part

of a *vicRKX* tricistronic operon shown to modulate adhesion, biofilm formation, genetic competence and stress tolerance in *S. mutans* (69-71). Also notably, the VicK sensor kinase harbours a PAS domain that functions as an input module in proteins that sense oxygen, redox potential, and light, suggesting it may play a role in the observed affect environmental conditions have on mutanamide production (72). Recently, the Cvitkovitch group reported the global transcriptome of a VicK deficient mutant (SmuvicK) and its parent UA159 strain that showed significant down-regulation of several genes (SMU.1334, SMU.1335, SMU.1336, SMU.1341, SMU.1342, SMU.1344) located within the TnSmu2 locus encoding mutanobactin A (49, 73). To validate microarray results and demonstrate a VicRK regulatory link on expression of several TnSmu2 genes, total RNAs from SmuvicK, Smuvic+ and *S. mutans* UA159 strains were isolated, and used for cDNA synthesis and quantitative real-time PCR (qRT-PCR) as described previously.

Expression analysis of 6 selected genes within the TnSmu2 locus using qRT-PCR revealed that loss of VicK or overexpression of the *vicRKX* operon altered transcription of the TnSmu2 genes (Figure 8). More specifically, loss of VicK resulted in repression of the candidate genes, whereas *vicRKX* overexpression resulted in their de-repression. Hence, transcriptional analysis suggests a positive regulatory role for the VicRK in modulating genes within the TnSmu2 locus responsible for mutanobactin and mutanamide production in *S. mutans*.

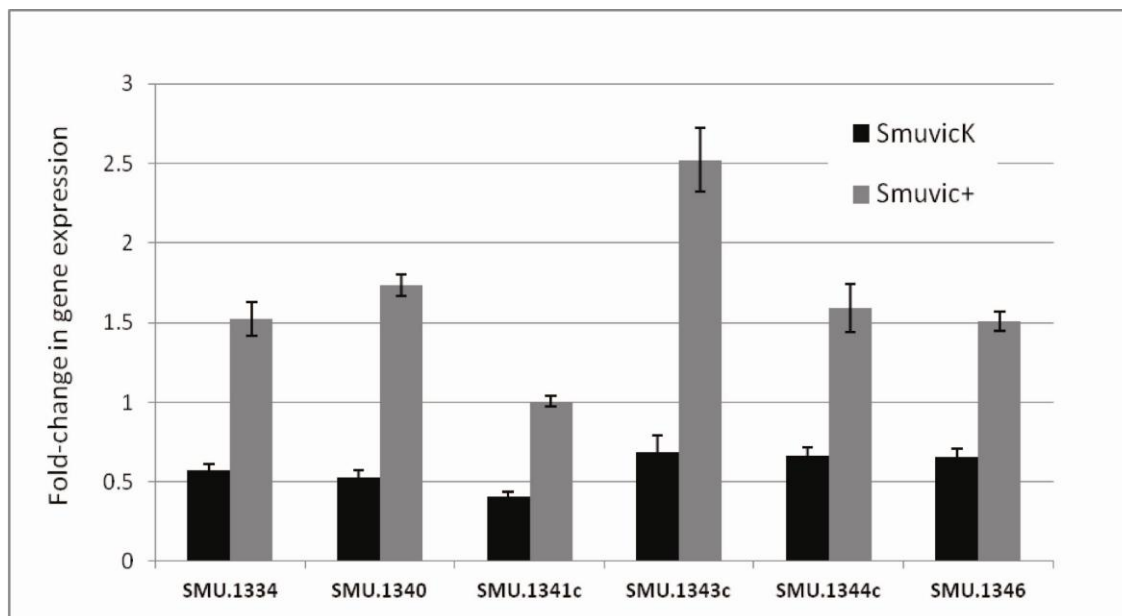


Figure 8 . Expression of selected genes within the TnSmu2 locus in the VicRK mutant versus UA159 parent strains. Using cultures grown to mid-log phase, cDNAs were isolated from *S. mutans* SmuvicK, Smuvic+ and UA159 strains and subjected to qRT-PCR analysis using primers specific for genes within the TnSmu2 locus. Fold-expression of genes in *S. mutans* UA159 was set at an user-defined value of 1.0. Results show the mean fold-expression from three independent experiments \pm std. error.

Isolation and Structure Elucidation of Mutanamide.

To isolate enough of the 399 m/z metabolite for structural and bioactivity analysis we carried out a large scale fermentation of wild type *S. mutans* at 5% CO_2 (g)/air for 48 hr. The liquid fermentations were processed using ethyl acetate liquid-liquid extraction, followed by silica flash chromatography and finally reverse phase-HPLC, ultimately yielding 1.7 mg of pure compound. High-resolution mass spectrometry gave a molecular ion $[\text{M}+\text{H}]^+$ of 399.2867 m/z and the chemical formula $\text{C}_{22}\text{H}_{42}\text{N}_2\text{S}_2$ (0.3ppm error). ^1H NMR yielded 7 unique ^1H signals, with a triplet at 0.86 ppm indicating a terminal methyl and 3 ^1H signals between 1.25 and 2.10 ppm belonging to methylene groups. A broad

singlet at 6.6 ppm was suggestive of an amide bond, however, this was unresolved pending further experiments. ^{13}C NMR provided 6 C signals, with a terminal methyl at 13.9 ppm, and 5 apparent methylene groups between 22.1 and 31.2 ppm. From this data, the compound was deduced to possess an alkyl chain 10 carbon atoms in length matching the alkyl tail size found on the mutanobactins. To explain the disparity between the low number of ^1H and ^{13}C signals and the large molecular weight and calculated molecular formula a symmetrical structure was proposed. Testing this hypothesis, 2D NMR experiments in conjunction with 1D data and MS/MS fragmentation were conducted and supported a structure with two alkyl chains linked through a N and O containing system. A hydrolysis experiment was performed where purified mutanamide was dissolved in 300 μL of deuterated TFA and its degradation monitored by NMR over time. After 24 hours, the sample was analyzed and found to be made up of three acyl metabolites, all possessing an amino group. Using 1D and 2D NMR, the putative structures of these fragments are shown, as well as the proposed mutanamide structure (Figure 9). From this structural information the 399 m/z product, now referred to as mutanamide, was known to possess alkyl tails, a structural feature often polyketide derived. To assess the involvement of PKS genes within the TnSmu2 operon in mutanamide biosynthesis, a mutant strain with a deletion of the PKS genes believed to be responsible for the biosynthesis of the alkyl tail found on the mutanobactins was generated ($\Delta\text{SMU}_1343/44$) and its metabolic output examined.

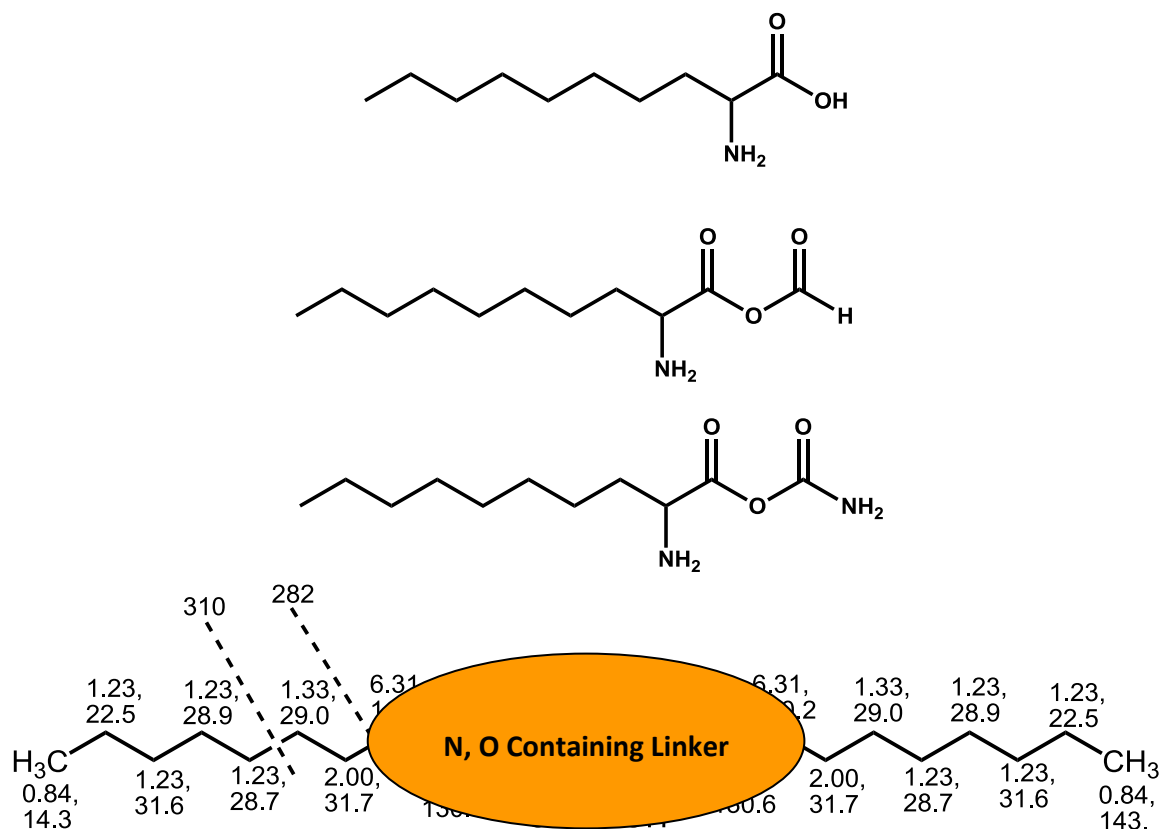


Figure 9. Proposed Mutanamide Structure Based on Partial Structures From Acid Hydrolysis, MS/MS Studies and NMR Experiments. NMR experiments performed on a Bruker 700 MHz spectrometer (in 100% deuterated TFA). Partial structures are proposed based on ^1H , ^{13}C , ^1H - ^1H COSY and long range ^1H - ^{13}C HMBC interactions.

Mutanamide Production is Linked to TnSmu2 Polyketide Synthase Genes.

S. mutans wild type, ΔTnSmu2 and $\Delta\text{SMU}_{1343/44}$ strains were again grown, extracted and analyzed using LC-MS as previously described (Figure 10). In contrasting the UV profiles a new peak was observed in the chromatogram of $\Delta\text{SMU}_{1343/44}$ with a $[\text{M}+\text{H}]^+$ molecular ion at 171 m/z in place of peaks corresponding to the mutanobactins and mutanamide. A pair wise comparison between wild type and $\Delta\text{SMU}_{1343/44}$ LC-MS data sets using PCA confirmed the 171 m/z metabolite to be the focal difference between

the two strains. To emphasize the metabolic shift, extracted ion chromatograms for mutanamide and the 171 m/z metabolite were generated and depict the loss of mutanamide production in Δ SMU_1343/44 which is replaced by an accumulation of the 171 m/z metabolite (Figure 10C). Interested in the identification of this compound, and its role in TnSmu2 biosynthetic operations, a large scale fermentation of Δ SMU_1343/44 was performed, yielding 2.6 mg of pure compound from 2 L of culture using previously described extraction methods.

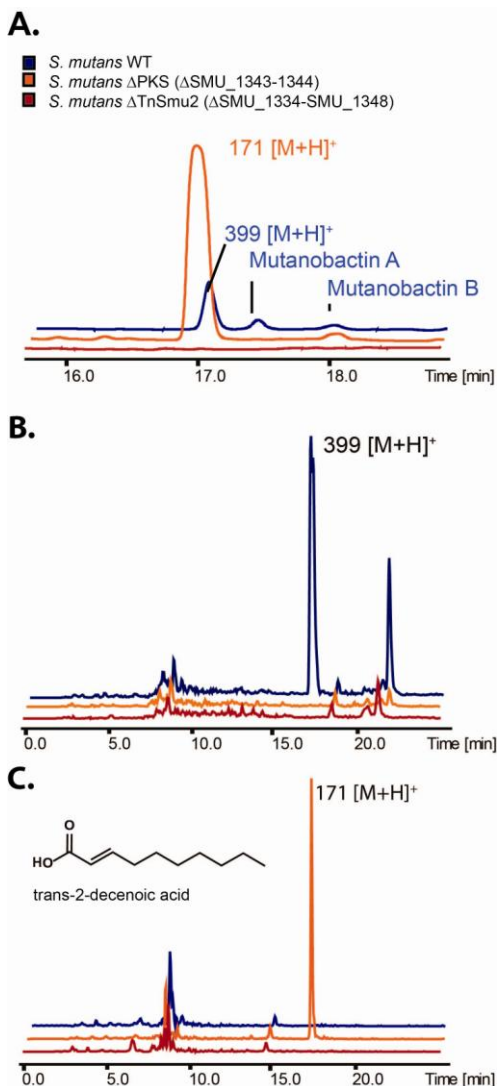


Figure 10. LC-MS Analysis of TnSmu2 Mutant Strains.

A) Comparing UV profiles of wildtype (blue trace), PKS deficient Δ SMU_1343/44 (orange trace) and complete operon deletion Δ TnSmu2 *S. mutans* strains (red trace) established correlations between metabolites of interest from metabolomic studies and specific biosynthetic genes within TnSmu2. Mass and fragmentation data from LC-MS(/MS) chromatograms were used to confirm metabolite identity. In deleting the PKS genes SMU_1343/44, UV peaks corresponding to the wildtype TnSmu2 metabolites disappeared and were replaced with a new large UV peak possessing a $[M+H]^+$ molecular ion at 171 m/z . **B)** Extracting LC-MS(/MS) chromatograms for the 399 m/z $[M+H]^+$ ion confirmed its presence only in wildtype *S. mutans*, and absence upon deletion of PKS genes. **C)** Extracting LC-MS profiles for the newly identified 171 m/z $[M+H]^+$ ion confirmed its detection only in Δ SMU_1343/44. Isolation and structural elucidation experiments identified the compound as the previously discovered *S. mutans* fatty acid signalling molecule *trans*-2-decenoic acid (SDSF).

^1H NMR revealed a terminal methyl group at 0.85 ppm with methylene groups between δ_{H} 1.25 and 2.2 ppm, reminiscent of the mutanamide data. However where the mutanamide ^1H spectra possessed only broad singlets, sharp signals appeared at δ_{H} 5.7 (doublet, $J=15.5$) and δ_{H} 6.72 ppm indicative of an alkene group in the *trans* configuration based on the coupling value,. The simple doublet at δ_{H} 5.7 ppm suggested the proton is between the alkene and some proton deficient terminal group, such as a carboxylic acid.

The ^{13}C NMR spectra provided 11 signals, with a terminal methyl at $\delta_{\text{C}} 13.95$ ppm, and 6 signals between $\delta_{\text{C}} 22.07$ and 31.30 ppm, again indicative of methylene groups.

Additional signals were observed at $\delta_{\text{C}} 123.21$ and 147.45 ppm from the double bond and two final signals at $\delta_{\text{C}} 165.68$ and 167.80 (quaternary carbon) ppm are believed to be associated with the terminal unit in a fatty acid type molecule. 2D NMR experiments confirmed the structure to be an unsaturated short chain fatty acid, and with a molecular weight of 169, allowed its identification as *trans*-2-decenoic acid. Interestingly, *trans*-2-decenoic acid had previously been isolated and characterized from *S.mutans* UA159 by bioactivity guided fractionation, selecting for metabolites with the ability to inhibit *C. albicans* germ tube formation (41). In that particular study however, 170L of culture were required to obtain enough material for structural elucidation.

From this accumulation of *trans*-2-decenoic acid upon the deletion of PKS genes, a hypothesis was developed with *trans*-2-decenoic acid being used as a monomer in the biosynthesis of mutanobactin and mutanamide. Previous studies by Wang *et al.*, used [1- ^{13}C] acetate and [2- ^{13}C] acetate feeding experiments to argue that the head to tail condensation of six acetate units was responsible for the 12 non-peptide derived carbons in the mutanobactin scaffold and that these units were derived from PKS machinery. Our results instead suggest a medium chain fatty acid, specifically *trans*-2-decenoic acid, is utilized by PKS genes within TnSmu2, extending it by an additional acetyl-CoA establishing the first biosynthetic substructure. Downstream, full lipopeptide assembly follows through the successive addition of amino acid monomers to the extended *trans*-2-decenoic acid moiety. The lack of a methylene unit within the acyl tail moiety of

mutanobactin can be readily explained by the possible action of the standalone enoyl reductase domain encoded at Smu.1335c.

This initial process of generating the acyl tail is known as lipoinitiation and has been reported to occur through variable biosynthetic mechanisms for different lipopeptides. In examining the TnSmu2 operon, Smu.1345c, a gene found early in the assembly line, stood out for its high homology to the didomain enzyme MycA, the enzyme responsible for the addition of decanoic acid to the lipopeptide mycosubtilin (74). Smu.1345c had previously been implicated in incorporating an aspartic residue in mutanobactin, however, feeding experiments with isotopically labelled aspartic acid showed no incorporation (Figure 11). Since both MycA and Smu.1345c possess fatty acyl ligase (AL) and acyl carrier protein (ACP) domains, and mycosubtilin is known to exist in homologous forms differing in acyl tail length, the promiscuity of fatty acid incorporation by the TnSmu2 operon was explored using fatty acid precursor feeding experiments.

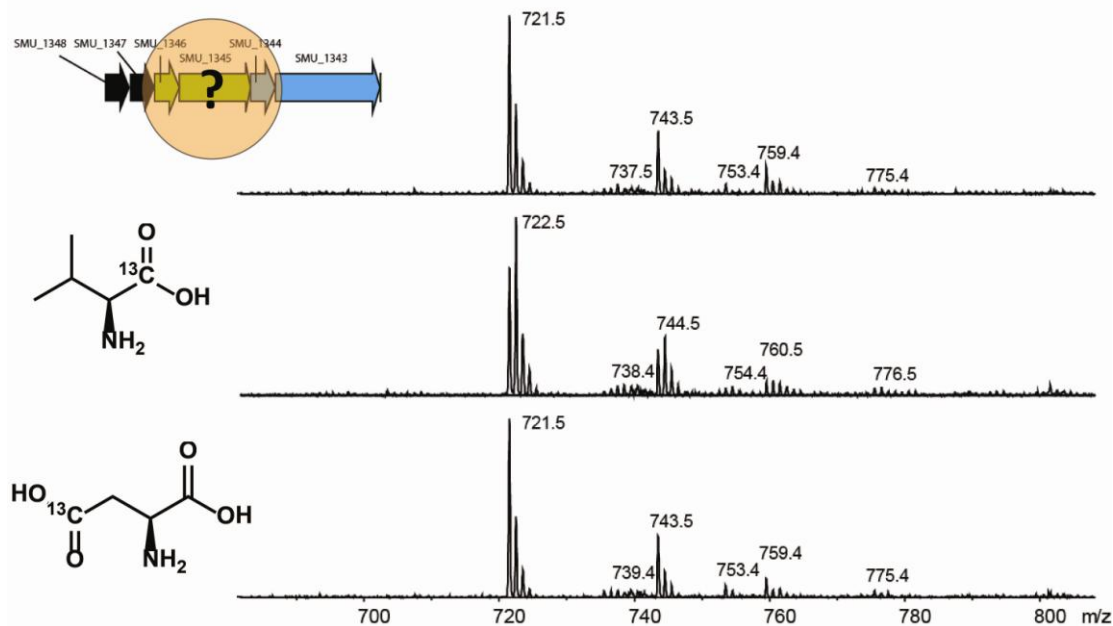


Figure 11. Aspartic Acid is Not Incorporated By Smu_1345 into mutanobactin A. By fermenting *S. mutans* in CDM supplemented with 500 μ M of isotopically labelled amino acids, the incorporation of specific monomers was questioned. Previous groups proposed SMU_1345 in the TnSMU2 operon incorporated an aspartic acid residue, however, no incorporation was observed in mutanobactin A based on its isotope pattern. Were it to be present, the isotope pattern would shift significantly, as seen with the valine positive control.

Medium Chain Fatty Acids Are Key Monomers in Mutanobactin/Mutanamide

Biosynthesis.

To test whether mutanobactin and mutanamide biosynthesis involve the incorporation of activated medium chain fatty acids feeding experiments were devised. *S. mutans* wild type and Δ TnSmu2 strains were grown in 40 mL of CDM supplemented with 500 μ M of 9-decenoic acid, 8-nonenic acid, or 7-octenoic acid. Cultures were grown for 48 hours, extracted as previously described and the generation of novel compounds examined using LC-MS (Figure 12). In each supplemented medium a decrease in mutanobactin production was observed in wild type strains, with the fatty

acids more closely resembling decanoic acid decreasing production most and 7-octenoic acid having almost no discernible decrease. The decrease in mutanobactin production suggested a derailment of the biosynthetic assembly line towards divergent metabolites and by extracting LC-MS chromatograms for modified versions of mutanobactin A (719 m/z for 9-decenoic acid, and 705 m/z for 8-nonenoic acid), bioengineered mutanobactins were identified and confirmed using MS/MS fragmentation (Figure 12). No detectable incorporation of 7-octenoic acid was observed suggesting the fatty acid incorporating machinery has a strong predisposition towards fatty acids near 10 carbons in length.

Due to apparently low levels of incorporation no mutanamide analogues could be identified under small scale fermentation conditions. However, by growing wild type *S. mutans* in 1L batches of 50% THYE supplemented with 500 μM of the fatty acids, mutanamide analogues could be identified with $[\text{M}+\text{H}]^+$ molecular ions at 397 m/z suggesting 9-decenoic acid incorporation and 383 m/z for 8-nonenoic acid incorporation. MS/MS analysis of the new compounds confirmed their identity as mutanamide analogues. Based on the observed mass differences in daughter ions, only a single fatty acid monomer appeared to be incorporated in the analogues, suggesting an asymmetric molecule. Interestingly, all analogues possessed the same daughter ion at 202.9 m/z suggesting a conserved structural moiety (Figure 13). From these large scale feeding experiments a small amount of the 9-decenoic acid fed mutanobactin A analogue was also able to be obtained for NMR analysis confirming the incorporation of 9-decenoic acid within the mutanobactin scaffold and cementing the incorporation of medium chain fatty acids in mutanobactin and mutanamide biosynthesis.

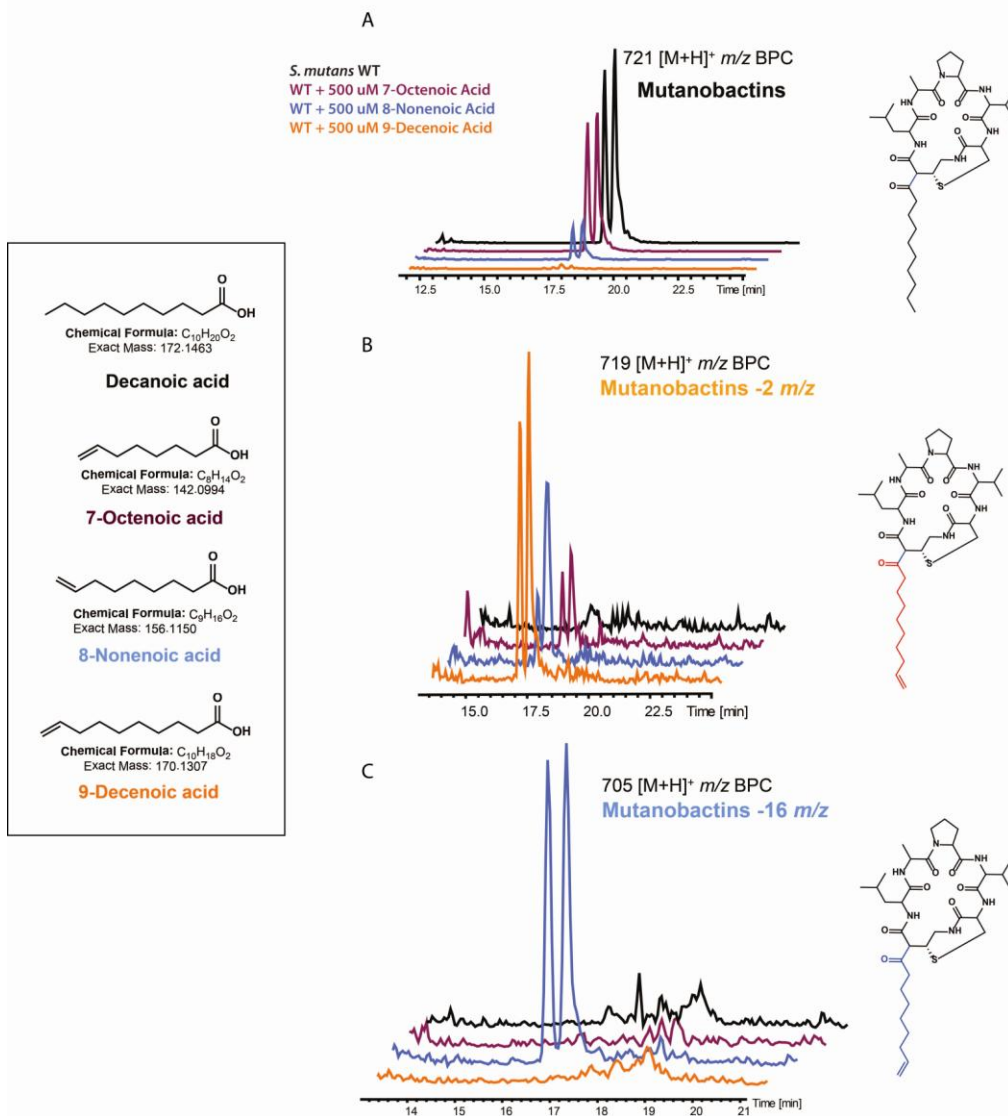


Figure 12. Supplementing *S. mutans* Cultures with Decanoic Acid Analogues Results in Novel Mutanobactin Analogues. Believing SMU_1345 to be a fatty acid-CoA ligase, responsible for incorporating decanoic acid in mutanobactin A biosynthesis, the ability to incorporate other fatty acids into mutanobactin was questioned. A) When *S. mutans* was grown in CDM supplemented with 500 μ M of fatty acids close in size to decanoic acid, mutanobactin A and C levels decreased proportionally as observed in the extracted ion chromatogram for 721 *m/z* [M+H]⁺ molecular ions. B) Supplementation with 9-decenoic acid led to new peaks with *m/z* of 719, suggesting the mutanobactin analogue shown. Large scale fermentations and NMR experiments confirmed the production of this novel mutanobactin. C) Successful incorporation of 8-nonenic acid led to a new molecular ion at 705 *m/z*, suggestive of a novel bioengineered mutanobactin supported by MS/MS data.

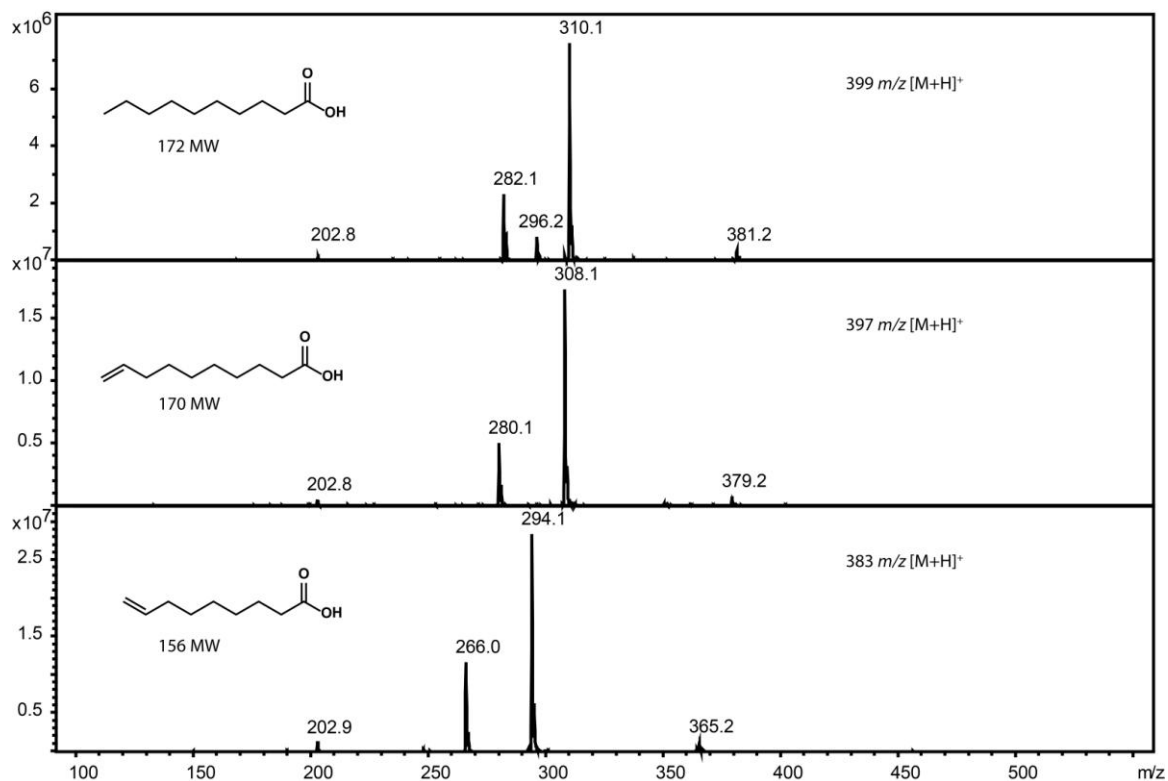


Figure 13. MS/MS Fragmentation Data of Mutanamide Analogues from Fatty Acid Feeding Studies Suggests Single Monomer Incorporation. Large scale fermentations of *S. mutans* supplemented with 500 μ M 9-decenoic acid (170 MW) or 8-nonenic acid (156 MW) produced novel mutanamide analogues as confirmed by MS/MS fragmentation patterns of 399 m/z (wildtype), 397 m/z (+ 9-decenoic acid), and 383 m/z (+ 8-nonenic acid) molecular ions.

TnSmu2 Biosynthetic Products Differentially Inhibit *C. albicans* Hyphal Formation.

Incorporation of an acyl tail moiety appears to be a unifying structural component present amongst all compounds reported to inhibit the hyphal transformation in *C.*

albicans. As a high degree of structural homology existed between mutanamide and

trans-2-decenoic acid which was previously shown to inhibit *C. albicans* hyphal

transformation, a similar activity was pursued using mutanamide. Since mutanobactin A

was also reported to inhibit *C. albicans* hyphal transition, a hyphal transition inhibition

assay was carried out as reported by Vilchez *et al.* (41), comparing the bioactivities of mutanobactin A, mutanobactin C, and mutanamide. By treating *C. albicans* with the TnSmu2 products in hyphal-inducing conditions the capability of the TnSmu2 metabolites to inhibit the transformation could be quantified using microscopy. Visually counting the number of cells in the hyphal state relative to the non-invasive yeast in the presence or absence of TnSmu2 products over time provided an accurate assessment of hyphal inhibition capacity between the TnSmu2 metabolites.

From these experiments it became obvious that, from the TnSmu2 products tested, mutanamide exhibited the most inhibitory activity (Figure 14). By qualitatively assessing treated versus non-treated *C. albicans* cells after 6 hours of growth, cells treated with 100 $\mu\text{g}/\text{mL}$ mutanamide were almost all in the yeast form, while a significantly greater number of cells exhibited germ tube formation following identical treatment with mutanobactin A or C. Compared to an untreated control however, all TnSmu2 metabolites tested possessed significant inhibitory activity. To measure the true extent of mutanamide's efficacy, a more in-depth quantitative evaluation of inhibition was performed.

Following 4 hours of growth in the presence of 100 $\mu\text{g}/\text{mL}$ mutanamide *C. albicans* cells were completely inhibited from transitioning into their invasive germ tube form (Figure 14B/C). In contrast, at the same time-point and dosage, inhibitory activities of mutanobactin A and C, showed mutanobactin A to be more active than mutanobactin C with ~30% and ~70% of *C. albicans* cells exhibiting germ tube formation respectively. Even at 10 $\mu\text{g}/\text{mL}$ mutanamide almost no cells showed hyphal transformation and even

with 1 $\mu\text{g}/\text{mL}$ concentration, at most 50% of cells were in their invasive form. At 1 $\mu\text{g}/\text{mL}$ both mutanobactin A and B failed to exhibit any inhibitory activity against the pathogenic conversion. In a stand alone assay, the activity of mutanamide was measured over time revealing that even after 6 hours of growth 100 $\mu\text{g}/\text{mL}$ and even 10 $\mu\text{g}/\text{mL}$ concentrations were adequate to abolish the hyphal transition. From these results, and studies previously performed on *S. mutans* derived *trans*-2-decenoic acid, and other fatty acid based molecules, it appears that inhibition of germ tube formation in *C. albicans* is modulated primarily by medium chain fatty acids. In the case of the mutanobactins, the observed activity is believed to result directly from the acyl tail, and suggests that the peptide core may in fact be a hindrance for this particular activity. A question then arises as to what role the peptide core is playing, and within the context of what biological activity?

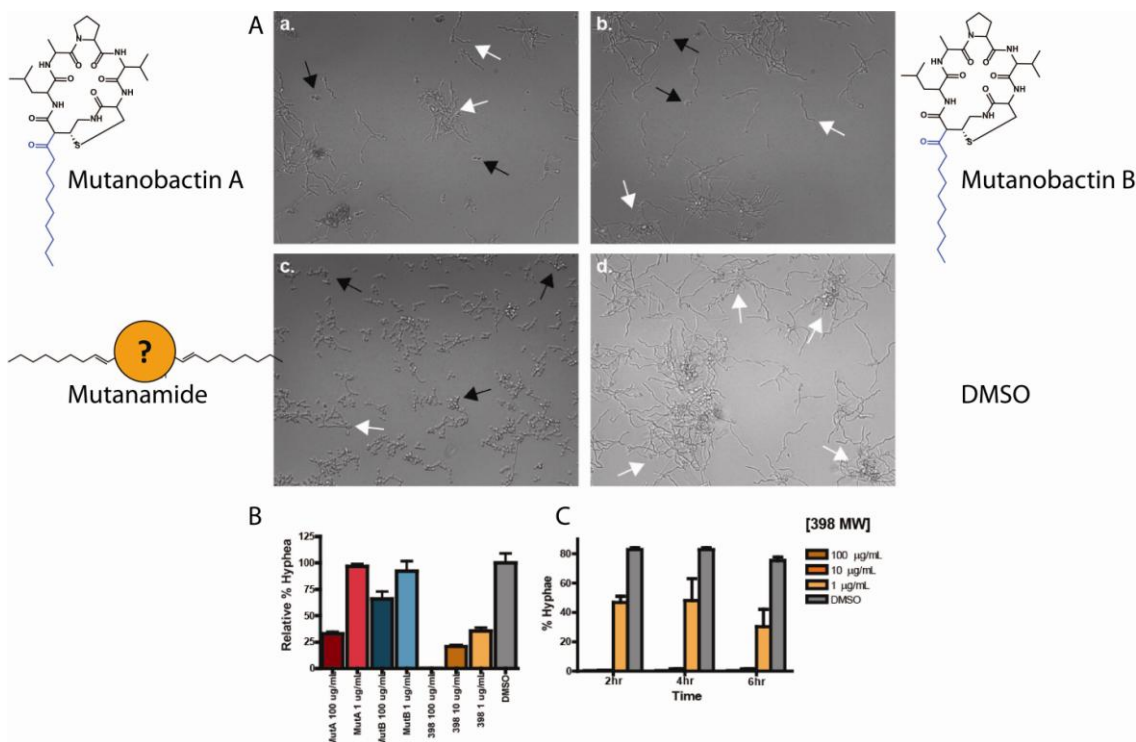


Figure 14. Comparison of TnSmu2 Product's Ability to Inhibit the Hyphal Transformation of *Candida albicans*. A) *C. albicans* cells were grown in a medium promoting germ tube formation in the presence of 100 μ g/mL mutanobactin (a.), mutanobactin (b.), mutanamide (c.), or DMSO (d.) Following 4 hours of incubation, cell morphology was examined using phase contrast microscopy and the inhibitory activity of the TnSmu2 products compared qualitatively. Compared to the DMSO control, where almost all cells were in a hyphal form (white arrows), a moderate number of cells treated with mutanobactin A and B remained in their yeast state (black arrows), whereas treatment with mutanamide almost completely inhibited the hyphal transition in all cells. B-C) Inhibition was quantified by counting the number of hyphal cells relative to yeast cells (200 total cells counted), after 4 hours of growth, confirming the increased efficacy of mutanamide compared to the mutanobactins (B). C) Mutanamide retained the ability to inhibit hyphal transformation even after 6 hours of growth with complete and almost complete inhibition at 100 and 10 μ g/mL respectively.

TnSmu2 Products Elicit an Immune Response in Dendritic Cells.

The mixed NRP-PK surfactin has recently been shown to exhibit anti-inflammatory activity in a number of studies (75, 76). Since the structurally related TnSmu2 products are secreted metabolites by a human microbiome member, we sought to explore their effects on host cells in an immunological perspective. Dendritic cells (DCs) were chosen due to their role as messengers between innate and adaptive immunity, a role defined by their localization in tissues in contact with the external environment where they can process antigen material and present it on their surface as a marker to other immune cells. DCs isolated from rat spleens were co-incubated with purified mutanobactin A and C, the most abundant TnSmu2 products, as well as *trans*-2-decenoic acid for 24 and 48 hours. Following co-incubation, cells were assayed for immune response by measuring levels of the pro-inflammatory cytokine IL-12, the anti-inflammatory cytokine IL-10, and the both pro- and anti-inflammatory cytokine IL-6.

All compounds tested elicited an immune response from DCs to varying degrees (Figure 15). Mutanobactins A and C (referred to as B in Figure 15), and *trans*-2-decenoic acid all induced similarly high levels of IL-12 at both 250 and 25 μ M with a slight increase from 24 to 48 hours. A moderate induction in anti-inflammatory IL-10 was noted for the mutanobactins, which, together with IL-12 data, suggests their nature to be more pro-inflammatory. In contrast, *trans*-2-decenoic acid induced significantly more IL-10 secretion, which increased significantly from 24 to 48 hours, almost matching IL-12 levels. In this regard, *trans*-2-decenoic acid appears to induce high IL-12 levels first, with

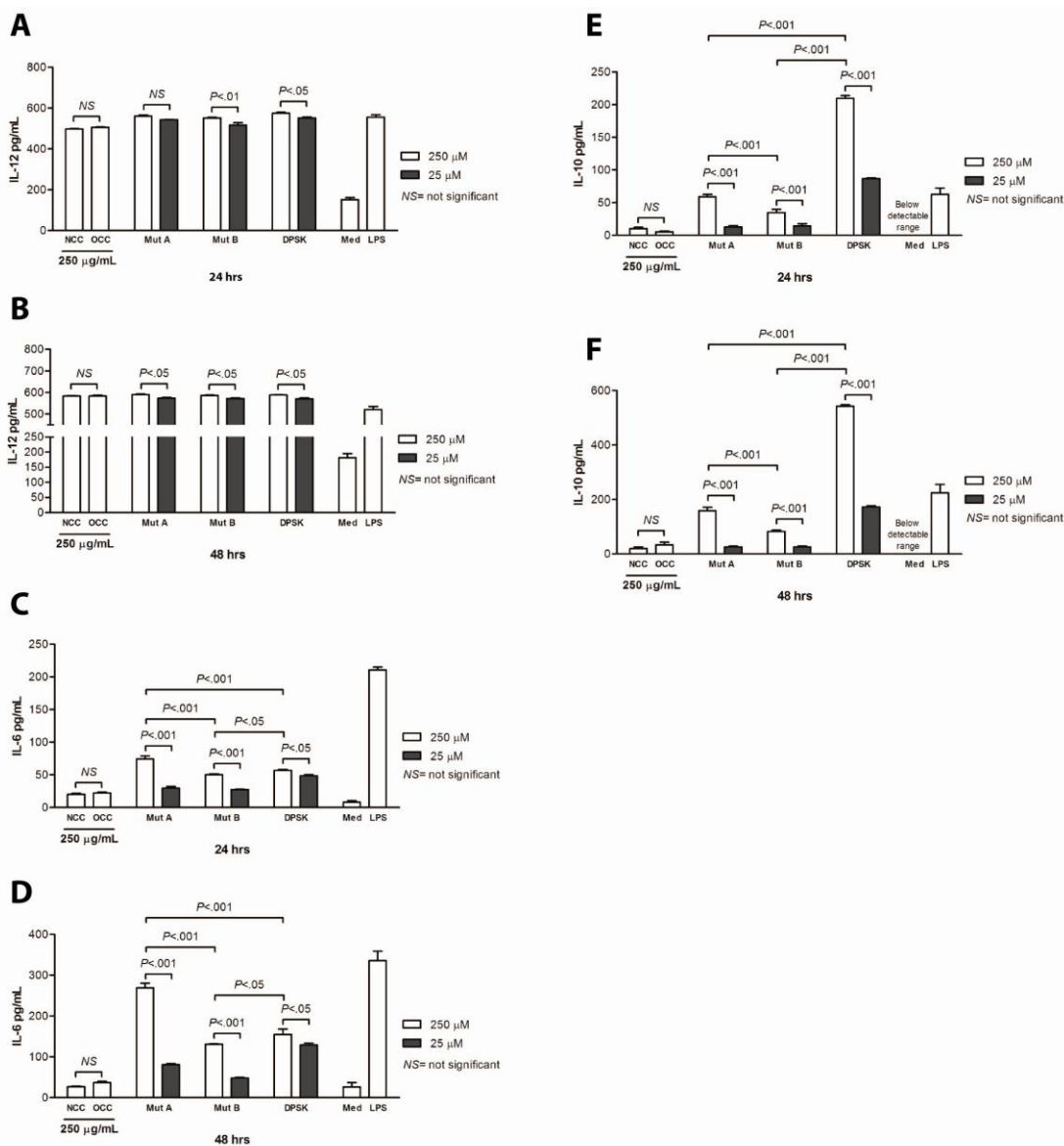


Figure 15. TnSmu2 Biosynthetic Products Elicit an Immune Response in Mouse Dendritic Cells. Dendritic cells isolated from mice spleens were incubated with or without LPS (100 ng/mL, Sigma-Aldrich) and combined with mutanobactin A (MutA), its stereoisomer mutanobactin C (labelled as MutB) or trans-2-decenoic acid (DPSK). Compounds were dissolved in PBS and added to the culture at varying doses in the presence or absence of nuclear factor kappa B (NF- κ B) inhibitor, pyrrolidine dithiocarbamate (10 μ mol/L, PDTc, Sigma) and incubated at 37°C for 24 (A,C, and E) and 48 (B, D, and F) hours. Supernatants were collected and analyzed for cytokine levels using the Bio-Plex Luminex system (Bio-Rad, Canada). Supernatant levels of IL-12 (A & B), IL-6 (C & D), and IL-10 (E & F) were measured using a Bio-Rad cytokine 2-plex panel kit. Fluorescence data was acquired and analyzed by Bio-Plex Manager software (version 5.0, Bio-Rad Laboratories).

compensatory levels of anti-inflammatory IL-10 following. All TnSmu2 compounds induced modest levels of IL-6.

This data suggests that the mutanobactins are proinflammatory antigens, whereas the nature of *trans*-2-decenoic acid is difficult to deduce from its stimulation of both pro- and anti-inflammatory cytokines depending on treatment duration. The addition of the peptide core in the mutanobactins clearly has an effect on the nature of the immune response, appearing to make the molecules more proinflammatory. As for *trans*-2-decenoic acid, previous studies examining the related compound 10-hydroxy-2-decenoic acid noted its apparent anti-inflammatory effects; however, further studies are required to determine the full effects of *trans*-2-decenoic acid (77, 78) on the host immune system. From these results it is not yet possible to confidently assign the individual TnSmu2 compounds as either anti- or pro-inflammatory; however, their ability to elicit a pronounced immune response warrants further study using *in vivo* models. Understanding the initiation of adaptive immunity in the oral cavity will provide insight and potential intervention for oral infectious diseases and potentially further our understanding of the impact of oral disease on systemic conditions.

Here, we report a more complete catalogue of the metabolic output from the TnSmu2 NRPS-PKS operon within *S. mutans* generated by interrogating LC-MS data sets from wild type and Δ TnSmu2 extracts using PCA. Using this approach a number of unreported mutanobactin analogues were observed, while not omitting previously reported compounds. Interestingly, a number of the new compounds differed significantly from the known mutanobactin scaffold with some exhibiting significantly higher

molecular weights. Alongside the higher molecular weight peptides, another divergent product was identified which appeared nonpeptidic and had a significantly lower molecular weight from the mutanobactins. Feeding experiments confirmed the molecule to be fatty acid derived and linked to the TnSmu2 operon through PKS enzymes. Cumulatively, experimental results generated here provide increased insight into mutanobactin and mutanamide biosynthesis, allowing for the generation of a proposed assembly line (Figure 16). Overall, this study has expanded what's known about secondary metabolism within *S. mutans*, raising interesting questions regarding biosynthetic logic and the biological activity of human microbiome derived metabolites within a host specific setting.

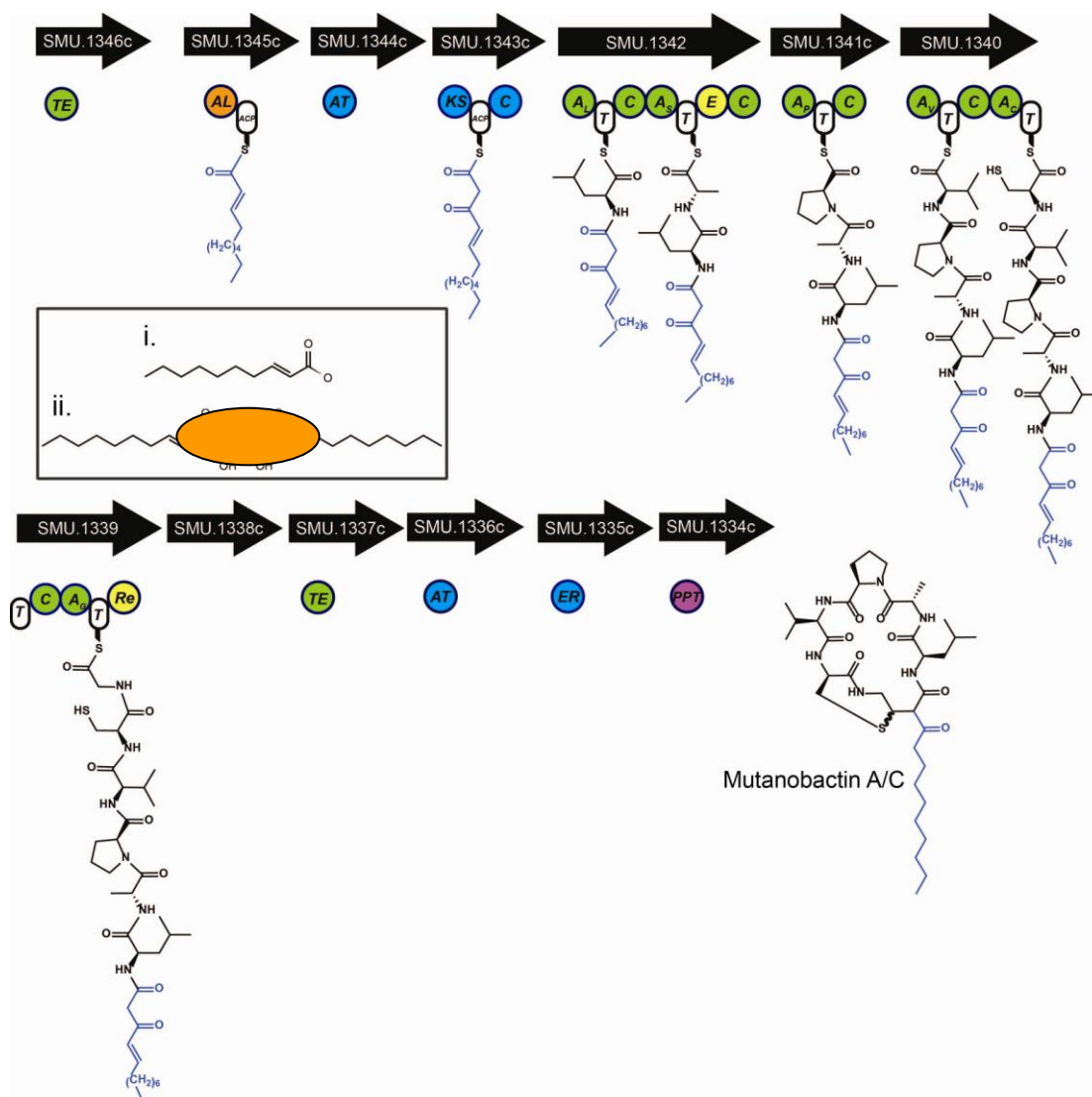


Figure 16. Proposed Biosynthetic Pathway for the Mutanobactins and Mutanamide.

2.5 Materials and Methods

All experiments were performed by Nikola Lukenda except where noted.

Bacterial Strains and Reagents. *Streptococcus mutans* genomic strain UA159 was used in all studies. *Candida albicans* ATCC no. 90028 was used for hyphal inhibition assays. All reagents and chemicals were purchased from Sigma Aldrich unless otherwise stated.

S. mutans mutants were constructed by Martha Cordova from the Cvitkovitch lab.

Mutant Construction. Complete deletion of TnSmu2 in *S. mutans* was generated using in-frame allelic exchange, substituting the biosynthetic operon for a erythromycin resistance cassette. Knockout was confirmed using PCR and primers specific to SMU_1340 (Forward: AGCCAGCGTCATCTTCTGTCACC, Reverse: AGGGAGTGCAGGTTGGCGGA) and SMU_1343 (Forward: TCGACCACTGACCGGATTCCCA, Reverse: TGCTTCATTAGAAGCGATGCACCA). Polyketide synthase mutant (Δ Smu. 1343c/1344c) was obtained using similar methodology. A full list of plasmids and primers used are listed in Supplemental Table S1.

Fermentation, Analysis and Isolation of TnSmu2 Biosynthetic Products. All *S. mutans* strains were grown using Todd-Hewitt broth supplemented with 10% yeast

extract (THYE broth), THYE broth supplemented with erythromycin (10 $\mu\text{g}/\text{mL}$), or a chemically defined media (CDM) as previously reported at 37°C with 5% CO_2 without shaking unless otherwise mentioned (79). Anaerobic growth was achieved using a BD GasPak™ (260626) self contained anaerobic system. For isolation of TnSmu2 products, 1L batches of 50% THYE were inoculated in 2.8 L Fernbach Flasks with 10 mL of overnight *S.mutans* WT or mutant seed culture and incubated for 48 hours. Liquid-liquid extraction using ethyl acetate (2:1, 1:1 vol/vol) was performed on the supernatant following centrifugation (8500 rpm for 20 min) and the resulting organic phase concentrated under vacuum. The crude extract was fractionated using a Combiflash® Rf normal phase MPLC system (Teledyne Technologies Inc.) with a 12g RediSep® Rf silica Flash column. The following program of solvent A (hexanes) and B (ethyl acetate) was employed: 0-2 min, 0%B; 2-16 min, a linear gradient to 100% B; 16-18 min, isocratic 100% B. A 100% MeOH over 10 min wash followed. Resulting fractions were pooled by 25% ethyl acetate increments, yielding 5 fractions, and concentrated to dryness under vacuum prior to analysis by HPLC-ESI-MS (Dionex UltiMate 3000 HPLC system with variable UV detection in line to a Bruker amaZon X ion-trap mass spectrometer operating in positive ionization mode with auto MSn). Analytical scale analysis was performed on a 250 x 4.60 mm Phenomenex Luna 5 μ C18(2) 100Å (Serial n. 516161-20) column with a flowrate of 1 ml min⁻¹ and the following program consisting of solvents A (H₂O + 0.1% Formic acid) and B (Acetonitrile + 0.1% Formic acid): 0-5 min, equilibration at 5% B; 5-58 min, curve 8 gradient to 95%B; 58-60 min, linear gradient to 100% B; 60-65 min, constant 100% B; 65-67 min, linear gradient to 5% B; 67-75 min, re-equilibration at 5%

B. For multivariate analysis, a 50 x 3.0 mm Phenomenex Gemini-NX 3u C-18 110A column (Serial n. 567333-1) was used with the following program using an identical solvent system: 0-3 min, 2% B; 3-23 min, linear gradient to 100% B; 23-27 min 100% B; 27-29 min, linear gradient to 2% B; 29-35 min, re-equilibration at 2% B. Isolation of TnSmu2 biosynthetic products was achieved using semi-preparative HPLC with a 250 x 10 mm Phenomenex Luna 5u C18(2) 100A column (Serial n. 473442-7) with a flowrate of 3 ml min⁻¹ and the following gradient using the same solvent system as described previously: 0-4 min, 55% B; 4-34 min, linear gradient to 100% B; 34-36 min, 100% B; 36-37 min, linear gradient to 55% B; 37-40 min, re-equilibration at 55% B. High-resolution mass spectral data was obtained using a Thermo Scientific LTQ Orbitrap XL. NMR experiments were performed using a Bruker Avance 700 MHz spectrometer with all samples dissolved in dimethyl-d₆-sulfoxide “100%” (CDN Isotopes).

Multivariate Analysis of Wild type and Mutant *S. mutans* Extracts. Wild type and mutant *S. mutans* were grown overnight in 10 mL of CDM and used to inoculate (1:100) 40 mL cultures of fresh CDM in quadruplicate (N=4) which were then grown for 48 h under standard conditions. Cultures were lyophilized, and brought up in 1 mL of 80% MeOH/H₂O with the soluble portion analyzed using HPLC-ESI-MS operating in positive mode with a 150-1500 *m/z* mass window. Multivariate analysis was performed on the resulting data sets using Bruker Daltonics Profile Analysis 2.0. Pairwise comparisons between wild type and mutant strains using PCA and T-test models were performed using rectangular bucketing with baseline subtraction of data prior to analysis. Bucket

parameters were defined as $\Delta R_t = 0.2$ min, with a kernel size of 0.02 min, and $\Delta m/z = 0.5$ m/z with a kernel size of 0.150 m/z .

Feeding Experiments with Isotopically Labelled Precursor Amino Acids. *S. mutans* UA159 was grown overnight in CDM, diluted 100-fold, and grown for 48 hours at 37°C in a 5% CO₂ air mixture in fresh CDM supplemented with 500 μM of DL-Valine-1-¹³C, DL-Aspartic-4-¹³C acid, or Glycine 1-¹³C, ¹⁵N. Cultures were lyophilized, and brought up in 80% MeOH/H₂O, with the soluble portion analyzed using HPLC-ESI-MS operating in positive mode with a 150-1500 m/z mass window.

Generation of Novel Mutanobactin and Mutanamide Analogues Through Directed Medium Chain Fatty Acid Feeding Experiments. *S. mutans* UA159 was grown overnight in CDM, diluted 100-fold and grown for 48h at 37°C in 5% CO₂ air mixture in CDM supplemented with 500 μM 9-decenoic acid, 8-nonenoic acid, or 7-octenoic acid. Cultures were extracted and analyzed identically as for the isotopically labelled precursor feeding experiment. In order to detect mutanamide analogues 1L cultures of 50% THYE supplemented with 500 μM of a specific fatty acid were grown and extracted using ethyl acetate with the resulting crude extract analyzed using HPLC-ESI-MS.

Effect of Environmental Conditions on Mutanamide Production. *S. mutans* wild type and $\Delta TnSmu2$ strains were grown in 50 mL cultures in 50% THYE under anaerobic and 5% CO₂ (g) conditions. Crude extracts were generated using ethyl acetate liquid-liquid

extraction and analyzed using HPLC-ESI-MS as previously described. Mutanamide production was measured by integrating UV peak areas in LC chromatograms of extracts from the two conditions.

***C. albicans* Hyphal Formation Assay.** *C. albicans* pre-cultures were grown in YNB medium without amino acids and with ammonium sulfate (Bioshop® Canada Inc.; YNB406.100), supplemented with 0.1% maltose and 0.2% glucose at 30°C with agitation at 160 rpm for 24 h. To assay hyphal formation, pre-cultures were used to inoculate hyphal promoting media, consisting of YNB with 2.5mM N-acetylglucosamine added (Sigma A3286-5G). TnSmu2 biosynthetic products were dissolved in DMSO and added at the noted concentrations. Care was taken to add no more than 1 µL of DMSO to 100 µL cultures to avoid secondary effects. Cultures were grown under noted *C. albicans* conditions and were examined using light microscopy every 2 hours to assay cell morphology. Specifically, percentage of hyphal cells = number of hyphal cells/200 total cells counted.

Microscopy. For light microscopy, a Nikon Eclipse TS100 microscope was used to examine *C. albicans* cell morphology at a total magnification of 200x. To generate microscopy images, a Leica DMI 6000 B microscope equipped with a Hamamatsu Orca ER-AG camera was used at 200x total magnification.

The following experiments were designed by Nikola Lukenda and Janice Kim from Dr. Khan's lab at McMaster University, conducted by Janice Kim, and results interpreted by Nikola Lukenda.

Animals. Male (8-10 week old) C57BL/6 mice (Taconic) were kept in sterilized, filter-topped cages under specific pathogen-free conditions and fed autoclaved food. All experiments were approved by the animal ethics committee of McMaster University and conducted under the Canadian guidelines for animal research.

Isolation of DCs from spleens. Mice were sacrificed by cervical dislocation and spleens were excised and placed in Spleen Dissociation Medium (STEMCELL Technologies) and incubated for 30 min at room temperature. They were then strained through a 70- μ m nylon mesh filter (BD Falcon) and washed with PBS supplemented with 2% fetal bovine serum (FBS) and 1 mmol/L EDTA. Splenic DCs were isolated using a CD11c positive isolation kit (EasySep®, STEMCELL Technologies) according to the manufacturer's guidelines.

Ex vivo DC culture. DCs (10⁶ cells/mL) isolated using CD11c positive selection were grown in RPMI medium 1640 supplemented with 10% fetal bovine serum (FBS), 100 U/mL penicillin, 100 μ g/mL streptomycin, and 50 μ M 2-ME (Invitrogen Life Technologies). Cells were incubated with or without LPS (100 ng/mL, Sigma-Aldrich), combined with compounds to be tested (dissolved in PBS) at varying doses, and

incubated at 37°C for 24 and 48 hours. Supernatants were collected and analyzed for cytokine levels using the Bio-Plex Luminex system (Bio-Rad, Canada). Supernatant levels of interleukin (IL)-12, and IL-6 were measured using a Bio-Rad cytokine 2-plex panel kit. Fluorescence data was acquired and analyzed by Bio-Plex Manager software (version 5.0, Bio-Rad Laboratories).

3 CHAPTER 2:

Development of a LC-MS Selected Reaction Monitoring (SRM) Method for the Detection and Quantification of a *S. mutans* Pheromone

Submitted as: Evaluation of XIP as a novel death effector, and its effects on genetic transformation in *Streptococcus mutans*

Authors: Iwona B. Wenderska¹, Nikola Lukenda², Martha Cordova¹, Nathan Magarvey², Dilani B. Senadheera^{1*} and Dennis G. Cvitkovitch¹

Author Affiliations: ¹Department of Oral Microbiology, Faculty of Dentistry, University of Toronto, Toronto, ON. ²Department of Biochemistry and Biomedical Sciences and the Michael G. DeGroot Institute for Infectious Disease Research, McMaster University, Hamilton, ON.

3.1 Chapter Forward

*Having identified nonribosomal peptides from *S. mutans* as cross kingdom signalling and immunostimulatory metabolites, the potential of ribosomally produced peptides as human relevant metabolites was explored. The following chapter summarizes a collaborative effort between the Magarvey lab, to design and develop an LC-MS method to quantify levels of *S. mutans* peptide pheromones in culture supernatant, and the Cvitkovitch at the University of Toronto who used this method to examine pheromone signalling genes. The specific system studied, ComRS, has established implications in genetic transformation of *S. mutans*, an important factor for genetic heterogeneity and adaptation. Emphasis is placed on work done by Nikola Lukenda within the context of this thesis; however, readers are encouraged to obtain the published manuscript for full experimental details.*

3.2 Abstract

In *Streptococcus mutans*, ComX, an alternate sigma factor, drives the transcription of late-competence genes most of which are essential for genetic transformation. Two signaling pathways, ComDE and ComRS, modulate ComX activity in response to the competence stimulating peptide (CSP) and the SigX-inducing peptide (XIP), respectively. *comRS* genes, encoding the ComR regulatory protein and the ComS precursor to the XIP, function as the proximal regulatory system for ComX activation.

Using liquid chromatography-mass spectrometry, here we show that mature XIP was absent in the cell-free supernatants of *comR/S*-deficient mutants. XIP was also drastically reduced in ComX-deficient cultures, suggesting a ComX-mediated positive feedback mechanism for XIP synthesis. We have also reported the individual and combinatorial effects of CSP and XIP on transformation, cell killing and gene expression in two different growth media (i.e. THYE and CDM) previously reported. In accordance with other reports, loss of *comR/S* or *comX* completely abolished competence, which was not restored by the addition of XIP or CSP. Viability assays with 10 μ M XIP resulted in killing nearly 82% of cells relative to the no-peptide control, suggesting a novel role for XIP as a potent effector of cell death that can perhaps be exploited for targeted killing of *S. mutans*.

3.3 Introduction

Genetic heterogeneity allows for the robust adaptation of a bacterial community to changing environmental conditions, and can be acquired through the development of genetic competence (80). The acquisition of novel, heritable DNA by the process of genetic transformation, not only propagates antibiotic resistance and virulence determinants, but also shapes bacterial genomes contributing to rapid evolutionary changes (81-85). In a mixed biofilm environment such as dental plaque, the exchange of genetic material via transformation is thought to be a common occurrence between the residential consortia (86, 87). Through a collaboration with Dr. Cvitkovitch at the University of Toronto, signalling systems using two known secreted competence-inducing peptides were investigated for their ability to modulate transformation under different growth conditions, and act as effectors of cell death in *Streptococcus mutans*.

The current competence model of *S. mutans* encompasses multiple signal input systems that modulate transcription of *comX*, which encodes an alternate sigma transcription factor, ComX (SigX) (88-93). ComX is critical for the expression of late-competence genes whose products modulate DNA uptake and recombination (94-97). A role for ComX in cell death was also demonstrated (96-100). Recently, Mashburn-Warren *et al.* (2010) identified the ComR regulatory protein of the ComRS signalling pathway as the proximal regulator necessary for *comX* expression (91). ComR, in conjunction with its cognate signal peptide, XIP (SigX inducing peptide), modulates *comX* transcription in *S. mutans* (91). The XIP precursor encoded by *comS* is

consequently exported extracellularly, processed to its mature form, and then internalized via the Opp/Ami transporter to interact with ComR for *comX* regulation (91). The loss of ComR in *S. mutans* abolishes natural competence as determined by transformation levels below the limit of detection (<0.001 transformation frequency) (91). This striking effect of ComR on transformability has not been observed by deletion mutagenesis of the ComCDE quorum sensing system first demonstrated to modulate the competence phenotype via regulation of ComX in *S. mutans* (97, 101, 102). The *comC* gene encodes the precursor competence stimulating peptide (CSP), and the *comDE* genes encode the CSP detection unit comprising the sensor kinase (ComD) and its cognate response regulator (ComE) (101). At a threshold CSP concentration, ComD is autophosphorylated (103). Transphosphorylation of ComE, in turn, induces expression of several so called “early-genes” including, *comC*, *comAB* that encodes an ABC transporter and processing system for CSP maturation and export, as well as *comX* (97, 104). Until now, the induction of *comX* expression by ComE has not been attributed as a direct control, as no binding site for ComE has been observed in the *comX* promoter (105). It is known that the addition of CSP cannot restore *comX* expression in a *comR* mutant, while XIP does not require a functional *comE* gene to induce the expression of *comX* (91). These observations highlight the central role of ComRS in the competence pathway of *S. mutans*.

Stemming from the report by Mashburn-Warren *et al.*, the current study compared the effects of XIP and CSP on *S. mutans* genetic transformation, cell killing and gene expression under two different growth media known to facilitate competence. Herein, we

have identified a novel role for XIP as an effector of cell death in *S. mutans*, and further show that its activity in transformation and cell killing are inhibited when grown in nutrient rich, Todd-Hewitt yeast extract (THYE) medium optimal for CSP activity. Instead, XIP functions optimally in a chemically-defined medium (CDM) to elicit cell killing and transformation at levels comparable to that of CSP in THYE growth medium. Using liquid chromatography-mass spectrometry (LC-MS), we quantified mature XIP in the cell free-supernatant of UA159, and further report that XIP was absent in supernatants of ComR- and ComS-deficient mutants. Taken together, results from this study provide insight into the effects of XIP and CSP in the competence and cell killing pathways of this pathogen.

3.4 Results and Discussion

Measurement of XIP in the culture supernatants of *S. mutans* UA159, *comR* and *comS* knockout mutants.

In this study, Wenderska *et al.*, compared the individual and combinatorial effects of CSP and XIP on genetic transformation, cell killing and gene expression of *S. mutans* using strains grown in both THYE and CDM growth media. Transformation results showed that CSP and XIP elicit comparable levels of transformation frequencies in THYE and CDM respectively. In accordance with other reports, loss of *comR* or *comX* completely abolished competence, which was not restored by the addition of XIP or CSP (Figure 17A) (91). In $\Delta SMcomS$, abolishment of transformation could be attributed to the lack of ComS and its XIP derivative. Addition of XIP was able to complement transformation deficiency of $\Delta SMcomS$ but only when grown in CDM medium. It was also likely that loss of ComR would limit expression of *comS* by inhibiting ComR-modulated positive feedback regulation of the *comS* locus, and hence, limit XIP present in the supernatant. Therefore, we measured the mature XIP levels present in the supernatants of *S. mutans* UA159, *comR*, *comS* and *comX* mutant strains after 24h of growth using HPLC- MS/MS.

Synthetic XIP (sXIP) provided by the Cvitkovitch lab was analyzed by LC-MS/MS. This data provided an authentic standard for confirming XIP presence in culture supernatants, while also providing the MS/MS data required for development of a selected reaction monitoring (SRM) MS experiment (Figure 18). Fragmentation of sXIP

produced a characteristic peptide ladder, allowing for annotation of daughter ions corresponding to losses of the C-terminal amino acids leucine, serine, and tryptophan. The fragmentation pattern of sXIP was identical to the pattern observed for a putative native XIP from a *S. mutans* supernatant extract showing a similar retention time and m/z of 877 (Figure 18). In both spectra, the strongest MS/MS signal was observed at 658 m/z , corresponding to a XIP fragment missing a water, leucine, and serine moiety. This transition was used as the basis for a 15 min SRM LC-MS/MS experiment, and showed good sensitivity and selectivity in both sXIP and *S. mutans* extract chromatograms, allowing its application in quantifying XIP levels in *S. mutans* cultures (Figure 18 C.)

In UA159, XIP was detected at concentrations ranging from 95 ng/mL to 750 ng/mL. Consistent with the loss of transformability in $\Delta SMcomR$ and $\Delta SMcomS$, XIP was absent in their cell free supernatants (Figure 17B). Also interestingly, XIP was significantly decreased ($p < 0.05$) in $\Delta SMcomX$ supernatant. These results suggested mature XIP could be detected in cell supernatants even after 24h of incubation, which warrants examination of *S. mutans* XIP-induced transformability beyond the early-lag phase normally used. Further, these results suggested that the ComX regulon modulates the production, export or processing of the ComS peptide. Taken collectively, transformation and expression studies confirmed that signaling via ComRS and ComX is essential for the transformation phenotype of *S. mutans* and that this XIP-mediated signaling functions downstream of the ComCDE signaling cascade.

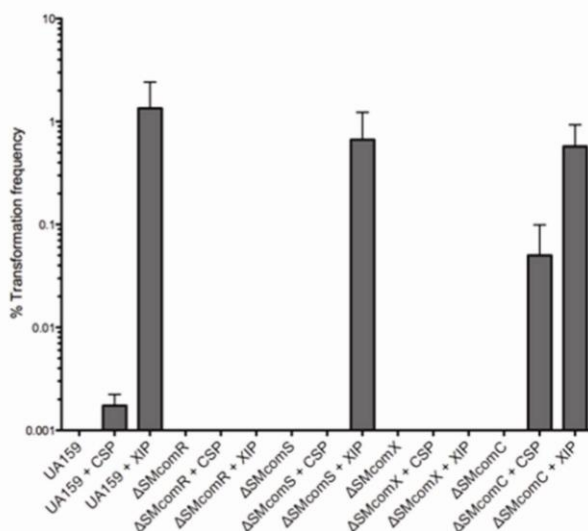
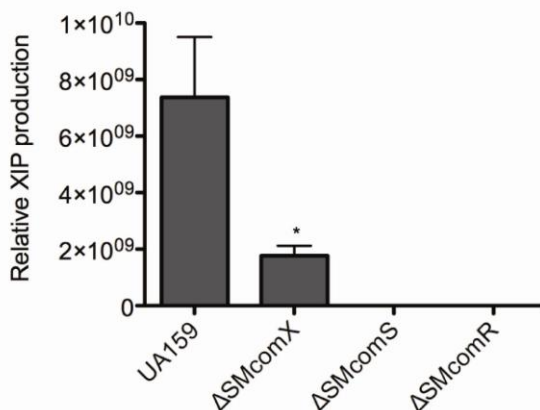
A.**B.**

Figure 17. Loss of Transformation Frequency Correlates with Decreased XIP Levels in Culture Supernatant as Measured by SRM LC-MS. A) *S. mutans* UA159 and mutant strains were subcultured to an OD600 of 0.1 in CDM. Plasmid DNA pDL277 carrying a spectinomycin resistance cassette was added alone or with 0.4 μ M sCSP or 10 μ M sXIP to the cultures. The cultures were grown for another 1.5h and differentially plated. % Transformation frequency = (specr CFUs)/(total CFUs). Results depicted here are an average of at least three independent experiments, error bars represent the standard error of the mean. B) The levels of XIP in the supernatant of each of the strains grown to stationary phase were quantified using HPLC-ESI-MS/MS. Data demonstrated here is a representation of at least 3 separate experiments, error bars indicate standard deviation. Statistical analyses were performed using a Student's T-test: *p<0.05.

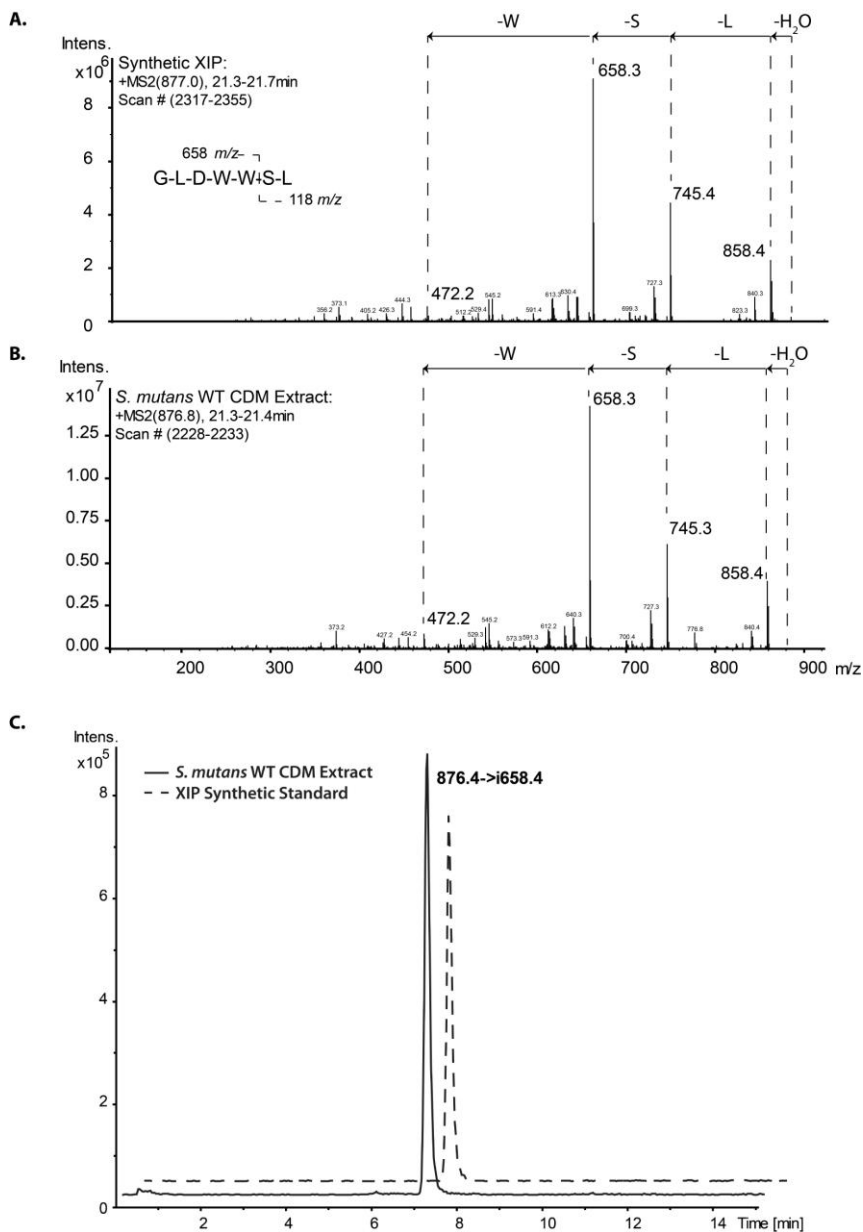


Figure 18. Development of a Selected Reaction Monitoring (SRM) LC-MS Experiment for *S. mutans* XIP. A) Synthetic XIP (sXIP) was analyzed by LC-MS/MS with auto MSn enabled to identify the best transition to monitor for SRM, and to act as an authentic standard for native XIP detection in *S. mutans* extracts (B). In both the sXIP and *S. mutans* extract samples, a 877 m/z molecular ion was observed with an identical retention time and MS/MS fragmentation pattern. Partial amino acid mapping was possible, confirming the ion as belonging to the *S. mutans* as XIP peptide pheromone. C) By monitoring the MS/MS fragmentation of the parent 877 m/z ion to the daughter 658 m/z ion, corresponding to a loss of serine, leucine and water fragments, a highly sensitive and selective SRM method was developed.

3.5 Materials and Methods

The following experiment was designed and performed by Nikola Lukenda with mutant strains and XIP and CSP standards provided by Iwona B. Wenderska from Dr. Cvitkovitch's lab at the University of Toronto. Please refer to the published manuscript for full materials and methods.

Bacterial strains and growth conditions. *S. mutans* UA159 (49) and its mutant strains in *comC* (Δ SM*comC*), *comD* (Δ SM*comD*), *comE* (Δ SM*comE*) (101) and *comX* (Δ SM*comX*) (106) were used in this study. The *comS* mutant (Δ SM*comS*) and the *comR* mutant (Δ SM*comR*) were constructed using a non-polar ligation PCR mutagenesis method described previously (107), and confirmed using nucleotide sequencing and real-time PCR. *S. mutans* strains were grown at 37°C with 5% CO₂ in either THYE, containing 0.3% yeast extract (Difco Laboratories) or CDM as described previously (91). Erythromycin and spectinomycin were used as needed at concentrations of 10 µg/mL and 1 mg/mL, respectively. Synthetic XIP (sXIP) and CSP (sCSP) peptides were synthesized using F-MOC chemistry (Advanced Protein Technology Centre, Hospital for Sick Kids, Toronto, Canada). Stock concentrations of 1µM of XIP and 0.4mM CSP were prepared in DMSO and water, respectively, for use in our studies. Growth kinetics were monitored using an automated growth reader (Bioscreen C; Labsystems, Finland) as previously described (71).

XIP detection and quantification. *S. mutans* UA159 and mutant strains were grown overnight in CDM medium, diluted 100-fold and grown for 48h at 37°C in 5% CO₂ air mixture. Next, cell free supernatants (CFSs) were obtained by centrifugation of cultures at 4500 rpm for 20 min and filter sterilization using a 0.45µm syringe filter. CFSs were then lyophilized and, once dry, reconstituted in 2 mL of 5% MeOH/H₂O (v/v) prior to analysis by HPLC-ESI-MS/MS (Dionex UltiMate 3000 HPLC system with variable UV detection in line to a Bruker amaZon X ion-trap mass spectrometer operating in positive ionization mode with auto MS/MS enabled). Analytical scale analysis was performed on a 250 x 4.60 mm Phenomenex Luna 5µ C18(2) 100Å column (Serial no. 516161-20) with a flow rate of 1 ml min⁻¹ and the following program consisting of solvents A (water + 0.1% formic acid) and B (acetonitrile + 0.1% formic acid): 0-2 min, equilibration at 5% B; 2-18 min, linear gradient to 100% B; 18-20 min, constant 100% B, 20-20.5 min, linear decrease to 5% B; 20.5-23 min re-equilibration at 5% B. The identity of XIP in culture supernatants was confirmed by comparison to the retention time and MS/MS fragmentation of synthetic XIP obtained from the Advanced Protein Technology Centre, Hospital for Sick Kids, Toronto, using identical HPLC-MS/MS methods. Relative quantification of XIP in CFSs was carried out by extracting TIC MS chromatograms for XIP molecular ions (876 m/z [M+H]⁺ and 438 m/z [M+2H]²⁺), while for quantifying XIP levels, a directed LC-MS/MS experiment was performed using selected-reaction monitoring (SRM) tandem mass spectrometry. The SRM *m/z* transition 876.4 → 658.4 was monitored, corresponding to a -SL loss from the GLDWWSL parent ion, generating a GLDWW daughter ion. Resulting peak areas were integrated and final concentrations

calculated from a linear calibration curve created using CDM spiked with XIP and processed in an identical way to CFSs. Peak areas from each sample were standardized to optical densities of 48-h culture samples prior to centrifugation for HPLC-MS/MS analysis. Results were obtained for four independent experiments and statistics were conducted using the Student's T-test.

4 Chapter 3:

Expanding the Catalogue of Immunomodulatory Effector Molecules from the Probiotic *Lactobacillus plantarum* WCFS1

4.1 Chapter Forward

*As a second candidate system for NRP discovery in the human microbiome the gut commensal *Lactobacillus plantarum* was chosen. As a clinically verified probiotic, *L. plantarum* exerts positive effects on the host's immune system with evidence implicating secreted metabolites as being responsible. An examination into the genome of *L. plantarum* revealed a series of NRPS genes hypothesized to produce an NRP with immunomodulatory capability. Previous experiments from this thesis, using *S. mutans* mutanobactins, have already revealed the immune modulating effect of NRPs and many more examples can be found in the literature. As such, a strategy similar to the one which successfully identified the mutanobactins was developed, while not ignoring the potential of other secreted factors as being responsible.*

4.2 Abstract

A significant number of experimental and clinical studies have validated the beneficial role probiotic bacteria play in host health. Despite successful use in both therapeutic and in preventative treatments, the exact chemical underpinnings to most probiotic's modes of action remain undefined. Current models focus on cell wall components, bioactive fatty acids, or microbial proteins, neglecting the remaining rich pool of bacterial small molecules that are known to exist. Here, we sought to combine natural product discovery, and metabolomic profiling, with immunological assays to discover immunomodulatory small molecules produced by *Lactobacillus plantarum* WCFS1. Therapeutically, *L. plantarum* has a strong clinical and experimental precedent in conferring beneficial health effects to the host, and in modulating NF- κ B signalling. From a natural products angle, *L. plantarum* is of interest as it is the only sequenced lactobacilli known to possess enzymatic machinery for secondary metabolism. Specifically, genes encoding for nonribosomal peptide synthetases (NRPSs) are present within its genome, capable of producing a nonribosomal peptide (NRP) - a molecular class with proven immunomodulatory activity. To guide discovery we performed a series of experiments corroborating metabolomic profiles of extracts from *L. plantarum* grown to different growth phases, and from mutant strains devoid of secondary metabolism, to immunological assays monitoring cytokine profiles upon extract treatment. From these experiments, we identified the potential of crude *L. plantarum* extracts to modulate cytokine levels from dendritic cells (DCs) in a NF- κ B dependant manner. Furthermore,

we assigned that activity to a novel molecular class, the pyroglutamic acid dipeptides (pyroGlu-X), which are produced in higher abundance by stationary phase cells, have a strong literature precedent for immunomodulation, and have never before been isolated from a biological source. In contrasting NRPS mutant strains, we noted a decreased immune response from DCs treated with extracts from mutant strains. We have not yet however, despite significant efforts, identified the NRP product. Together, these results extend the immunomodulatory activity attributed to *L. plantarum* WCFS1 to include the pyroGlu-X peptides, and allude to the existence of other immunologically relevant metabolites produced by NRPS machinery.

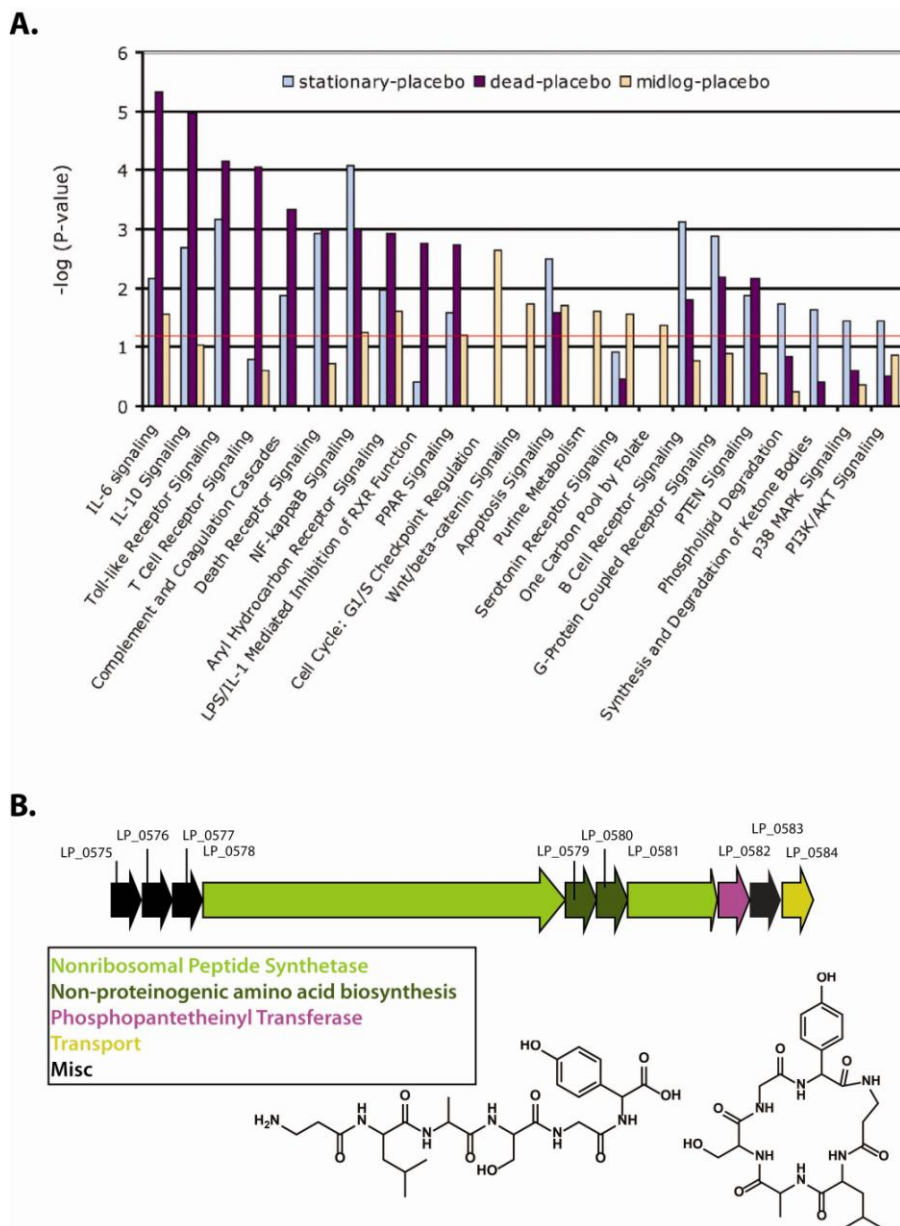
4.3 Introduction

Lactobacilli, through their natural occurrence in the human microbiome, key role in food fermentations, and therapeutic application as probiotics, have developed a deep, multifaceted relationship with humans. Central to this relationship is the beneficial effect conferred to host health in the treatment and prevention of numerous disorders including enteric infections, postantibiotic syndromes, inflammatory bowel disease, irritable bowel syndrome, and other immunological conditions (108-111). This therapeutic potential has led to rigorous scientific interest in identifying the exact molecular mechanisms by which lactobacilli achieve health improving effects. Currently, three modes of action have been proposed, with health improving organisms functioning to competitively exclude pathogenic bacteria, to modulate signalling pathways within the host, correcting errant signalling, or eliciting beneficial pathways, or to modulate the host's immune system (112, 113).

Achieving these activities implies the existence of effector molecules secreted by the lactobacilli, some of which have already been identified. In excluding competing organisms for instance, lactobacilli secrete ribosomally produced antimicrobial peptides, one of which, plantaracin, is induced specifically during gastrointestinal transit of *Lactobacillus plantarum* (114, 115). For immunomodulation, cell wall components are most often implicated, with direct evidence of purified lipoteichoic acid from the lactobacilli, *L. plantarum str. WCFS1*, modulating host immune response (116). Other studies showed lactobacilli derived peptidoglycans alleviated colitis severity, and capsular

polysaccharides from a *Lactobacillus casei* strain suppressed pro-inflammatory responses (117, 118). It is thus apparent that relationships can be established between some specific effector molecules from lactobacilli and observed changes in the host. However, the full web of chemical signalling is far from elucidated.

Significant differences in immunomodulation exist between lactobacilli species, and even between strains of the same species, as observed for *L. plantarum* (119). Evidence of a much more complex chemical signalling system is further reinforced by *L. plantarum* WCFS1, which exhibits differential NF- κ B signalling modulation dependent on its growth stage. In a study by van Baarlen *et al.*, patients ingested *L. plantarum* as live cells at mid-log growth, live cells at stationary growth, and heat killed stationary cells (120). Biopsies were performed, and the transcriptional profile of patient's duodenal cells were measured, revealing only stationary phase cells altered NF- κ B signalling pathways (Figure 19A) (120). Most interestingly, induction of both pro- and anti-inflammatory signalling pathways were observed, reflective of a tolerance-like response. Histological inspection confirmed no inflammation in patients, despite increased signalling in inflammatory pathways. Such a result supports the concept that *L. plantarum* enhances immune system alertness while modulating excessive pro- or anti-inflammatory signals, establishing and maintaining immune homeostasis. In disorders where disproportionate immune responses are etiological factors, such as inflammatory bowel disease (IBD), and inflammatory bowel syndrome (IBS), homeostatic preservation is an intriguing therapeutic target. Since heat killed stationary cells did not elicit the same result, cell wall



components were unlikely responsible, suggesting some yet to be discovered effector molecule.

Evidence of novel effectors has since grown, with studies confirming the ability of the supernatant from *L. plantarum* cultures to suppress proinflammatory cytokines through a NF- κ B pathway (121). In 2009, Petrof *et al.*, expanded the scope of *L. plantarum* supernatant activity, showing its unique capacity to inhibit multiple NF- κ B pathways as well as proteasome function, where other lactobacilli could not (122). *L. plantarum*'s uniqueness is further emphasized by its status as the only LAB to possess nonribosomal peptide synthetase (NRPS) genes within its genome, making it capable of producing a nonribosomal peptide (NRP), a class of metabolite with a strong immunomodulatory precedent (Figure 19B). That the NRP derived syringolin and salinosporamide are potent proteasome inhibitors, and another NRP, cyclosporine, is a clinically used immunosuppressant, fosters a specific interest into the metabolic effectors produced by *L. plantarum* (123-125).

Here, we sought to expand the catalogue of immunological effector molecules produced by *L. plantarum* WCFS1 by focusing on metabolite differences between NRPS wild type and mutant strains, as well as between mid-log and stationary growth phase cells. From fermentations, secreted metabolites were extracted and analyzed using metabolomic techniques, identifying compounds unique to a particular sample set. The same metabolite extracts were then used in *ex vivo* assays monitoring cytokine levels in primary dendritic cells. Using IL-12 as a primary marker for inflammation, due to its robustness and precedent in measuring immunomodulation across *L. plantarum* strains,

an increase in its levels were correlated to a series of compounds unique to stationary phase cells (119). These compounds were isolated and identified as a novel class of bacterial metabolite consisting of an N- terminal pyroglutamic acid moiety with variable amino acids at the C terminus. At least 12 dipeptide combinations have been identified with three confirmed to induce IL-12 in an NF- κ B dependant pathway. While no promising candidate compounds were identified in comparing NRPS wild type/knockout samples, a differential effect on IL-12 induction was noted, suggesting other novel, potentially NRP derived, effectors may yet still exist alongside the newly discovered pyroglutamic acid dipeptides.

4.4 Results and Discussion

***L. plantarum* Extracts Elicit a Growth Phase Dependent Cytokine Response.**

The process of identifying immunomodulatory metabolites from *L. plantarum* began by ensuring crude metabolite extracts were capable of eliciting a differential immune response. Cultures of wild type and mutant strains (IM1 and IM2), with inactivated NRPS genes (provided by Dr. Fischbach), were grown to either stationary or mid-log growth phase and crude metabolite extracts generated using a catch all method, ethyl acetate liquid-liquid partitioning. Immune response was compared by incubating mouse dendritic cells (DCs) with the metabolite extracts for 48 hours then measuring cytokine levels (Figure 20). Specifically, levels of the pro-inflammatory cytokine IL-12, and the both pro- and anti-inflammatory IL-6 were measured. Not surprisingly, all extracts tested induced IL-6 and IL-12 production compared to the media control, with the largest differentials being observed in IL-12 levels. DCs treated with extracts from stationary phase cultures exhibited the highest immune response, with IL-12 levels which far surpassed those of the positive control, LPS. Inactivation of NRPS genes also had a significantly detrimental effect on cytokine induction, however immune response was not completely abolished. It is apparent from these results that multiple captured small molecule factors, and not just growth phase dependent or nonribosomally produced metabolites are capable of inducing an immune response in DCs. Cytokine induction was suggested to occur through the NF- κ B signalling pathway as adding the NF- κ B pathway inhibitor PDTC significantly decreased extract activity.

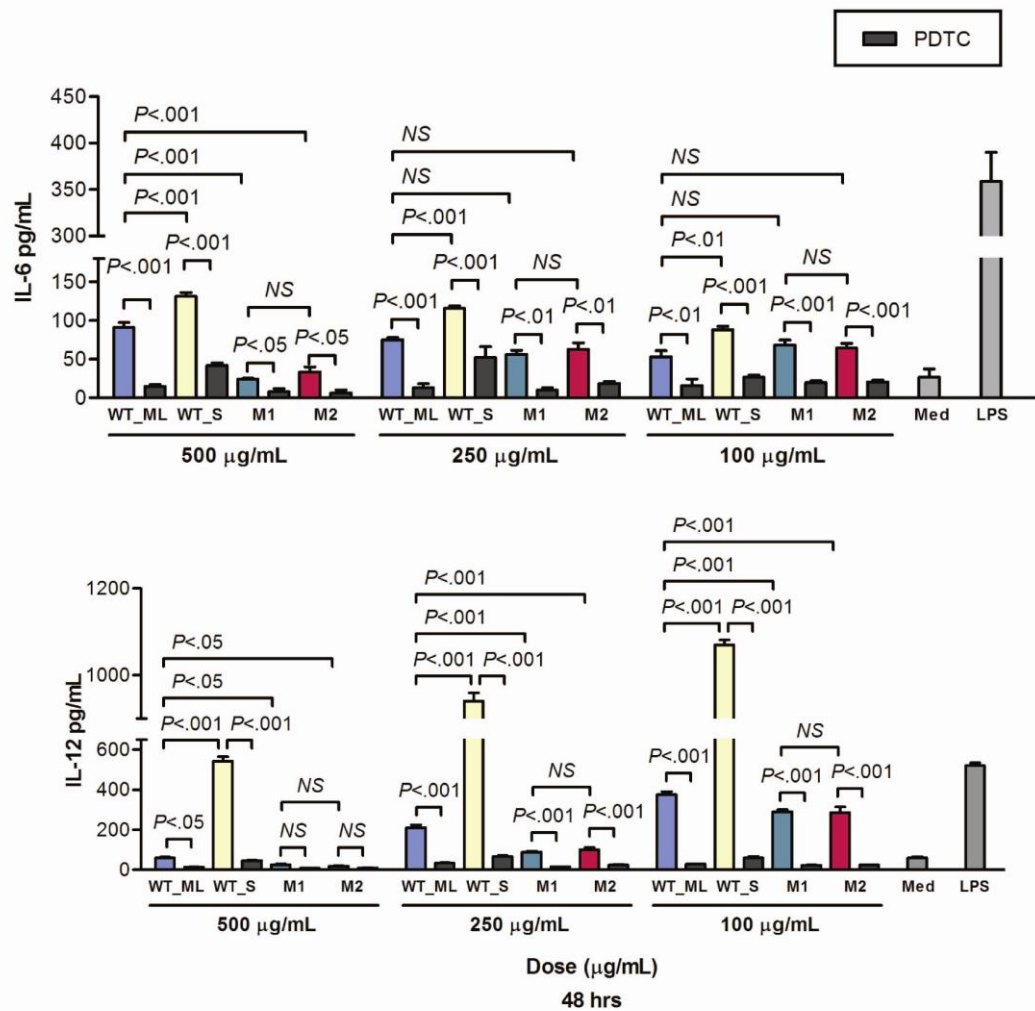


Figure 20. Differential Induction of Immune Response in DCs by *L. plantarum* Metabolite Extracts.

Dendritic cells isolated from mice spleens were co-incubated for 48 hours with *L. plantarum* metabolite extracts from wildtype cells grown to mid-log phase (WT_ML), stationary phase (WT_S), or from NRPS mutant strains grown to stationary phase (M1 and M2). *L. plantarum* extracts were dissolved in PBS and added to the culture at varying doses in the presence or absence of nuclear factor kappa B (NF-κB) inhibitor, pyrrolidine dithiocarbamate (10 µmol/L, PDTC, Sigma). Following incubation, supernatant interleukin (IL)-12 and IL-6 levels were measured using the Bio-Plex Luminex system (Bio-Rad, Canada) and a Bio-Rad cytokine 2-plex panel kit. Fluorescence data was acquired and analyzed by Bio-Plex Manager software (version 5.0, Bio-Rad Laboratories). Lipopolysacchride (LPS) when used, was added at a concentration of 100 ng/mL (Sigma-Aldrich), and a MRS media extract was added at 500 µg/mL.

Multivariate Analysis of *L. plantarum* Extracts Identifies Stationary Growth Phase Unique Metabolites.

Having confirmed the ability to extract immunomodulatory small molecules from *L. plantarum* fermentations, the molecular features within the extracts needed to be catalogued to identify compounds whose abundance correlates with immune responses. The same crude extracts used for the DC experiments were reconstituted in methanol and run on an LC-MS system with the resulting data sets interrogated using principal component analysis (PCA). A non-supervised statistical method, PCA is able to find and rank variances in LC-MS data sets, providing a visual representation of metabolic differences between sample sets. Concurrently, a supervised statistical method, the student's t-test was performed which lists the statistical significance of variances observed by PCA. A key step in multivariate analysis, is the defining of molecular features within a data set by their specific retention time and m/z . This process establishes a catalogue of every compound within a sample set which can then be used in pairwise comparisons to other samples. Using this method the metabolic differences between the tested *L. plantarum* extracts were catalogued, identifying compounds present in some samples and absent in others and those whose abundance varied between samples.

The first pairwise comparison was performed between NRPS wild type and mutant samples with the hope of identifying a divergent molecular feature with a m/z fitting the predicted NRP product (Figure 21). Quadruplicate extracts from *L. plantarum* NRPS mutant strains 1 (IM1) and 2 (IM2) formed a total pool of 8 LC-MS sample sets which were compared to the quadruplicate wild type sample sets of

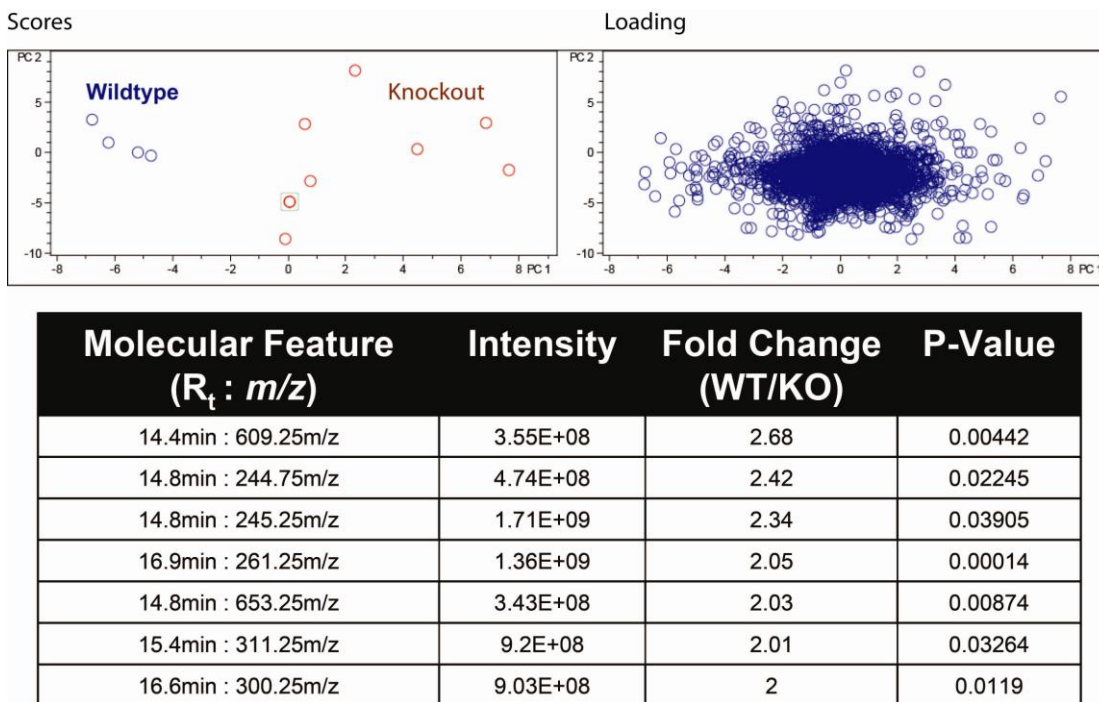


Figure 21. Multivariate Analysis of LC-MS Data from Wildtype and NRPS Mutant *L. plantarum* Metabolite Extracts. Untargeted metabolomic comparison of wildtype and NRPS inactivated *L. plantarum* strains using PCA. The Scores plot shows the grouping and differentiation of LC-MS data generated from wildtype (blue circles) and mutant (red circles) crude metabolic extracts (biological replicates, N=4 for wildtype, M1 and M2 extracts). The loading plot shows critical ions in the LC-MS data as determined by PCA represented by blue circles. Ions clustered closely together are common to both strains while those with negative PC 1 values are unique to the wildtype strain. In analyzing the LC-MS data 100.5-2000.5 m/z and 1.0-35.0 retention time ranges were defined. Results from the student's *t*-test comparison of wildtype and NRPS mutant sample sets are listed in a tabular format. Molecular features more abundant in wildtype samples are listed with their respective retention times, m/z 's, ion intensities, and change in abundance as measured by a fold change in MS signal intensity.

L. plantarum grown to stationary phase. Using PCA analysis and the student's *t*-test, no molecular features were identified as uniquely belonging to one particular group. From the scores plot in the PCA distribution, a significant amount of divergence is seen between the mutant sample sets, indicative of metabolic variability between them. The inability to cluster the sample sets tightly together is understood within the context of the

loading plot, where no key differentiating molecules are highlighted, suggesting either a high degree of statistical noise in analyzing the sample sets, or simply that no significant differences could be identified between the samples. The output from the student's *t*-test reinforces this result as the only differentiating molecular features differ by merely 2 fold in MS signal intensity. Of those compounds identified, each peak was manually confirmed to be present in both wild type and NRPS mutant samples, disrupting their identification as the desired NRP product.

Multivariate analysis comparing mid-log extracts to the highly immune stimulating stationary growth phase extracts yielded more promising results (Figure 22). From the scores plot in the PCA output, we see the stationary and mid-log samples group more tightly together than in the NRPS mutant strains. This close grouping signifies that LC-MS data for replicate samples closely resemble one another, yet differ significantly from the other, sample sets. Examination of the loading plot reveals this differentiation is the result of a few key identifiable metabolites with *m/z*'s in the 200-400 MW range, and similar retention times. Analyzing the data using the student's *t*-test quantifies the difference of these molecules, showing significantly higher levels, ranging from 6 to 14 fold more in stationary than mid-log extracts. Two of the detected molecular features, with *m/z* of 485.3 $[2M+H]^+$ and 276.8 $[M+H]^+$, were 11 and 7 times more abundant in the stationary samples respectively, and had their ions extracted manually from the LC-MS data for confirmation, targeting them for further analysis (Figure 23).

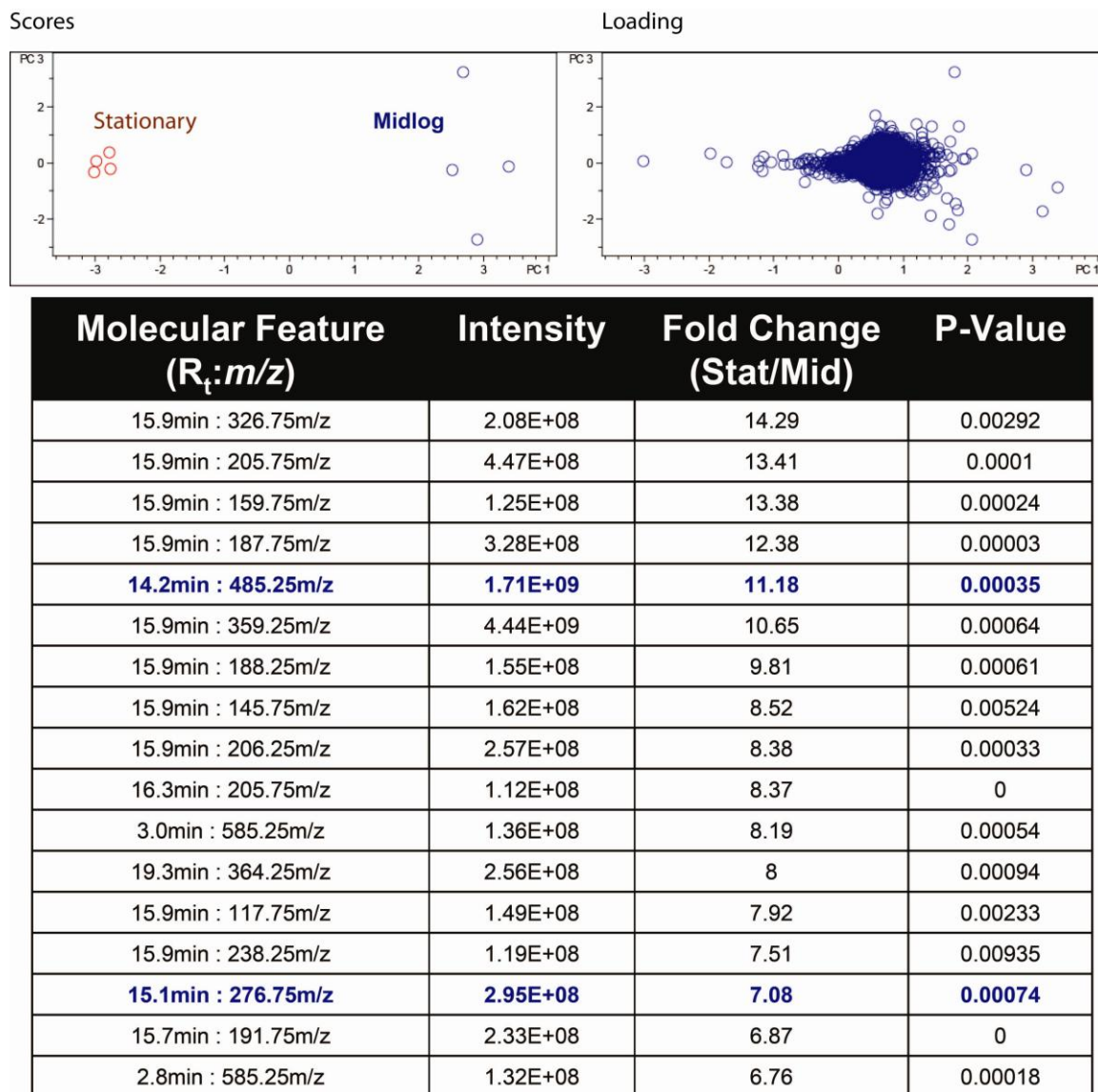


Figure 22. Multivariate Analysis of LC-MS Data from Stationary and Mid-Log *L. plantarum* Metabolite Extracts. **A)** Untargeted metabolomic comparison of metabolite extracts from *L. plantarum* grown to its stationary or mid-log growth phase (biological replicates, N=4). **B)** Results from the student's t-test comparison of stationary and mid-log extract sample sets. Molecular features more abundant in stationary samples are listed with their respective retention times, m/z 's, ion intensities, and change in abundance as measured by a fold change in MS signal intensity. Multivariate analysis was performed using the same parameters as previously described.

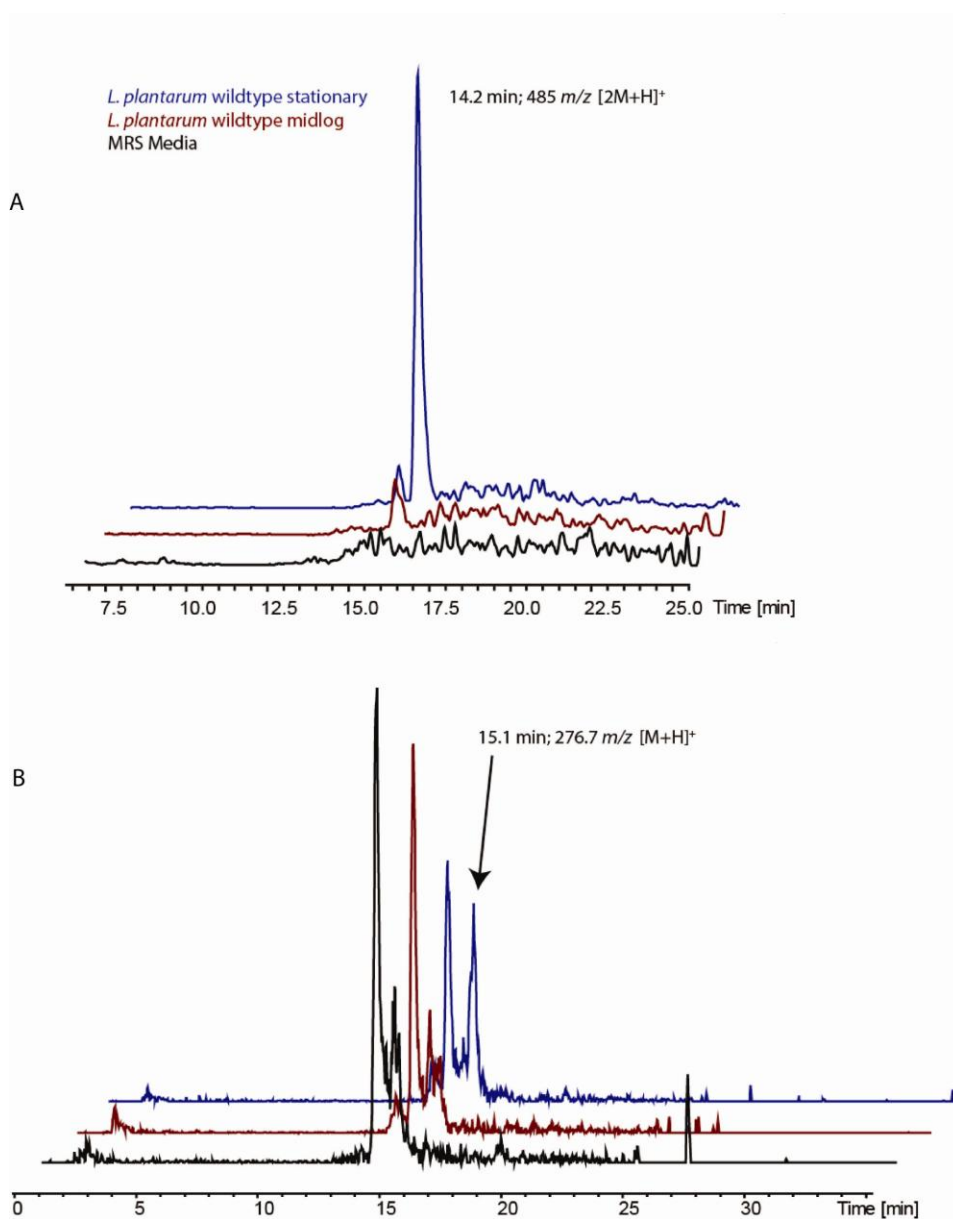


Figure 23. Extracted Ion Chromatograms for Stationary Growth Phase Unique Metabolites Identified by Multivariate Analysis. LC-MS data sets were manually extracted for ions of interest to confirm multivariate analysis results. Base peak chromatograms for molecular features with ions at 485 (A) and 277 m/z (B) are shown for wildtype stationary, mid-log, and MRS media sample sets.

Isolation and Characterization of *L. plantarum* Pyroglutamic acid Dipeptides.

Having identified a number of metabolites produced more abundantly by bacteria grown to stationary phase, where the extract elicited the strongest immune response, large scale fermentation and metabolite isolation experiments were devised to isolate these targeted compounds. A large scale fermentation (10 L) of *L. plantarum* was grown to stationary phase, extracted with ethyl acetate, and the resulting crude extract processed using silica flash-chromatography. Using LC-MS, flash fractions were monitored for the 485 m/z and 277 m/z compounds which were found in the 25% MeOH/DCM fraction. Using preparative scale HPLC, two peaks corresponding to these compounds were purified, allowing for structural studies.

A combination of MS/MS and NMR experiments led to the compounds identification as pyroglutamic acid containing dipeptides (pyroGlu-X), with the 485.3 m/z $[2M+H]^+$ being pyroGlu-Leu (MW 243) and the 276.8 m/z $[M+H]^+$ compound identified as pyroGlu-Phe (MW 276) (Figures 24 and 25). For the 276.8 m/z compound, MS/MS fragmentation first revealed the peptidic nature of the compound. Daughter ions corresponding to losses of water (259 m/z) and a carboxyl group (231 m/z) were observed, suggesting their initial loss, followed by the cleavage of the amide bond resulting in immonium ions for phenylalanine (120 m/z) and pyroglutamic acid (112 m/z). Additionally, a second fragmentation scheme was observed by daughter ions at 166 m/z and 112 m/z , which matched the loss of a pyroglutamic acid and phenylalanine moiety respectively, due to a breaking of the amide bond. 1D and 2D NMR experiments confirmed the 277 m/z compound as pyroGlu-Phe, with pyroGlu at the N-terminus.

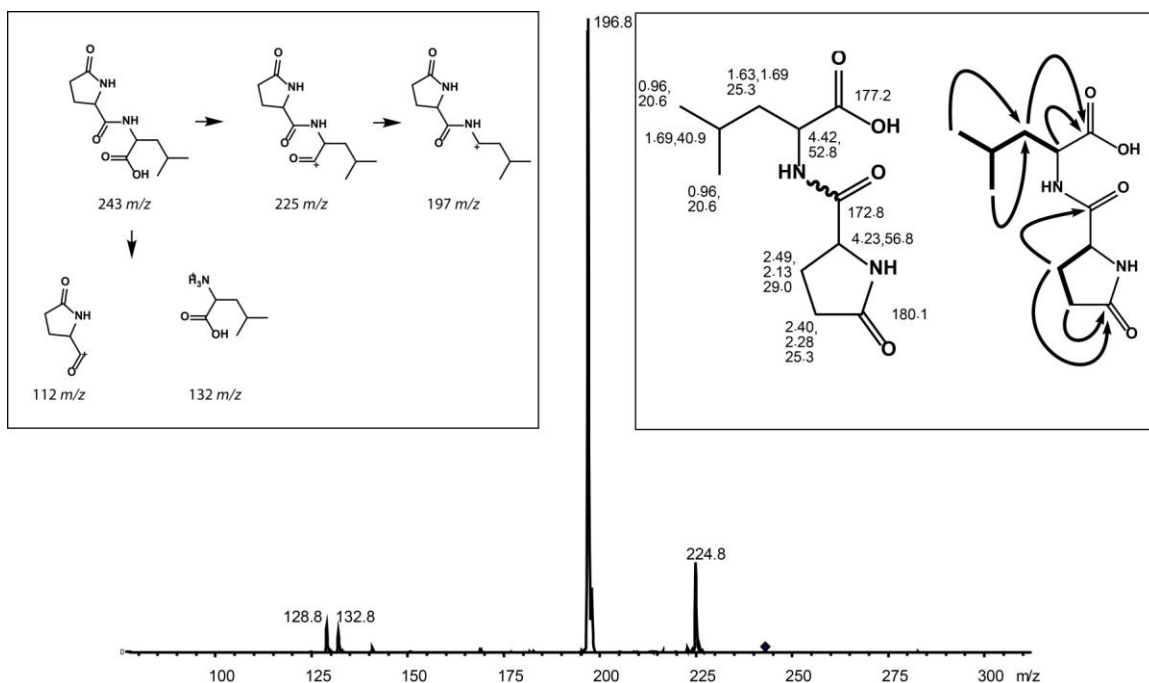


Figure 24. Structural Elucidation of PyroGlu-Leu by MS/MS Fragmentation Mapping and NMR Correlations. To generate MS/MS data, the mixture of pyroGlu-X dipeptides obtained from silica flash chromatography was analyzed by LC-MS/MS on a Dionex UltiMate 3000 HPLC system in line to a Bruker amaZon X ion-trap mass spectrometer operating in positive ionization mode with a scan window of 100-2000 m/z . NMR experiments were performed on a Bruker 700 MHz spectrometer with the sample dissolved in 100% CD_3OD . Amino acid composition and order were confirmed using 1H - 1H COSY (bold lines) and long range 1H - ^{13}C HMBC interactions (curly arrows). Highly similar spectral results were obtained for the stereoisomeric compound.

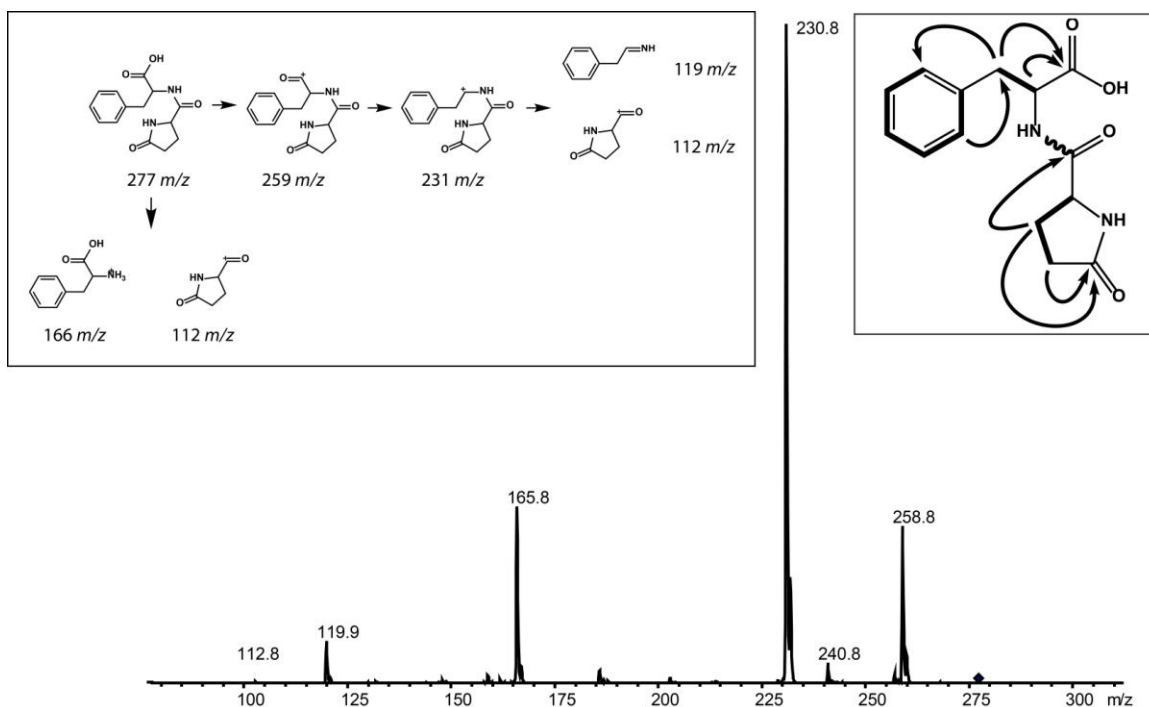


Figure 25. Structural Elucidation of PyroGlu-Phe by MS/MS Fragmentation Mapping and NMR Correlations. Structural data for pyroGlu-Phe was obtained using the same protocols and parameters as for pyroGlu-Leu.

Identical experiments were carried out to identify the $485.3\ m/z$ $[2M+H]^+$ compound. MS/MS fragmentation of the $[M+H]^+$ molecular ion at $243\ m/z$ produced two fragmentation schemes just as for pyroGlu-Phe. In the first, direct fragmentation of the amide bond resulted in two daughter ions at $132\ m/z$ and $112\ m/z$, corresponding to losses of pyroglutamic acid and leucine respectively. In another fragmentation scheme, losses of water ($225\ m/z$) and a carboxyl group ($197\ m/z$) were again observed, with no subsequent fragmentation. NMR experiments confirmed the substitution of a leucine monomer for phenylalanine at the C terminus suggesting the position of pyroGlu at the N terminus of the dipeptide to be a requisite feature for this class of *L. plantarum* metabolite. Returning to the 25% MeOH/DCM flash fraction, at least 12 analogous compounds were identified

by MS/MS patterns and are currently being isolated (Figure 26). Of these, a third compound was isolated with identical MS/MS and NMR spectral data as pyroGlu-Leu identifying it as a stereoisomer (data not shown). The compounds are believed to be diastereoisomers, and not enantiomers, as the two compounds possess different retention times (Figure 26). These analogous compounds all appear to retain pyroglutamic acid with a significant amount of redundancy in the other amino acid monomer including Cys, Ala, Val, Met, Tyr, Arg, Trp, and others to be determined.

Despite its absence in any known bacterial metabolites, pyroGlu itself was previously observed in lactic acid bacteria (LAB) and noted for its anti-microbial effects (126, 127). Biosynthetically, two main methods exist for pyroGlu production. The first requires pyroGlu cyclase activity which cyclize free glutamic acid, and the second uses aminopeptidase activity, which specifically liberates pyroGlu moieties. Both activities have been observed *in vitro* in LAB, including *L. plantarum* (126, 127). These results do not explain how the dipeptides are produced however and the role of nonribosomal peptide synthetase machinery cannot be overlooked, especially in understanding how the amide bond is formed between pyroGlu and the various amino acid monomers.

To the best of our knowledge the discovery of these compounds from a natural source is the first of its kind, with no precedent for naturally occurring pyroGlu-X dipeptides. Interestingly, the compounds are currently the subject of a patent awarded in 2011 (Anti-inflammatory peptide, US 2011/0183925 A1), where they were discovered by high throughput screening efforts for inhibitors of TNF- α converting enzyme (TACE) and

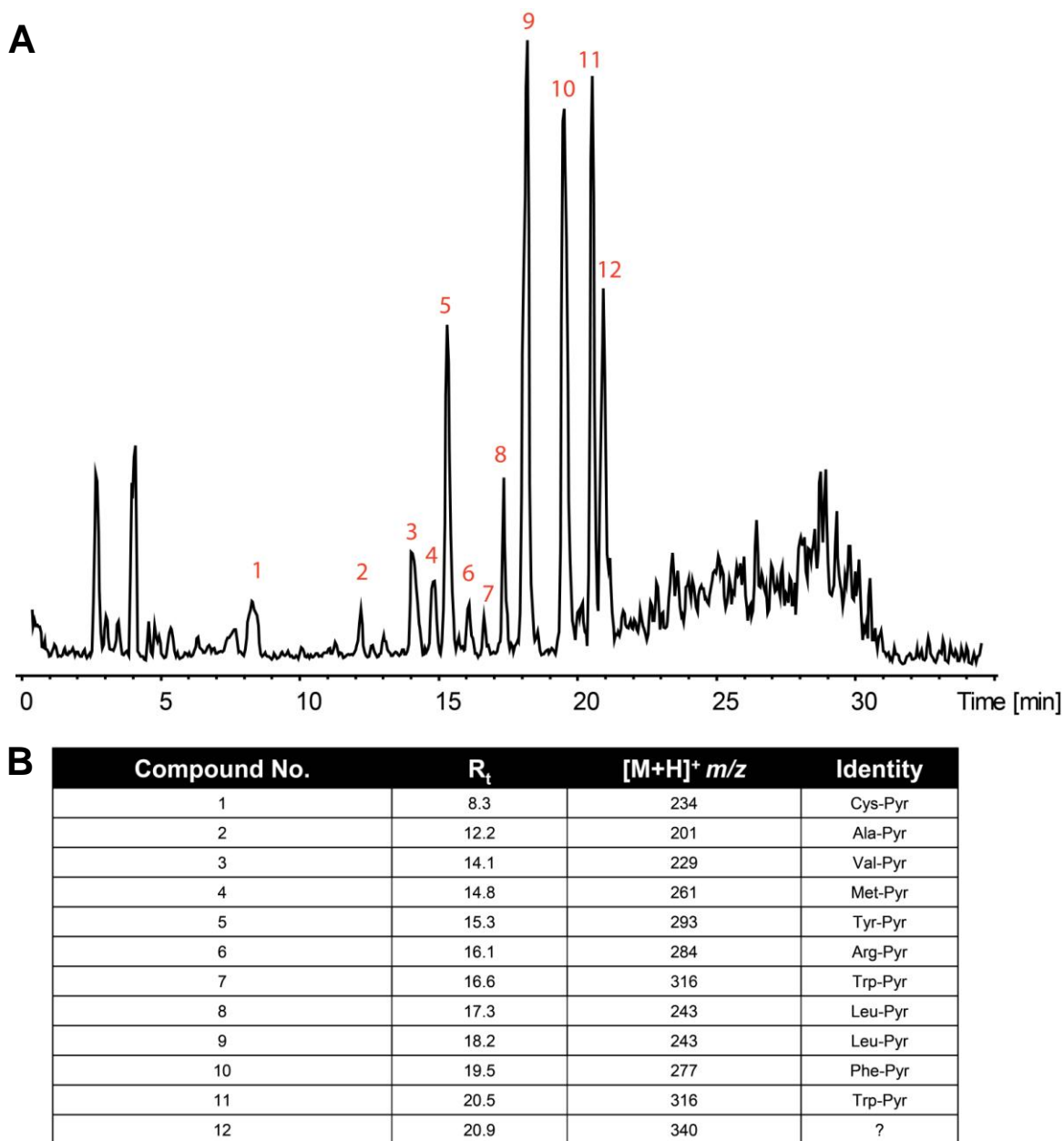


Figure 26. *L. plantarum* Produces Multiple Analogues of PyroGlu-X Dipeptides.
A-B) By analyzing the LC-MS/MS data from the 25% MeOH/DCM silica flash fraction, metabolites were identified with MS/MS fragmentation patterns resembling those of pyroGlu-Leu and pyroGlu-Phe facilitating their identification as pyroGlu-X dipeptides, and even for the prediction of their amino acid composition as listed.

caspase-1, two enzymes responsible for the production of pro-inflammatory cytokines. pyroGlu-Phe and pyroGlu-Leu both scored well on the screen, and in *in vitro* assays inhibited TACE activity by 15% and 40% respectively at 200 μ M. A kit measuring TACE activity has since been purchased to test the pyroGlu-X dipeptides identified from *L. plantarum* independently, and as a mixture assessing synergistic potential. In an unrelated study, a correlation was made between pyroGlu levels, LAB abundance and the severity of inflammatory bowel disease in sufferers, further supporting immunomodulatory activities (128). While a strong literature precedent for biological activity is important, the biological activity of the pyroGlu-X dipeptides isolated from *L. plantarum* remained to be confirmed.

Using the same *ex vivo* assay as for the original extracts, DCs were incubated with pyroGlu-Leu (C1: 242 MW A), the stereoisomer of pyroGlu-Leu (C2: 242 MW B) and pyroGlu-Phe (C3: 276 MW) and immune response was measured by means of IL-6 and IL-12 production. Following incubation for 24 hours a modest induction in IL-6 was observed, which increased slightly over 48 hours, similar to the original effects from the crude extracts. (Figure 27). Interestingly, IL-6 levels increased with decreasing dosages, with 2.5 μ M inducing the highest IL-6 levels after 24 hours. By 48 hours however, the immune response of DCs treated with different dipeptides were similar, showing the compounds to be slightly more efficacious than the media control, and significantly lacking to LPS. NF- κ B signalling was again implicated as addition of the NF- κ B pathway inhibitor PDTC, decreased immune response. The 25% MeOH/DCM flash fraction which possessed all of the pyroGlu-X dipeptides was also tested and while not producing a

drastic change in IL-6 levels, a similar trend was observed for it too increased immune response with decreased test material.

As with the crude extracts, measuring IL-12 produced much more robust results (Figure 28). Following 24 hours of incubation all of the dipeptides, at concentrations as low as 2.5 μ M, induced as potent an immune response in DCs as LPS, and by 48 hours, far exceeded the response by LPS. In fact, using 250, 25, or 2.5 μ M resulted in the same high immune response suggesting assay saturation. With IL-12, the NF- κ B pathway was again implicated, as adding PDTC almost abolished immune response. The recapitulation of IL-12 induction by the pyroGlu-X dipeptides confirms their identity as the immunostimulatory metabolites unique to stationary phase *L. plantarum* fermentations as suggested by multivariate analysis of LC-MS data sets. However, the physiological implications of the immune response by *L. plantarum* cannot be determined by *ex vivo* DC assays alone and requires testing in additional cell lines and ultimately *in vivo*.

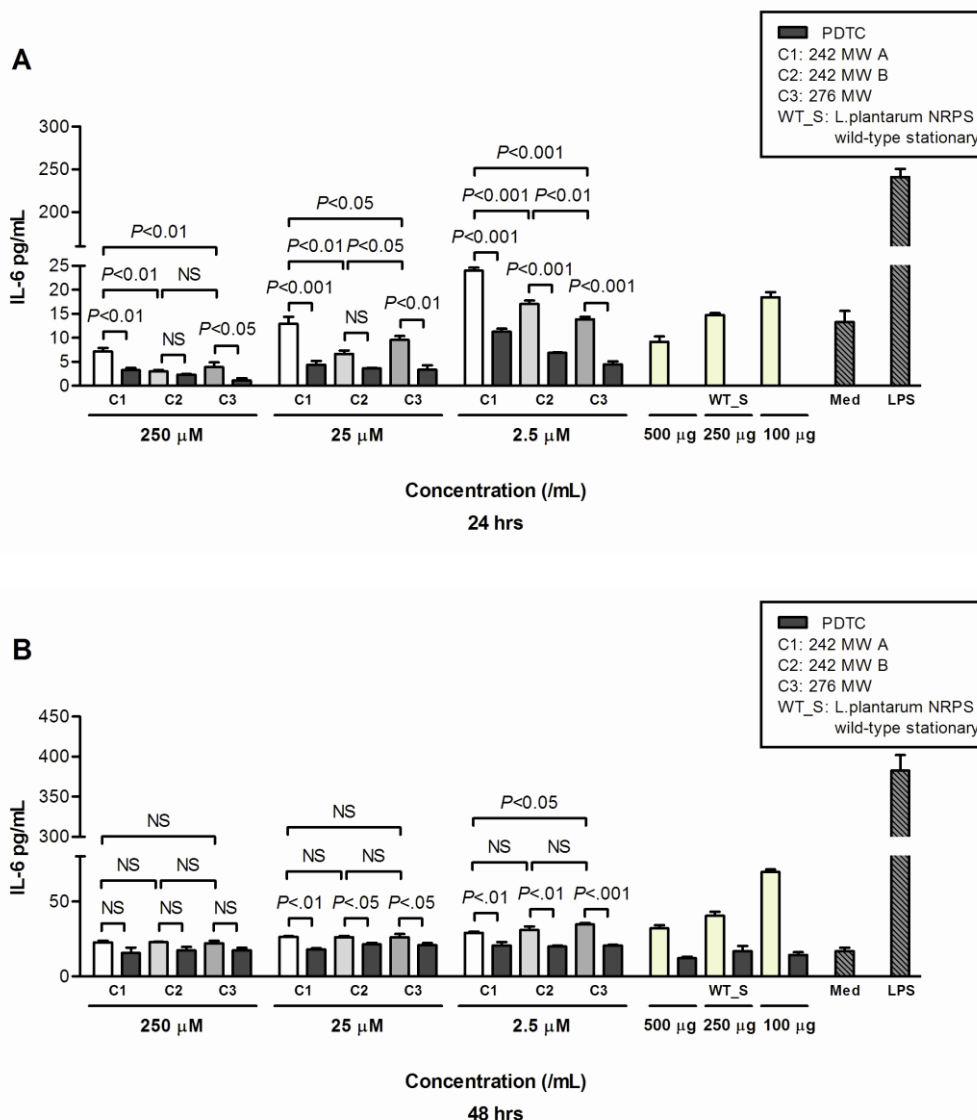


Figure 27. *L. plantarum* PyroGlu-X Dipeptides Modestly Induce IL-6 Expression in Mouse Dendritic Cells. Dendritic cells isolated from mice spleens were incubated with or without LPS (100 ng/mL, Sigma-Aldrich) and combined with pyroGlu-Leu A (C1: 242 MW A), its stereoisomer pyroGlu-Leu B (C2: 242 MW B) or pyroGlu-Phe (C3:276 MW). Additional cells were incubated with the 25% MeOH/DCM silica flash fraction containing the mixture of pyroGlu-X dipeptides (WT_S). Compounds were dissolved in PBS and added to the culture at varying doses in the presence or absence of nuclear factor kappa B (NF- κ B) inhibitor, pyrrolidine dithiocarbamate (10 μ mol/L, PDTC, Sigma) and incubated at 37°C for 24 and 48 hours. Supernatants were collected and analyzed for cytokine levels using the Bio-Plex Luminex system (Bio-Rad, Canada). Supernatant levels of IL-6 were measured using a Bio-Rad cytokine 2-plex panel kit. Fluorescence data was acquired and analyzed by Bio-Plex Manager software (version 5.0, Bio-Rad Laboratories).

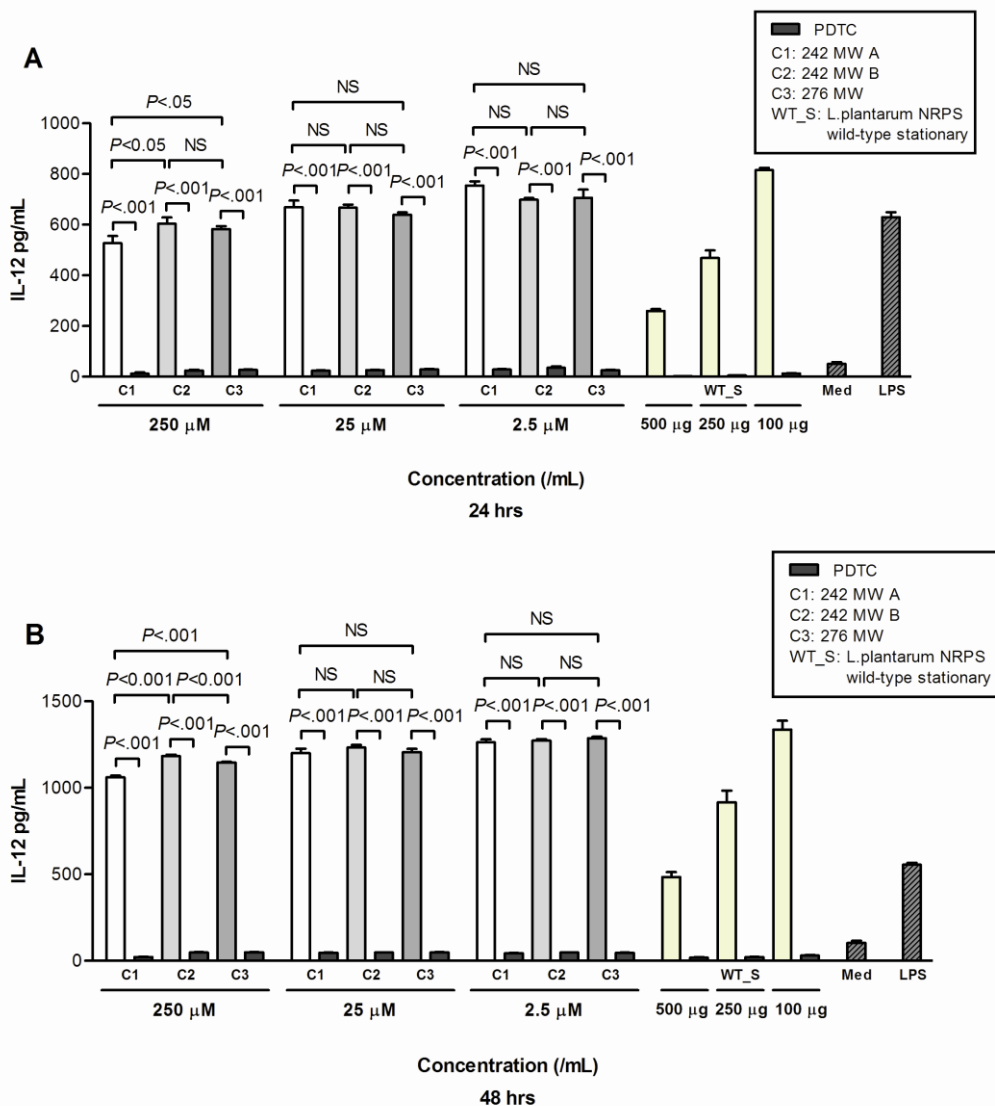


Figure 28. *L. plantarum* PyroGlu-X Dipeptides Strongly Induce IL-12 Expression in Mouse Dendritic Cells. Dendritic cells isolated from mice spleens were incubated with or without LPS (100 ng/mL, Sigma-Aldrich) and combined with pyroGlu-Leu A (C1: 242 MW A), its stereoisomer pyroGlu-Leu B (C2: 242 MW B) or pyroGlu-Phe (C3: 276 MW). Additional cells were incubated with the 25% MeOH/DCM silica flash fraction containing the mixture of pyroGlu-X dipeptides (WT_S). Compounds were dissolved in PBS and added to the culture at varying doses in the presence or absence of nuclear factor kappa B (NF- κ B) inhibitor, pyrrolidine dithiocarbamate (10 μ mol/L, PDTC, Sigma) and incubated at 37°C for 24 and 48 hours. Supernatants were collected and analyzed for cytokine levels using the Bio-Plex Luminex system (Bio-Rad, Canada). Supernatant levels of IL-12 were measured using a Bio-Rad cytokine 2-plex panel kit. Fluorescence data was acquired and analyzed by Bio-Plex Manager software (version 5.0, Bio-Rad Laboratories).

Supplementing Mice with PyroGlu-Phe Suppresses LPS Induced IFN-Gamma Production.

As an initial foray into *in vivo* studies, the safety and effects of the pyroGlu-X dipeptides were questioned using a non-specific mouse model. Mice were dosed daily with 100 µg of PyroGlu-Phe over a course of three days after which they were sacrificed and assessed for a systemic response. Broadly, no apparent negative effects were observed in the mice regarding weight changes or morbidity. TNF- α levels were also measured in serum collected from the mice, and found to be comparable to the negative saline control, suggesting compound injection elicited no significant systemic immune response (Figure 29A). To further explore the effects of pyroGlu-Phe on immune response, splenocytes were isolated from the mice and assayed for cytokine secretion (Figure 29B/C). Splenocytes from the saline and treated mice groups produced comparable amounts of TNF- α when stimulated with LPS, however, interestingly, the pyroGlu-Phe treated group secreted significantly lower amounts of interferon-gamma (IFN- γ) upon LPS challenge. This suggests that supplementation with pyroGlu-Phe does not provoke a systemic immune response within mice, however, is able to suppress IFN-gamma production in response to LPS stimulation. Considering the numerous implications of aberrant IFN- γ expression in autoimmune disorders and IBD, its modulation by *L. plantarum* pyroGlu-X dipeptides offers an interesting perspective on the probiotic's mechanism of action while hinting at a therapeutic role for the pyroGlu-X dipeptides within the context of a dietary supplement (129-131). These promising preliminary *in vivo* results require further investigation, including assessing the ability of

the pyroGlu-X dipeptides to suppress a systemic immune response within mice when injected with LPS systemically. The discovery of immunomodulatory small molecules from probiotic organisms can supersede the administration of live culture probiotics, placing emphasis on the main effector molecules, while subverting risks associated with live culture administration (132).

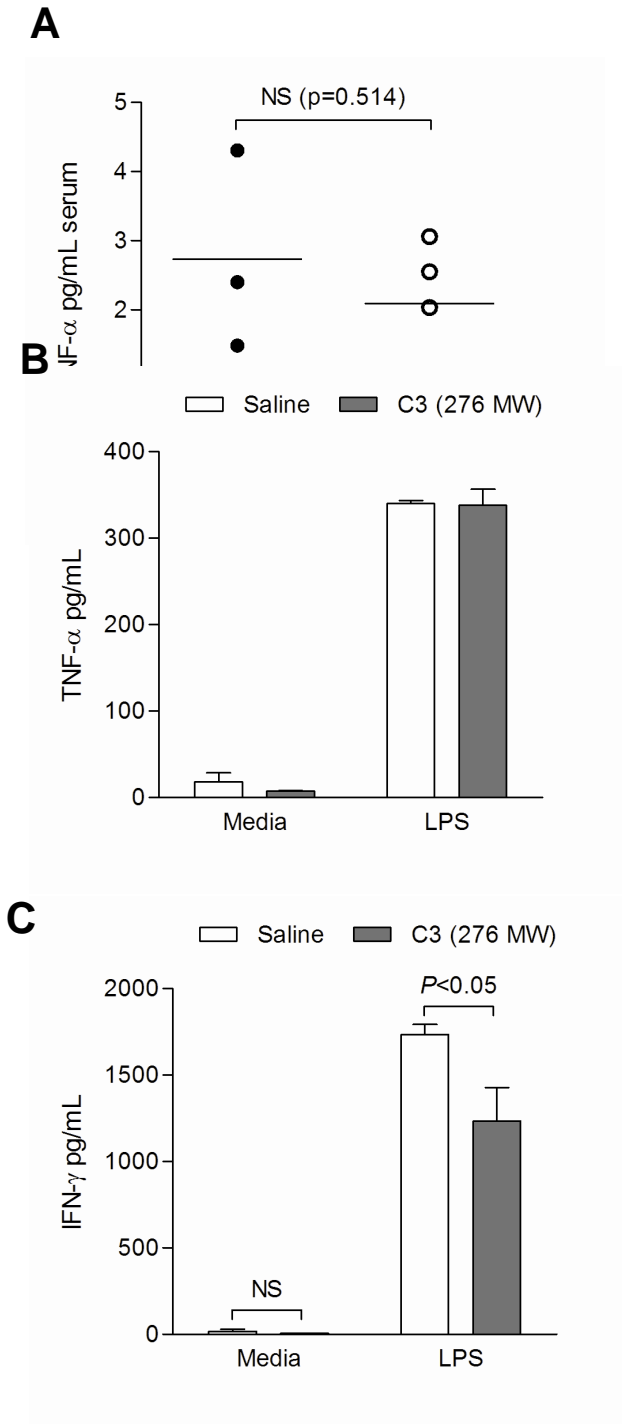


Figure 29. Supplementing Mice with PyroGlu-Phe Decreases IFN-Gamma Secretion by Splenocytes in Response to LPS.

A) Male C57BL/6 (Taconic) were injected intraperitoneally with 100 μ g of pyroGlu-Phe (C3 (276 MW)) for 3 days. Blood was taken from mice on day 3 and TNF- α was measured in serum by ELISA. **B-C)** Spleens were removed from mice and a single cell suspension was prepared. Cells were placed in 24-well plates at a concentration of 1×10^6 cells per well and LPS was added to a final concentration of 100 ng/mL. Cells were then incubated at 37°C and 5% CO₂. After 24 hours the supernatant was collected and TNF- α and IFN- γ cytokine levels measured by ELISA.

4.5 Materials and Methods

All experiments were performed by Nikola Lukenda except where noted.

Bacterial Strains, Fermentation Conditions and Reagents.

Lactobacillus plantarum WCFS1 wild type and NRPS insertional mutant strains (IM1 and IM2) were provided by Dr. Fischbach at the University of California, San Francisco. All reagents were purchased from Sigma-Aldrich unless otherwise listed. *L. plantarum* strains were cultured in de Man, Rogosa and Sharpe (MRS) media (BD sciences) or MRS media supplemented with erythromycin (10 µg/mL) at 37°C with no shaking. Cultures were grown to either mid-log (OD₆₀₀ of 1.0) or stationary phase (overnight growth).

Multivariate Analysis of *L. plantarum* Extracts. For metabolome analysis, 30 mL fermentations of *L. plantarum* strains were grown to either mid-log (OD₆₀₀=1; 6 hr) or stationary phase (until OD₆₀₀ stabilized at 1.8; 48 hr) and extracted using liquid-liquid partitioning (ethyl-acetate 2:1, 2x) with the resulting organic phase concentrated *in vacuo* (N=4). Dried material was reconstituted in 100% methanol and analyzed by HPLC-MS (Dionex UltiMate 3000 HPLC system with variable UV detection in line to a Bruker amaZon X ion-trap mass spectrometer operating in positive ionization mode with a scan window of 100-2000 *m/z*). Samples were run on a 50 x 3.00 mm Phenomenex Gemini-NX 3µ C18 110A column (Serial N. 507333-1) with a flowrate of 0.4 ml min⁻¹ and the following program consisting of solvents A (H₂O + 0.1% Formic acid) and B (Acetonitrile + 0.1% Formic acid): 0-3 min, 2% B; 3-23 min, linear gradient to 100% B;

23-27 min, 100% B; 27-29 min, linear gradient to 100% B; 19-35 min, 5% B. Remaining material was pooled for ex vivo cell assays. Multivariate analysis was performed on the resulting data sets using Bruker Daltonics Profile Analysis 2.0. Pairwise comparisons between wild type mid-log and stationary cultures and between wild type and mutant cultures using PCA and t-test models were performed using rectangular bucketing. Bucket parameters were defined as $\Delta R_t = 0.3$ min, with a kernel size of 0.150 min, and $\Delta m/z = 0.5$ m/z with a kernel size of 0.150 m/z . Retention time and m/z ranges examined were between 1.0-30.5 min and 100.5 to 2000.5 m/z respectively.

Isolation and Characterization of Stationary Growth Phase Dependent Metabolites.

To isolate compounds identified by multivariate analysis, 6 x 1L fermentations of wild type *L. plantarum* were grown to stationary phase and processed by liquid-liquid extraction (ethyl acetate 2:1, 2x). The organic phase was concentrated in *vacuo* and the crude extract fractionated using a Combiflash® Rf normal phase MPLC system (Teledyne Technologies Inc.) with a 24g RediSep® Rf silica Flash column. The following program of solvent A (hexanes) and B (ethyl acetate) was employed: 0-5 min, 0% B; 5-12 min, 25% B; 12-22 min, 50% B; 22-30 100% B. This was followed by a DCM (solvent A)/ MeOH (solvent B) program as follows: 0-7 min, 0% B; 7-15 min, 25% B; 15-22 min 50% B; 22-30 min 75% B; 30-40 min, 100% B. A total of 9 fractions were generated and interrogated by LC-MS for the compounds of interest. The 50% MeOH/DCM fraction was further fractionated using preparative HPLC with a 250 x 15 mm Phenomenex Luna 5 μ C18(2) 100Å column with a flow rate of 8 ml min⁻¹ and the

same HPLC solvent system as described earlier and the following program: 0-5 min, 5% B; 5-23 min linear gradient to 45% B; 23-25 min, linear gradient to 100% B; 25-29 min, 100% B; 29-30.5 min, linear gradient to 5% B; and 30.5-35 min, 5% B. LC-MS/MS fragmentation data for pyroGlu-X dipeptides was obtained by analyzing the 50% MeOH/DCM fraction with HPLC-autoMS/MS using a 250 x 4.60 mm Phenomenex Luna 5 μ C18(2) 100Å (Serial n. 516161-20) column with a flowrate of 1 ml min⁻¹ and the same program as for their isolation. High-resolution mass spectral data was obtained using a Thermo Scientific LTQ Orbitrap XL. NMR experiments were performed using a Bruker Avance 700 MHz spectrometer with all samples dissolved in methanol-d₄ 99.8% (Sigma Aldrich). From this, 1.7 mg of pyroGlu-L-Leu, 1.8 mg of pyroGlu-D-Leu, and 2.2 mg of pyroGlu-Phe were obtained.

The following experiments were designed by Nikola Lukenda and Janice Kim from Dr. Khan's lab at McMaster University, and conducted by Janice Kim with results interpreted by Nikola Lukenda.

Animals. Male (8-10 week old) C57BL/6 mice (Taconic) were kept in sterilized, filter-topped cages under specific pathogen-free conditions and fed autoclaved food. All experiments were approved by the animal ethics committee of McMaster University and conducted under the Canadian guidelines for animal research.

Isolation of DCs from spleens. Mice were sacrificed by cervical dislocation and spleens were excised and placed in Spleen Dissociation Medium (STEMCELL Technologies) and incubated for 30 min at room temperature. They were then strained through a 70- μ m nylon mesh filter (BD Falcon) and washed with PBS supplemented with 2% fetal bovine serum (FBS) and 1 mmol/L EDTA. Splenic DCs were isolated using a CD11c positive isolation kit (EasySep®, STEMCELL Technologies) according to the manufacturer's guidelines.

***Ex vivo* DC culture.** DCs (10⁶ cells/mL) isolated using CD11c positive selection were grown in RPMI medium 1640 supplemented with 10% fetal bovine serum (FBS), 100 U/mL penicillin, 100 μ g/mL streptomycin, and 50 μ M 2-ME (Invitrogen Life Technologies). Cells were incubated with or without LPS (100 ng/mL, Sigma-Aldrich) and combined *Lactobacillus plantarum* fractions dissolved in PBS were added to the culture at varying doses in the presence or absence of nuclear factor kappa B (NF- κ B) inhibitor, pyrrolidine dithiocarbamate (10 μ mol/L, PDTC, Sigma) and incubated at 37°C for 24 and 48 hours. Supernatants were collected and analyzed for cytokine levels using the Bio-Plex Luminex system (Bio-Rad, Canada). Supernatant levels of interleukin (IL)-12, and IL-6 were measured using a Bio-Rad cytokine 2-plex panel kit. Fluorescence data was acquired and analyzed by Bio-Plex Manager software (version 5.0, Bio-Rad Laboratories).

***In vivo* assessment of systemic immune response.** Male C57BL/6 (Taconic) were injected intraperitoneally with 100 µg of pyroGlu-Phe for 3 days. Blood was taken from mice on day 3, placed at room temperature for 2 hours, followed by centrifugation at 2000g for 20 minutes. TNF- α was measured in serum by ELISA. Spleens were removed from mice and a single cell suspension was prepared. The cell suspension was centrifuged and the cell pellet was re-suspended in lysis medium to remove red blood cells. Cells were placed in 24-well plates at a concentration of 1×10^6 cells per well. LPS was added to a final concentration of 100ng/mL. Cells were placed in 37 degree humidified incubator at 5% CO₂. After 24 hours, supernatant was collected and centrifuged and cytokine levels were measured by ELISA.

5 Chapter 4:

**Faecalienes are Anti-Inflammatory Metabolites from Crohn's Disease Associated
*Faecalibacterium Prausnitzii***

5.1 Chapter Forward

As a third system of study the Crohn's disease associated Faecalibacterium prausnitzii was chosen due to its divergence from the S. mutans and L. plantarum projects. With F. prausnitzii an anti-inflammatory secreted metabolite was believed to exist based on experiments using cell free supernatants, however, unlike with S. mutans and L. plantarum, no NRPS or PKS biosynthetic operons were identified in the available genomic data. This contrast provided an intriguing opportunity to expand the scope of this thesis to search for novel, non NRP or PK, bioactive secondary metabolites from human microbiota. As such, chemical isolation techniques and biological assays developed from work on S. mutans and L. plantarum were applied and modified to facilitate the discovery of novel secondary metabolites from F. prausnitzii.

5.2 Abstract

In a 2008 study published by Sokol *et al.*, the microbial composition of Crohn disease (CD) patients was profiled at the time of surgical intervention, the only “cure” for Crohn’s, and again 6 months later. While a decrease in the abundance and diversity of intestinal bacteria had already been established as a marker in Crohn disease patients, the authors extended the hypothesis by successfully narrowing that dysbiosis to one specific bacterium, *Faecalibacterium prausnitzii*. Microbial profiling experiments combined with patient follow up studies exposed a strong correlation between decreased *F. prausnitzii* levels and the recurrence of CD. Spurred by this finding, the mechanisms of *F. prausnitzii* immunomodulation were questioned using *in vitro* and *in vivo* systems. *In vitro* experiments suggested that a secreted metabolite with anti-inflammatory activity was responsible, as cells treated with bacterial supernatant secreted decreased levels of the pro-inflammatory cytokine IL-8. From these findings, the authors proposed that secreted anti-inflammatory metabolites from *F. prausnitzii* were counterbalancing the dysbiosis in CD, leading to improved immunomodulation and providing a promising treatment strategy. Here we report the discovery of a novel class of anti-inflammatory metabolite secreted by *F. prausnitzii*. Large scale fermentations of *F. prausnitzii* were extracted, fractionated, and by using anti-inflammatory activities as a guide, led to the discovery of three novel, but related, anti-inflammatory compounds.

5.3 Introduction

Inflammatory bowel disease (IBD) affects millions of individuals worldwide with over 2.8 million, and 200 000 sufferers in the US and Canada respectively. A family of disorders, IBD is characterized by a dysregulated immune response to intestinal microbiota resulting in chronic and relapsing inflammation of the gastrointestinal tract. The two most common forms of IBD, Crohn's disease (CD) and ulcerative colitis (UC), rely on a genetic predisposition within the immune system of the host which is triggered by intestinal microbiota initiating an inflammatory cascade (133-135). In studying the microbial nature of this disease two approaches have been taken, one global, examining the overall state of intestinal microbiota, and the other specific, searching for individual candidate organisms linked to the disease. Early experiments employed culture-based techniques to catalogue intestinal flora, however, these methods were inherently flawed as more than 70% of microbes remained unexplored (136, 137). Only with the recent development of culture-independent and metagenomic techniques, and their application to IBD, has the relationship between IBD and gut flora begun to be properly characterized.

Metagenomic approaches treat the entire microbial community being studied as a single entity, fragmenting and analyzing all genomic DNA available in an unbiased way. Obtained genomic DNA is then screened for 16s rRNA genes by DNA hybridization, and microbial diversity determined by 16s rRNA gene sequencing and phylogenetic analysis. Other techniques include fluorescence in situ hybridization (FISH) and real time quantitative polymerase chain reaction (RT Q-PCR). Using these methods faecal

microbiota have been compared repeatedly between healthy and diseased individuals revealing a significant decrease in microbial diversity in individuals with Crohn's disease, specifically within the phylum Firmicutes (138, 139). While these experiments helped illustrate the global state of intestinal flora in Crohn's, no specific candidate organisms had yet been confirmed to be major disease factors.

In 2008, Sokol *et al.*, assessed the composition of microbiota of CD patients at the time of, and 6 months following surgical removal of the ileum, the final section of the small intestine where inflammation typically occurs (140). Using FISH, the authors focused their analysis in CD patients on the bacterium *Faecalibacterium prausnitzii*, a member of the Firmicutes phylogeny, previously reported to be depleted in IBD patients (141, 142). Sokol *et al.* confirmed and quantified the depletion of *F. prausnitzii* revealing its absence significantly correlated with the reoccurrence of CD. Probing its role in CD, *in vitro* experiments suggested the existence of a secreted metabolite, as the bacterial supernatant and not the bacterium itself, was responsible for abolishing IL-1 β induced NF- κ B activity, decreasing levels of the pro-inflammatory cytokine IL-8 (Figure 30A). Other *in vitro* experiments showed increased anti-inflammatory IL-10 levels, and decreased pro-inflammatory TNF- α and IL-12, upon treating human blood cells with the supernatant. Expanding studies to *in vivo* experiments, using a mouse colitis model, *F. prausnitzii* supernatant, and no other cellular components, reduced colitis severity and improved mouse survival from 20 to 100% over 20 days (Figure 30B). From these findings, the authors proposed that secreted anti-inflammatory metabolites from *F. prausnitzii* were counterbalancing the dysbiosis in CD, leading to improved

immunomodulation and providing a promising treatment strategy. Numerous studies have since confirmed *F. prausnitzii*'s role as a etiological factor in CD, but none have explored the molecular nature of its role (143-147).

A collaboration was established with Dr. Philippe Langella of the INRA, lead author on the Sokol paper, whereby our natural product expertise would be used to identify metabolites secreted by *F. prausnitzii*, responsible for its role in mitigating CD. Large scale fermentations of *F. prausnitzii* were extracted and fractionated, with fractions selected for further processing by their anti-inflammatory activity. Using this process we identified a series of related compounds from the *F. prausnitzii* supernatant which have anti- IL-8 activity in an *in vitro* cell based assay.

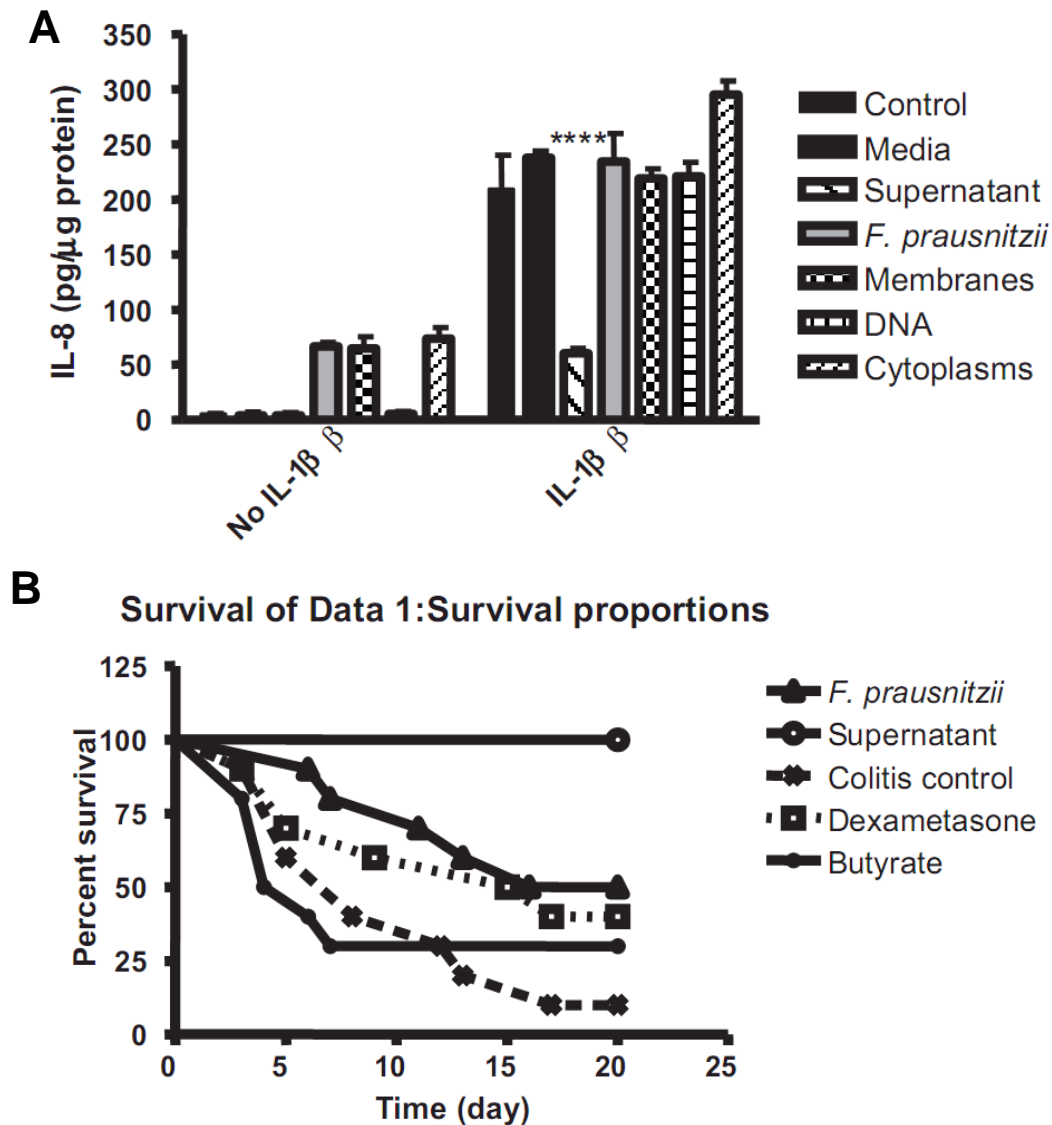


Figure 30. *Faecalibacterium prausnitzii* Supernatant Exhibit's Anti-Inflammatory Activity on Caco-2 Cells and Provides Protective Effects on Mice After TNBS Challenge. Replicated from Sokol *et al.*, 2008. **A**) A soluble, secreted factor from *F. prausnitzii* exerts anti-inflammatory effects as only its supernatant, and not its intracellular, or structural components, modulate IL-1 β induced IL-8 secretion. The values are expressed as the mean \pm SEM in pg/ μ g of proteins. **** = $P < 0.001$. **B**) An intraperitoneal injection of 200 μ L of *F. prausnitzii* supernatant significantly increased mouse survival compared to administration of live bacteria (10⁹-10¹⁰ CFU in 200 μ L), or other factors. Each group included 10 mice. Statistical analysis was performed using the log rank test.

5.4 Results and Discussion

Extraction Optimization for *F. prausnitzii* Anti-Inflammatory Metabolites.

Crude metabolite extracts from *F. prausnitzii* fermentations were generated using HP-20 resin or ethyl acetate liquid-liquid partitioning, and compared for their ability to recapitulate cell free supernatant anti-inflammatory effects. Two 20L fermentations were split into 10L pools and extracted by each method, generating HP-20, and ethyl acetate derived crude mixtures in duplicate. HP-20 extraction resulted in more bio-mass compared to ethyl acetate, indicative of broader metabolite capture. When both mixtures were tested for their anti-inflammatory activity, however, both completely abolished IL-8 secretion from TNF- α treated HT-29 cells. Further inspection of treated cells revealed detachment from the assay plate, indicative of poor cell health. Believing poor cell state to result from the complexity of the extract, crude mixtures were split into 22 pools by preparative HPLC. Anti-inflammatory activity was again assayed and again, cells treated with HP-20 derived fractions exhibited poor physiology while HT-29 cells treated with ethyl acetate had normal morphology and, some pools retained anti-inflammatory ability (E18, E19). As such, subsequent extraction of *F. prausnitzii* metabolites would use ethyl acetate derived mixtures for guided isolation of anti-inflammatory metabolites.

Guided Isolation of *F. prausnitzii* Anti-Inflammatory Compounds.

A 30 L fermentation of *F. prausnitzii* was extracted using ethyl acetate liquid-liquid extraction with the resulting crude mixture split into 7 pools using silica flash

chromatography. Each pool was tested for its ability to modulate IL-8 levels from TNF- α stimulated HT-29 cells as an anti-inflammatory marker. Cells treated with pools 1 and 7 measured the lowest IL-8 levels, with 1 mM samples abolishing IL-8 secretion while maintaining a healthy cell state, as determined microscopically (Figure 31). As pool 7 yielded only 1.9 mg of material, pool 1 was chosen for further metabolite mining, beginning with LC-MS analysis. By UV and MS base peak chromatogram (BPC), three main peaks were observed with m/z 's of 244 [M-H]⁻ (R_t 14.0 min), 244 [M-H]⁻ (R_t 14.5 min) and 228 [M-H]⁻ (R_t 17.0 min). All compounds, hereon referred to as faecalienes, shared similar UV absorbances in the 300 nm range which along with their related masses, suggested structural similarities (Figure 32). Preparative HPLC was used to purify target compounds allowing structural elucidation preceding bioactivity testing.

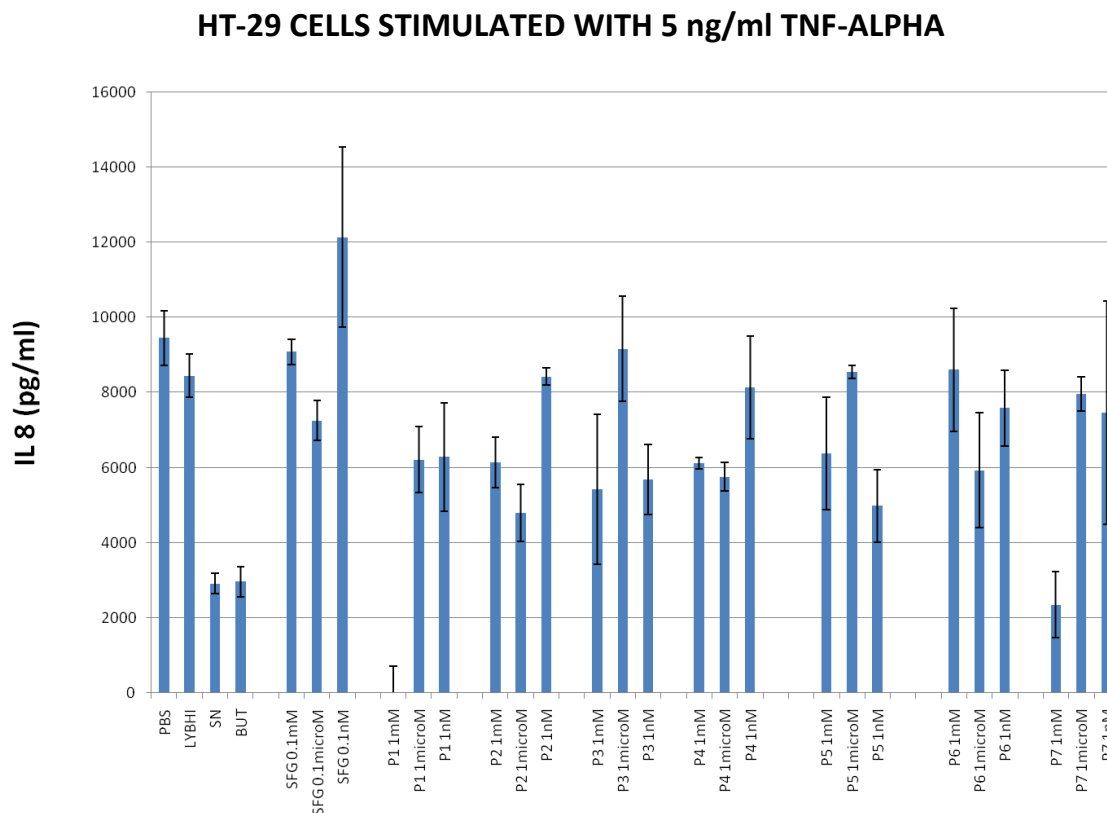


Figure 31. Anti-Inflammatory Guided Fractionation of *F. prausnitzii* metabolites.

Thirty litres (30 L) of *F. prausnitzii* supernatant were extracted with ethyl acetate and partitioned using silica flash chromatography into seven pools. Each pool was tested for its anti-inflammatory ability by adding varying concentrations of the extracts to HeLa cells concurrently with TNF- α stimulation and incubating for 6 hours. After incubation, supernatants were collected and IL-8 levels measured using ELISA. Addition of *F. prausnitzii* supernatant (20% v/v) (SN) and butyrate (40 mM) (BUT) to cells acted as positive controls, while phosphate buffered saline (PBS) and fermentation media (20% v/v) (LYBHI) were negative controls. SFG samples correspond to a partially purified metabolite. N=3 for all treatments.

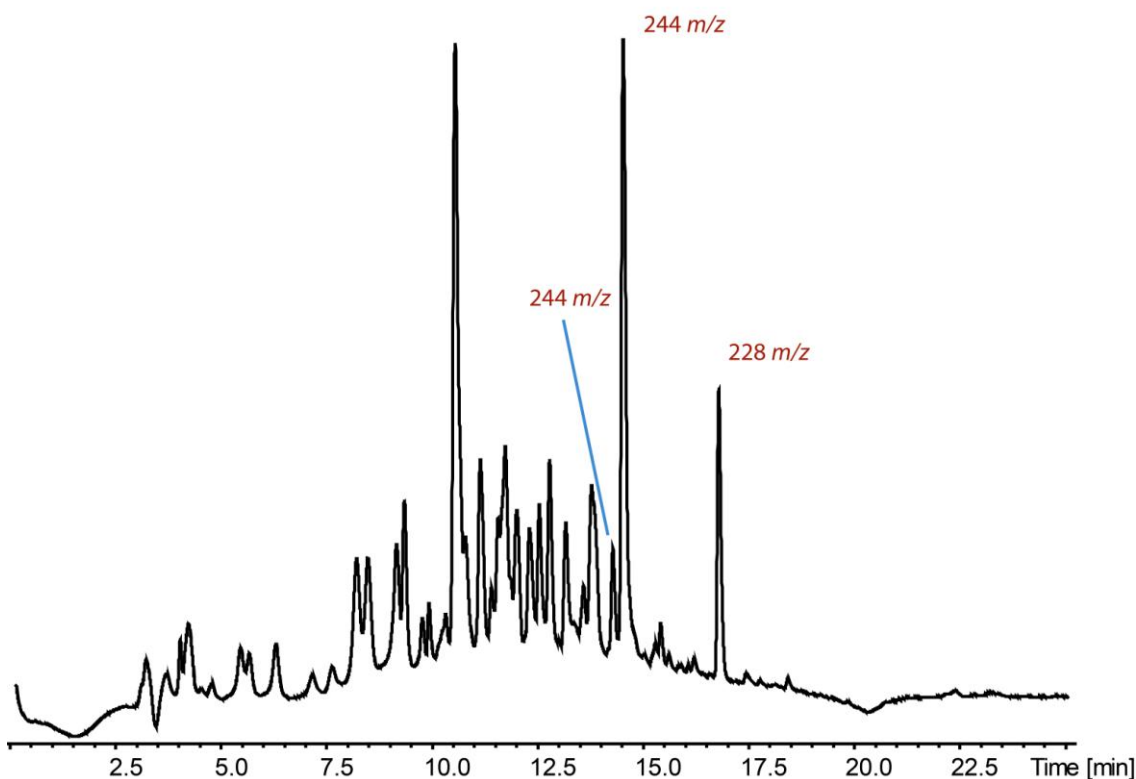


Figure 32. Identification of Structurally Related *F. prausnitzii* Metabolites in Anti-Inflammatory Pool P1. A UV chromatogram from LC-MS analysis of P1 highlights the complexity of the mixture. Peaks chosen for isolation, based on similar UV and m/z properties are labelled.

Structural Characterization of the Faecalienes.

HRESIMS analysis of faecaliene A (m/z 244 $[M-H]^-$, R_t 14.5 min), provided a molecular ion with m/z 244.0447 corresponding to a molecular formula of $C_{13}H_{10}NO_2S$ ($[M-H]^-$, calcd 244.0438, 3.9 ppm error). MS/MS experiments were performed, however, only two daughter ions were observed corresponding to losses of a water and methyl group. (Data not shown) Faecaliene A's UV spectrum suggested the presence of a phenyl group which was supported by four 1H NMR signals between δ_H 7.46-8.21 ppm (4H). Additional 1H -NMR signals were observed at δ_H 2.45 ppm (3H) corresponding to a

methyl group, and at δ_{H} 3.46 ppm (2H), indicating a methylene group, accounting for a total of 9 proton signals. The two outstanding protons predicted by the HRESIMS formula were attributed to exchangeable hydroxyl and amide protons supported by ^{13}C -NMR peaks at δ_{C} 146.1 and 166.6 ppm respectively. From the ^{13}C spectrum, the presence of a benzyl group was expanded to a naphthalene scaffold by the presence of 9 signals between δ_{C} 116.4-125.7 ppm, leading to a proposed structure (Figure 33). The outstanding carbon required for a naphthalene skeleton was found by an HMBC interaction between the benzene proton H-7 and C-6 at δ_{C} 146.1 ppm, shifted due to a hydroxyl group. Long range ^1H - ^{13}C HMBC and ^1H - ^1H COSY interactions were used to confirm the polycyclic nature of faecaliene A. COSY data revealed a single spin system comprising the four protons between δ_{H} 7.46-8.21 ppm, forming the backbone of the naphthalene moiety. These protons exhibited HMBC interactions with key C atoms, C-6, C-11, and C-13, confirming the naphthalene structure. HMBC interactions between the methylene protons H-2 (δ_{H} 3.46 ppm) and the naphthalene scaffold at C-4 (δ_{C} 120.9 ppm) and the amide C-2 (δ_{C} 166.6 ppm) confirmed the polycyclic scaffold of faecaliene A, leaving only the functional groups to be assigned. The methyl group indicated by H-14 at δ_{H} 2.45 ppm was placed at C-5 by HMBC interactions with C-4 and C-6, and the hydroxyl group was assigned to C-6 by HMBC interactions with the methyl protons H-14, and naphthalene proton H-7. A literature search of faecaliene A identified it as a novel compound based on the known 1H-Naphtho[2,1-b][1,4]thiazin-2(3H)-one scaffold (CAS 136928-66-0), which lacks the naphthalene methyl and hydroxy groups.

Faecaliene B (m/z 228 $[M-H]^-$, R_t 17.0 min) afforded a molecular ion at m/z 228.0495 that corresponded to a molecular formula of $C_{13}H_{10}NOS$ ($[M-H]^-$, calcd 228.0489, 2.6 ppm error). As such, the loss of a single O atom was the differentiating factor from faecaliene A. Furthermore, 1H - and ^{13}C -NMR spectra of faecaliene B were remarkably similar to A, maintaining the decorated naphthalene scaffold. Faecaliene B however, lacked the methylene group observed at δ_H 3.46 ppm and instead, possessed an additional methyl signal at δ_H 2.92 ppm and δ_C 18.0 ppm. From this data, a structure was proposed with faecaliene B containing a thiozole group instead of an amide ring, suggested by ^{13}C -NMR shifts at δ_C 163.5 ppm and δ_C 135.3 ppm. HMBC interactions between the new methyl protons H-13 (3H, δ_H 2.92 ppm) and the thiozole C-2 (δ_C 163.5 ppm), and between methyl protons H-14 (3H, δ_H 2.55 ppm) and the thiozole C-3 (δ_C 135.3 ppm) confirmed the structure of faecaliene B (Figure 33). A literature precedent exists for faecaliene B however, previously identified as Naphtho[1,2-d]thiazol-5-ol, 2,4-dimethyl- (CAS 858189-61-4).

High resolution ESIMS of faecaliene C (m/z 244 $[M-H]^-$, R_t 14.0 min) revealed a molecular formula of $C_{13}H_{11}NO_2SNa$ ($[M+Na]^+$, m/z 268.0397, calcd 268.0403), exactly matching that of faecaliene A. A comparison of the NMR data revealed similarity to faecaliene B, with both maintaining the thiozole scaffold, however some differences were noted in the ^{13}C -NMR spectrum. Firstly, the naphthalene hydroxyl, previously seen at δ_C 147.3 ppm in faecaliene B was missing, and in its place a signal at δ_C 201.2 ppm corresponding to a ketone was observed. HMBC interactions between methyl protons H-14 and the ketone C-5, and the naphthalene proton H-6 with C-5, confirmed the ketone

position within the scaffold. The ^{13}C spectrum also lacked a naphthalene signal previously assigned to C-4 (δ_{C} 111.0) in faecaliene B, and instead had an upfield shift at δ_{C} 74.4 ppm, suggestive of a hydroxyl group. HMBC interactions confirmed the hydroxyl group was attached to C-4 by interactions between C-4 (δ_{C} 74.4) and the methyl protons H-14 (Figure 33). Although highly similar to the known faecaliene B, no literature precedent could be found for faecaliene C.

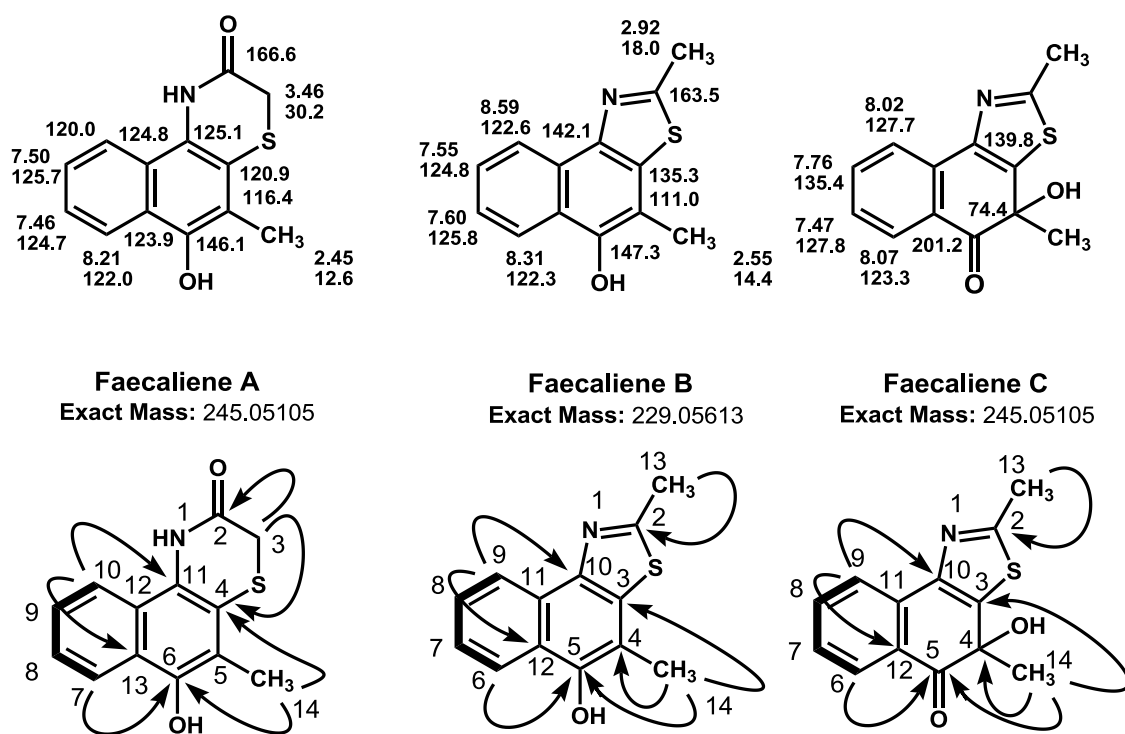


Figure 33. Structural Elucidation of the Faecalienes by 1D and 2D NMR. Structural elucidation of the faecalienes was achieved using a combination of ^1H - ^1H COSY (bold lines), ^1H - ^{13}C HMBC interactions (curly arrows), and 1D ^1H - and ^{13}C -NMR experiments.

Faecalienes Reduce IL-8 Secretion in HeLa Cells.

F. prausnitzii culture supernatants exhibit a remarkable ability to reduce the production of IL-8, one of the major chemokine mediators in inflammatory response. In the original Sokol *et al.*, paper IL-8 was used as a robust measure of immunomodulatory activity, and for the faecalienes to recapitulate this effect would support an anti-inflammatory role. Three unrelated metabolites were isolated from P1 as controls and were identified as various diketopiperazines. The IL-8 assay was performed independently three times, and in each assay only the faecalienes significantly reduced IL-8 secretion induced by TNF- α (Figure 34). Anti-IL-8 activity was observed using concentrations as low as 2.5 μ M. Due to DMSO and methanol being toxic to HeLa cells, the faecalienes were sparingly reconstituted in PBS, suggesting the faecalienes exhibit IL-8 reducing activity at even significantly lower concentrations. Experiments to determine the full efficacy of the faecalienes are currently ongoing.

To fully characterize the faecalienes as anti-inflammatory metabolites from *F. prausnitzii*, significant challenges exist. From 30L of supernatant, enough crude extract was generated to obtain mg quantities of the faecalienes. While this was enough material to elucidate their structures and confirm their ability to reduce TNF- α induced IL-8 production, such a low yield is a significant impediment to further research. Specifically, to fully appreciate the anti-inflammatory activity of the faecalienes mouse studies are required, including using a colitis model. This would require faecalienne amounts outside the possible yield of isolation from the natural source. Efforts are currently being explored to synthesize the faecalienes with a promising avenue found in the patent

GB 593025 (Polynuclear thiazoles and selenazoles, Kodak Ltd., 1947), where faecaliene B was first reported. Such efforts are worthwhile based on the potent therapeutic potential *F. prausnitzii* supernatant was previously shown to possess. The discovery of the faecalienes as novel immunomodulatory metabolites supports the designation of *F. prausnitzii* as a probiotic commensal member of the human microbiota, and further supports the argument of this thesis that human microbiota are a rich reservoir of novel host relevant metabolites.

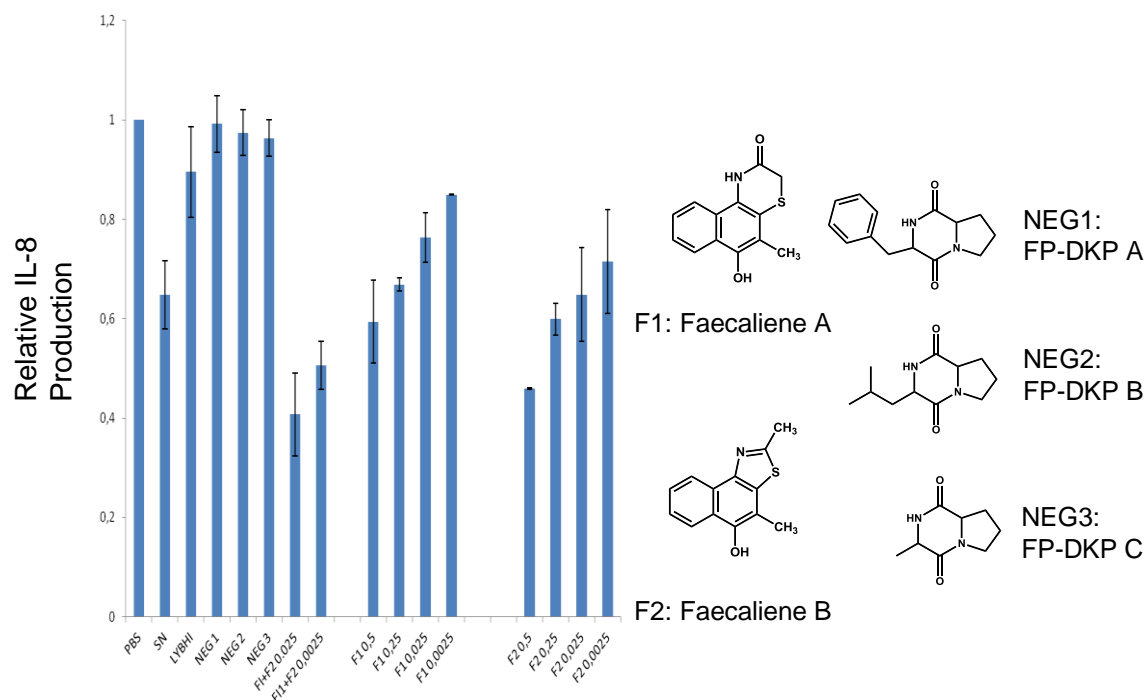


Figure 34. Faecalienes are Anti-Inflammatory Metabolites Secreted by *F. praunstizii*. Varying concentrations of the faecalienes were added to HeLa cells concurrently with TNF- α and incubated for 6 hours. After incubation, supernatants were collected and IL-8 levels measured using ELISA. Addition of *F. praunstizii* supernatant (20% v/v) (SN) to cells acted as a positive control, while phosphate buffered saline (PBS) and fermentation media (20% v/v) (LYBHI) were negative controls. NEG1, NEG2, and NEG3 correspond to diketopiperazines also isolated from P1. Concentrations are shown on the X-axis in M (mol/L). Synergistic effects of the faecalienes were also examined by adding them together at individuals concentrations of 25 μ M and 2.5 μ M.

5.5 Materials and Methods

All experiments were conducted by Nikola Lukenda except where noted.

Bacterial supernatants were provided by Dr. Emma Allen-Vercoe from the University of Guelph.

Bacterial Fermentations. *F. prausnitzii* A2-165 (DSM 17677), isolated from human fecal stool, was grown at 37°C in LYHBHI medium (Brain–heart infusion medium supplemented with 0.5% yeast extract (Difco) and 0.5% L-cysteine (Sigma-Aldrich)) supplemented with cellobiose (1 mg/ml; Sigma–Aldrich), maltose (1 mg/ml; Sigma), and cysteine (0.5 mg/ml; Sigma) in an anaerobic chamber. When necessary, the bacterium was grown in a semi-defined medium composed of: KH_2PO_4 (2.62 g/l), $(\text{NH}_4)_2\text{SO}_4$ (2 g/l), NaCl (2 g/l), CaCl_2 (15 mg/l), MgCl_2 (150 mg/l), MnCl_2 (15 mg/l), FeCl_3 (4mg/ml), Vitamin B12 (5mg/l), Vitamin B (Thiamin) (1mg/l), Biotin (1 mg/l), PABA (1 mg/l), Folic acid (1 mg/l), Vitamin K (2 mg/l), 30 mM Acetate, cellobiose (1 mg/ml), maltose (1 mg/ml), glucose (1 mg/l), 2% yeast extract and cysteine (0.5 mg/ml) in an anaerobic chamber.

Extraction of *F. prausnitzii* Anti-Inflammatory Metabolites. Liquid-liquid partitioning (ethyl acetate 2:1, 2x) and HP-20 (2.5% w/v) were used independently to extract 10 L fermentations of *F. prausnitzii*. Metabolite bound HP-20 resin was washed with methanol

with the resulting organic phase concentrated *in vacuo*, followed by preparative HPLC to generate 22 fractions which were tested for their anti-inflammatory capacity. The organic phase from ethyl-acetate extraction was treated identically.

Isolation and Analysis of Anti-Inflammatory *F. prausnitzii* Metabolites. Crude mixtures of *F. prausnitzii* secreted metabolites were generated by extracting 30 L of cell free culture with ethyl acetate (2:1, 2x), resulting in aqueous and organic phases. The anti-inflammatory activity of both phases was measured, with the organic phase undergoing further fractionation. A Combiflash® Rf normal phase MPLC system (Teledyne Technologies Inc.) with a 24g RediSep® Rf silica Flash column was used with the following program using DCM (solvent A)/ MeOH (solvent B) program as follows: 0-5 min, 0% B; 5-10 min, 15% B; 10-15 min 25% B; 15-20 min 35% B; 20-25 min, 50% B; 25-30 min, 70% B; and 30-40 min, 100% B. A total of 7 pools resulted, with the anti-inflammatory ability of each tested. Active pools underwent further fractionation using preparative HPLC with a 250 x 15 mm Phenomenex Luna 5 μ C18(2) 100Å column with a flow rate of 8 ml min⁻¹, a solvent system of solvent A (H₂O + 0.1% Formic acid) and B (Acetonitrile + 0.1% Formic acid) and the following program: 0-5 min, 5% B; 5-23 min linear gradient to 45% B; 23-25 min, linear gradient to 100% B; 25-29 min, 100% B; 29-30.5 min, linear gradient to 5% B; and 30.5-35 min, 5% B. Analytical scale analysis was performed using a 250 x 4.60 mm Phenomenex Luna 5 μ C18(2) 100Å (Serial n. 516161-20) column with a flowrate of 1 ml min⁻¹ and the same solvent system and program as previously described. Compounds isolated with a purity >90% had their anti-

inflammatory ability assayed following structural characterization. High-resolution mass spectral data was obtained using a Thermo Scientific LTQ Orbitrap XL. NMR experiments were performed using a Bruker Avance 700 MHz spectrometer with all samples dissolved in methanol-d₄ 99.8% (Sigma Aldrich).

The following experiment was conducted by Dr. Rebeca Martin from Dr. Langella's group at the INRA, with results interpreted by Nikola Lukenda.

Eukaryotic cell culture and experiments. HeLa cells (ATCC CCL-2) were grown in Dulbecco's Modified Eagle's minimal essential medium (DMEM) (GibcoBRL) supplemented with 10% (w/v) fetal bovine serum (FBS, GibcoBRL), 2mM L-glutamine (GibcoBRL) and with penicillin G/streptomycin (5000 IU/ml, 5000 µg/ml) (Sigma-Aldrich). Cultures were incubated in 25 cm² tissue culture flasks (Nunc) at 37 °C in a 5% (v/v) CO₂ atmosphere until confluence. For anti-inflammatory assays, 50000 cells per well were seeded in 24-well culture plates (Nunc) and cultivated, with a daily change of the culture medium during 6 days. The assays were performed seven days after seeding. Twenty-four hours before bacterial challenge, the culture medium was changed for a medium with 5% FBS. The bacterial supernatant at 20% , the control medium, PBS (GibcoBRL) or the molecules to test were added and the cells were stimulated simultaneously with human recombinant TNF-alpha (5 mg/ml; Sigma–Aldrich) in DMEM with 5% FBS for 6 h. After incubation, cell supernatants were collected and frozen at -80°C with a cocktail of protease inhibitors EDTA-free (Roche).

IL-8 ELISA and Protein Concentration.

HeLa cells were washed with PBS and lysed in PBS. Protein concentrations were determined in cell lysates using the Bradford reagent (Sigma-Aldrich) according to the manufacturer's instructions. The IL-8 level was determined in cell supernatants using Human IL-8 ELISA kit (Biolegend) according to the manufacturer's recommendations.

6 Conclusions

At the onset of this thesis an argument was made for the search for nonribosomal peptides and polyketides from human microbiota on the basis of their predicted biological activity within the human environment. A hypothesis developed where physiological effects from targeted candidate organisms could be linked to their NRP and PK products. Through experimentation on the human microbiome members *Streptococcus mutans*, *Lactobacillus plantarum*, and *Faecalibacterium prausnitzii*, this hypothesis was proven partly true.

In the oral microbiome, novel NRP and PK derived products from the TnSmu2 biosynthetic operon in *S. mutans* were identified and shown to affect pathogenesis in an oral yeast pathogen, as well as to possess host immune implications. The biosynthesis of these metabolites, the mutanobactins and mutanamide, were then studied using mutagenesis experiments, precursor feeding experiments, and structural elucidation experiments, revealing the significance of fatty acids in the production of TnSmu2 biosynthetic products. From these studies a number of yet to be characterized naturally occurring, and bioengineered products were also identified, allowing for further expansion of the TnSmu2 biosynthetic repertoire and elucidation of the role that *S. mutans* NRPs and PKs play in the human oral environment.

As a second support to the thesis hypothesis, *L. plantarum*, a member of the oral and gut microbiome was chosen for study, as it too, like *S. mutans*, possessed genetic elements predictive of NRP production. Furthermore, *L. plantarum* had an assayable

biological activity through its modulation of the host immune system, which was predicted to occur through the NRP, and would allow for its guided isolation. Genetic inactivation of the NRPS genes significantly decreased the immune response of dendritic cells to *L. plantarum* metabolic extracts, however, detailed analytical analysis of the same extracts yielded no NRP candidates. Differential immune induction was also noted in metabolite extracts from *L. plantarum* grown to mid-log versus stationary growth, and comparison of these metabolic extracts yielded the pyroglutamic acid containing dipeptides. *Ex* and *in vivo* assays suggested a protective role for these metabolites, particularly in modulating the cytokine IFN- γ , whose aberrant expression has been linked to inflammatory bowel disease and irritable bowel syndrome. PyroGlu-X dipeptides have never before been isolated from a natural source and their origins are believed to be nonribosomal. As such, surprisingly from this study nonribosomal, or modified dipeptides, were still identified as host significant metabolites from *L. plantarum* despite not being the original NRP target, reinforcing the significance of this class of metabolite in modulating host health.

For a third candidate system the Crohn's disease associated *F. prausnitzii* was chosen in order to probe for human relevant metabolites outside of NRPs and PKs, as *F. prausnitzii* lacks any NRPS or PKS genes. *F. prausnitzii* was still predicted to secrete an antiinflammatory metabolite however, as established by previous studies on its cell free supernatant. By guiding metabolite isolation by antiinflammatory assays, a number of novel compounds, known as the faecalienes, were identified and isolated from cell free supernatants. Structurally, these compounds differ significantly from the previously

studied NRPs from *S. mutans* and *L. plantarum*, yet early evidence supports a significant role in modulating the host's immune system. From studying the bioactive metabolites from *F. prausnitzii*, *L. plantarum*, and *S. mutans* has become apparent that although human microbiota can achieve significant host effects through NRPs and PKs, other, possibly yet unknown chemical scaffolds may still exist with potent actions towards the human host.

7 **References**

1. Gill, S. R., Pop, M., Deboy, R. T., Eckburg, P. B., Turnbaugh, P. J., Samuel, B. S., Gordon, J. I., Relman, D. A., Fraser-Liggett, C. M., and Nelson, K. E. (2006) Metagenomic analysis of the human distal gut microbiome, *Science* 312, 1355-1359.
2. Hooper, L. V., Littman, D. R., and Macpherson, A. J. (2012) Interactions between the microbiota and the immune system, *Science* 336, 1268-1273.
3. Holmes, E., Kinross, J., Gibson, G. R., Burcelin, R., Jia, W., Pettersson, S., and Nicholson, J. K. (2012) Therapeutic modulation of microbiota-host metabolic interactions, *Sci Transl Med* 4, 137rv136.
4. (2012) Structure, function and diversity of the healthy human microbiome, *Nature* 486, 207-214.
5. Donnet-Hughes, A., Perez, P. F., Dore, J., Leclerc, M., Levenez, F., Benyacoub, J., Serrant, P., Segura-Roggero, I., and Schiffrin, E. J. (2010) Potential role of the intestinal microbiota of the mother in neonatal immune education, *Proc Nutr Soc* 69, 407-415.
6. Turnbaugh, P. J., Ley, R. E., Mahowald, M. A., Magrini, V., Mardis, E. R., and Gordon, J. I. (2006) An obesity-associated gut microbiome with increased capacity for energy harvest, *Nature* 444, 1027-1031.
7. Hooper, L. V., and Gordon, J. I. (2001) Commensal host-bacterial relationships in the gut, *Science* 292, 1115-1118.
8. Uemura, N., Okamoto, S., Yamamoto, S., Matsumura, N., Yamaguchi, S., Yamakido, M., Taniyama, K., Sasaki, N., and Schlemper, R. J. (2001) *Helicobacter pylori* infection and the development of gastric cancer, *N Engl J Med* 345, 784-789.
9. Loesche, W. J. (1986) Role of *Streptococcus mutans* in human dental decay, *Microbiol Rev* 50, 353-380.
10. Round, J. L., and Mazmanian, S. K. (2009) The gut microbiota shapes intestinal immune responses during health and disease, *Nat Rev Immunol* 9, 313-323.
11. Wright, G. D. (2012) Antibiotics: a new hope, *Chem Biol* 19, 3-10.
12. Shanahan, F. (2010) Gut microbes: from bugs to drugs, *Am J Gastroenterol* 105, 275-279.
13. Clardy, J., Fischbach, M. A., and Walsh, C. T. (2006) New antibiotics from bacterial natural products, *Nat Biotechnol* 24, 1541-1550.
14. Vera, M. D., and Joullie, M. M. (2002) Natural products as probes of cell biology: 20 years of didemnin research, *Med Res Rev* 22, 102-145.
15. Bron, P. A., van Baarlen, P., and Kleerebezem, M. (2012) Emerging molecular insights into the interaction between probiotics and the host intestinal mucosa, *Nat Rev Microbiol* 10, 66-78.
16. Pestova, E. V., Havarstein, L. S., and Morrison, D. A. (1996) Regulation of competence for genetic transformation in *Streptococcus pneumoniae* by an auto-

- induced peptide pheromone and a two-component regulatory system, *Mol Microbiol* 21, 853-862.
17. Macfarlane, S., and Macfarlane, G. T. (2003) Regulation of short-chain fatty acid production, *Proc Nutr Soc* 62, 67-72.
 18. Cani, P. D., Bibiloni, R., Knauf, C., Waget, A., Neyrinck, A. M., Delzenne, N. M., and Burcelin, R. (2008) Changes in gut microbiota control metabolic endotoxemia-induced inflammation in high-fat diet-induced obesity and diabetes in mice, *Diabetes* 57, 1470-1481.
 19. Cummings, J. H. (1981) Short chain fatty acids in the human colon, *Gut* 22, 763-779.
 20. Ng, S. C., Hart, A. L., Kamm, M. A., Stagg, A. J., and Knight, S. C. (2009) Mechanisms of action of probiotics: recent advances, *Inflamm Bowel Dis* 15, 300-310.
 21. Rossi, M., Amaretti, A., and Raimondi, S. (2011) Folate production by probiotic bacteria, *Nutrients* 3, 118-134.
 22. Goodwin, B. L., Ruthven, C. R., and Sandler, M. (1994) Gut flora and the origin of some urinary aromatic phenolic compounds, *Biochem Pharmacol* 47, 2294-2297.
 23. Woodworth, J. R., Nyhart, E. H., Jr., Brier, G. L., Wolny, J. D., and Black, H. R. (1992) Single-dose pharmacokinetics and antibacterial activity of daptomycin, a new lipopeptide antibiotic, in healthy volunteers, *Antimicrob Agents Chemother* 36, 318-325.
 24. Sheldrick, G. M., Jones, P. G., Kennard, O., Williams, D. H., and Smith, G. A. (1978) Structure of vancomycin and its complex with acetyl-D-alanyl-D-alanine, *Nature* 271, 223-225.
 25. Shaw, L. M. (1989) Advances in cyclosporine pharmacology, measurement, and therapeutic monitoring, *Clin Chem* 35, 1299-1308.
 26. Vezina, C., Kudelski, A., and Sehgal, S. N. (1975) Rapamycin (AY-22,989), a new antifungal antibiotic. I. Taxonomy of the producing streptomycete and isolation of the active principle, *J Antibiot (Tokyo)* 28, 721-726.
 27. Umezawa, H., Maeda, K., Takeuchi, T., and Okami, Y. (1966) New antibiotics, bleomycin A and B, *J Antibiot (Tokyo)* 19, 200-209.
 28. Hofle, G., Glaser, N., Leibold, T., and Sefkow, M. (1999) Epothilone A-D and their thiazole-modified analogues as novel anticancer agents, *Pure Appl Chem* 71, 2019-2024.
 29. Sieber, S. A., and Marahiel, M. A. (2005) Molecular mechanisms underlying nonribosomal peptide synthesis: approaches to new antibiotics, *Chem Rev* 105, 715-738.
 30. Fischbach, M. A., and Walsh, C. T. (2006) Assembly-line enzymology for polyketide and nonribosomal Peptide antibiotics: logic, machinery, and mechanisms, *Chem Rev* 106, 3468-3496.
 31. Magarvey, N. A., Ehling-Schulz, M., and Walsh, C. T. (2006) Characterization of the cereulide NRPS alpha-hydroxy acid specifying modules: activation of alpha-

- keto acids and chiral reduction on the assembly line, *J Am Chem Soc* 128, 10698-10699.
32. Kohli, R. M., and Walsh, C. T. (2003) Enzymology of acyl chain macrocyclization in natural product biosynthesis, *Chem Commun (Camb)*, 297-307.
 33. Stachelhaus, T., Mootz, H. D., and Marahiel, M. A. (1999) The specificity-conferring code of adenylation domains in nonribosomal peptide synthetases, *Chem Biol* 6, 493-505.
 34. Challis, G. L., Ravel, J., and Townsend, C. A. (2000) Predictive, structure-based model of amino acid recognition by nonribosomal peptide synthetase adenylation domains, *Chem Biol* 7, 211-224.
 35. Rausch, C., Weber, T., Kohlbacher, O., Wohlleben, W., and Huson, D. H. (2005) Specificity prediction of adenylation domains in nonribosomal peptide synthetases (NRPS) using transductive support vector machines (TSVMs), *Nucleic Acids Res* 33, 5799-5808.
 36. Li, M. H., Ung, P. M., Zajkowski, J., Garneau-Tsodikova, S., and Sherman, D. H. (2009) Automated genome mining for natural products, *BMC Bioinformatics* 10, 185.
 37. Lautru, S., Deeth, R. J., Bailey, L. M., and Challis, G. L. (2005) Discovery of a new peptide natural product by *Streptomyces coelicolor* genome mining, *Nat Chem Biol* 1, 265-269.
 38. Gross, H., Stockwell, V. O., Henkels, M. D., Nowak-Thompson, B., Loper, J. E., and Gerwick, W. H. (2007) The genomisotopic approach: a systematic method to isolate products of orphan biosynthetic gene clusters, *Chem Biol* 14, 53-63.
 39. McAlpine, J. B., Bachmann, B. O., Pirae, M., Tremblay, S., Alarco, A. M., Zazopoulos, E., and Farnet, C. M. (2005) Microbial genomics as a guide to drug discovery and structural elucidation: ECO-02301, a novel antifungal agent, as an example, *J Nat Prod* 68, 493-496.
 40. von Reuss, S. H., Bose, N., Srinivasan, J., Yim, J. J., Judkins, J. C., Sternberg, P. W., and Schroeder, F. C. (2012) Comparative metabolomics reveals biogenesis of ascarosides, a modular library of small-molecule signals in *C. elegans*, *J Am Chem Soc* 134, 1817-1824.
 41. Vilchez, R., Lemme, A., Ballhausen, B., Thiel, V., Schulz, S., Jansen, R., Sztajer, H., and Wagner-Dobler, I. (2010) *Streptococcus mutans* inhibits *Candida albicans* hyphal formation by the fatty acid signaling molecule trans-2-decenoic acid (SDSF), *Chembiochem* 11, 1552-1562.
 42. Yang, J. Y., Karr, J. R., Watrous, J. D., and Dorrestein, P. C. (2011) Integrating 'omics' and natural product discovery platforms to investigate metabolic exchange in microbiomes, *Curr Opin Chem Biol* 15, 79-87.
 43. Robinette, S. L., Bruschiweiler, R., Schroeder, F. C., and Edison, A. S. (2012) NMR in metabolomics and natural products research: two sides of the same coin, *Acc Chem Res* 45, 288-297.
 44. Kersten, R. D., and Dorrestein, P. C. (2009) Secondary metabolomics: natural products mass spectrometry goes global, *ACS Chem Biol* 4, 599-601.

45. Smith, C. A., Want, E. J., O'Maille, G., Abagyan, R., and Siuzdak, G. (2006) XCMS: processing mass spectrometry data for metabolite profiling using nonlinear peak alignment, matching, and identification, *Anal Chem* 78, 779-787.
46. Forseth, R. R., Fox, E. M., Chung, D., Howlett, B. J., Keller, N. P., and Schroeder, F. C. (2011) Identification of cryptic products of the gliotoxin gene cluster using NMR-based comparative metabolomics and a model for gliotoxin biosynthesis, *J Am Chem Soc* 133, 9678-9681.
47. Vinayavekhin, N., and Saghatelian, A. (2009) Regulation of alkyl-dihydrothiazole-carboxylates (ATCs) by iron and the pyochelin gene cluster in *Pseudomonas aeruginosa*, *ACS Chem Biol* 4, 617-623.
48. Cortina, N. S., Krug, D., Plaza, A., Revermann, O., and Muller, R. (2012) Myxoprincomide: a natural product from *Myxococcus xanthus* discovered by comprehensive analysis of the secondary metabolome, *Angew Chem Int Ed Engl* 51, 811-816.
49. Ajdic, D., McShan, W. M., McLaughlin, R. E., Savic, G., Chang, J., Carson, M. B., Primeaux, C., Tian, R., Kenton, S., Jia, H., Lin, S., Qian, Y., Li, S., Zhu, H., Najar, F., Lai, H., White, J., Roe, B. A., and Ferretti, J. J. (2002) Genome sequence of *Streptococcus mutans* UA159, a cariogenic dental pathogen, *Proc Natl Acad Sci U S A* 99, 14434-14439.
50. Raaijmakers, J. M., De Bruijn, I., Nybroe, O., and Ongena, M. (2010) Natural functions of lipopeptides from *Bacillus* and *Pseudomonas*: more than surfactants and antibiotics, *FEMS Microbiol Rev* 34, 1037-1062.
51. Strieker, M., and Marahiel, M. A. (2009) The structural diversity of acidic lipopeptide antibiotics, *ChemBiochem* 10, 607-616.
52. Robbel, L., and Marahiel, M. A. (2010) Daptomycin, a bacterial lipopeptide synthesized by a nonribosomal machinery, *J Biol Chem* 285, 27501-27508.
53. Waterhouse, J. C., Swan, D. C., and Russell, R. R. (2007) Comparative genome hybridization of *Streptococcus mutans* strains, *Oral Microbiol Immunol* 22, 103-110.
54. Waterhouse, J. C., and Russell, R. R. (2006) Dispensable genes and foreign DNA in *Streptococcus mutans*, *Microbiology* 152, 1777-1788.
55. Argimon, S., and Caufield, P. W. (2011) Distribution of putative virulence genes in *Streptococcus mutans* strains does not correlate with caries experience, *J Clin Microbiol* 49, 984-992.
56. Duitman, E. H., Hamoen, L. W., Rembold, M., Venema, G., Seitz, H., Saenger, W., Bernhard, F., Reinhardt, R., Schmidt, M., Ullrich, C., Stein, T., Leenders, F., and Vater, J. (1999) The mycosubtilin synthetase of *Bacillus subtilis* ATCC6633: a multifunctional hybrid between a peptide synthetase, an amino transferase, and a fatty acid synthase, *Proc Natl Acad Sci U S A* 96, 13294-13299.
57. Aron, Z. D., Dorrestein, P. C., Blackhall, J. R., Kelleher, N. L., and Walsh, C. T. (2005) Characterization of a new tailoring domain in polyketide biogenesis: the amine transferase domain of MycA in the mycosubtilin gene cluster, *J Am Chem Soc* 127, 14986-14987.

58. Ansari, M. Z., Yadav, G., Gokhale, R. S., and Mohanty, D. (2004) NRPS-PKS: a knowledge-based resource for analysis of NRPS/PKS megasynthases, *Nucleic Acids Res* 32, W405-413.
59. Joyner, P. M., Liu, J., Zhang, Z., Merritt, J., Qi, F., and Cichewicz, R. H. (2010) Mutanobactin A from the human oral pathogen *Streptococcus mutans* is a cross-kingdom regulator of the yeast-mycelium transition, *Org Biomol Chem* 8, 5486-5489.
60. Wang, X., Du, L., You, J., King, J. B., and Cichewicz, R. H. (2012) Fungal biofilm inhibitors from a human oral microbiome-derived bacterium, *Org Biomol Chem* 10, 2044-2050.
61. Kanatomo, S., Nagai, S., Ohki, K., and Yasuda, Y. (1995) [Study on surfactin, a cyclic depsipeptide. I. Isolation and structure of eight surfactin analogues produced by *Bacillus natto* KMD 2311], *Yakugaku Zasshi* 115, 756-764.
62. Gu, J. Q., Nguyen, K. T., Gandhi, C., Rajgarhia, V., Baltz, R. H., Brian, P., and Chu, M. (2007) Structural characterization of daptomycin analogues A21978C1-3(d-Asn11) produced by a recombinant *Streptomyces roseosporus* strain, *J Nat Prod* 70, 233-240.
63. Bonmatin, J. M., Laprevote, O., and Peypoux, F. (2003) Diversity among microbial cyclic lipopeptides: iturins and surfactins. Activity-structure relationships to design new bioactive agents, *Comb Chem High Throughput Screen* 6, 541-556.
64. Debono, M., Turner, W. W., LaGrandeur, L., Burkhardt, F. J., Nissen, J. S., Nichols, K. K., Rodriguez, M. J., Zweifel, M. J., Zeckner, D. J., Gordee, R. S., and et al. (1995) Semisynthetic chemical modification of the antifungal lipopeptide echinocandin B (ECB): structure-activity studies of the lipophilic and geometric parameters of polyarylated acyl analogues of ECB, *J Med Chem* 38, 3271-3281.
65. Lakey, J. H., and Lea, E. J. (1986) The role of acyl chain character and other determinants on the bilayer activity of A21978C an acidic lipopeptide antibiotic, *Biochim Biophys Acta* 859, 219-226.
66. Lincke, T., Behnken, S., Ishida, K., Roth, M., and Hertweck, C. (2010) Closthioamide: an unprecedented polythioamide antibiotic from the strictly anaerobic bacterium *Clostridium cellulolyticum*, *Angew Chem Int Ed Engl* 49, 2011-2013.
67. Overy, D. P., Smedsgaard, J., Frisvad, J. C., Phipps, R. K., and Thrane, U. (2006) Host-derived media used as a predictor for low abundant, in planta metabolite production from necrotrophic fungi, *J Appl Microbiol* 101, 1292-1300.
68. Darvell, B. W. (1978) The development of an artificial saliva for in vitro amalgam corrosion studies, *J Oral Rehabil* 5, 41-49.
69. Senadheera, D., Krastel, K., Mair, R., Persadmehr, A., Abranches, J., Burne, R. A., and Cvitkovitch, D. G. (2009) Inactivation of VicK affects acid production and acid survival of *Streptococcus mutans*, *J Bacteriol* 191, 6415-6424.
70. Senadheera, M. D., Guggenheim, B., Spatafora, G. A., Huang, Y. C., Choi, J., Hung, D. C., Treglown, J. S., Goodman, S. D., Ellen, R. P., and Cvitkovitch, D. G.

- (2005) A VicRK signal transduction system in *Streptococcus mutans* affects *gtfBCD*, *gbpB*, and *ftf* expression, biofilm formation, and genetic competence development, *J Bacteriol* 187, 4064-4076.
71. Senadheera, M. D., Lee, A. W. C., Hung, D. C. I., Spatafora, G. A., Goodman, S. D., and Cvitkovitch, D. G. (2007) The *Streptococcus mutans* *vicX* gene product modulates *gtfB/C* expression, biofilm formation, genetic competence, and oxidative stress tolerance., *J. Bacteriol.* 189, 1451-1458.
 72. Taylor, B. L., and Zhulin, I. B. (1999) PAS domains: internal sensors of oxygen, redox potential, and light, *Microbiol Mol Biol Rev* 63, 479-506.
 73. Senadheera, D. B., Cordova, M., Ayala, E. A., Chavez de Paz, L. E., Singh, K., Downey, J. S., Svensater, G., Goodman, S. D., and Cvitkovitch, D. G. (2012) Regulation of bacteriocin production and cell death by the VicRK signaling system in *Streptococcus mutans*, *J Bacteriol* 194, 1307-1316.
 74. Hansen, D. B., Bumpus, S. B., Aron, Z. D., Kelleher, N. L., and Walsh, C. T. (2007) The loading module of mycosubtilin: an adenylation domain with fatty acid selectivity, *J Am Chem Soc* 129, 6366-6367.
 75. Park, S. Y., and Kim, Y. (2009) Surfactin inhibits immunostimulatory function of macrophages through blocking NK-kappaB, MAPK and Akt pathway, *Int Immunopharmacol* 9, 886-893.
 76. Hwang, M. H., Lim, J. H., Yun, H. I., Rhee, M. H., Cho, J. Y., Hsu, W. H., and Park, S. C. (2005) Surfactin C inhibits the lipopolysaccharide-induced transcription of interleukin-1beta and inducible nitric oxide synthase and nitric oxide production in murine RAW 264.7 cells, *Biotechnol Lett* 27, 1605-1608.
 77. Takahashi, K., Sugiyama, T., Tokoro, S., Neri, P., and Mori, H. (2012) Inhibition of interferon-gamma-induced nitric oxide production by 10-hydroxy-trans-2-decenoic acid through inhibition of interferon regulatory factor-8 induction, *Cell Immunol* 273, 73-78.
 78. Sugiyama, T., Takahashi, K., Tokoro, S., Gotou, T., Neri, P., and Mori, H. (2012) Inhibitory effect of 10-hydroxy-trans-2-decenoic acid on LPS-induced IL-6 production via reducing IkappaB-zeta expression, *Innate Immun* 18, 429-437.
 79. He, X., Wu, C., Yarbrough, D., Sim, L., Niu, G., Merritt, J., Shi, W., and Qi, F. (2008) The *cia* operon of *Streptococcus mutans* encodes a unique component required for calcium-mediated autoregulation, *Mol Microbiol* 70, 112-126.
 80. Johnsborg, O., Eldholm, V., and Havarstein, L. S. (2007) Natural genetic transformation: prevalence, mechanisms and function, *Res Microbiol* 158, 767-778.
 81. Cody, A. J., Field, D., Feil, E. J., Stringer, S., Deadman, M. E., Tsolaki, A. G., Gratz, B., Bouchet, V., Goldstein, R., Hood, D. W., and Moxon, E. R. (2003) High rates of recombination in otitis media isolates of non-typeable *Haemophilus influenzae*, *Infect Genet Evol* 3, 57-66.
 82. Didelot, X., and Maiden, M. C. (2010) Impact of recombination on bacterial evolution, *Trends Microbiol* 18, 315-322.

83. Kroll, J. S., Hopkins, I., and Moxon, E. R. (1988) Capsule loss in *Haemophilus influenzae* type b occurs by recombination-mediated disruption of a gene essential for polysaccharide export, *Cell* 53, 347-356.
84. Seifert, H. S., Ajioka, R. S., Marchal, C., Sparling, P. F., and So, M. (1988) DNA transformation leads to pilin antigenic variation in *Neisseria gonorrhoeae*, *Nature* 336, 392-395.
85. Feil, E. J., Maiden, M. C., Achtman, M., and Spratt, B. G. (1999) The relative contributions of recombination and mutation to the divergence of clones of *Neisseria meningitidis*, *Mol Biol Evol* 16, 1496-1502.
86. Cvitkovitch, D. G. (2001) Genetic competence and transformation in oral streptococci, *Crit Rev Oral Biol Med* 12, 217-243.
87. Marsh, P. D. (2004) Dental plaque as a microbial biofilm, *Caries Res* 38, 204-211.
88. Qi, F., Merritt, J., Lux, R., and Shi, W. (2004) Inactivation of the *ciaH* Gene in *Streptococcus mutans* diminishes mutacin production and competence development, alters sucrose-dependent biofilm formation, and reduces stress tolerance, *Infect Immun* 72, 4895-4899.
89. Ahn, S. J., Wen, Z. T., and Burne, R. A. (2006) Multilevel control of competence development and stress tolerance in *Streptococcus mutans* UA159, *Infect Immun* 74, 1631-1642.
90. Senadheera, D. B., Cordova, M., Ayala, E. A., Chavez de Paz, L. E., Singh, K., Downey, J. S., Svensater, G., Goodman, S. D., and Cvitkovitch, D. G. (2012) Regulation of bacteriocin production and cell death by the VicRK signaling system in *Streptococcus mutans*, *J Bacteriol*.
91. Mashburn-Warren, L., Morrison, D. A., and Federle, M. J. (2010) A novel double-tryptophan peptide pheromone controls competence in *Streptococcus* spp. via an Rgg regulator, *Mol Microbiol* 78, 589-606.
92. Okinaga, T., Xie, Z., Niu, G., Qi, F., and Merritt, J. (2010) Examination of the *hdrRM* regulon yields insight into the competence system of *Streptococcus mutans*, *Mol Oral Microbiol* 25, 165-177.
93. Okinaga, T., Niu, G., Xie, Z., Qi, F., and Merritt, J. (2010) The *hdrRM* operon of *Streptococcus mutans* encodes a novel regulatory system for coordinated competence development and bacteriocin production, *J Bacteriol* 192, 1844-1852.
94. Lee, M. S., and Morrison, D. A. (1999) Identification of a new regulator in *Streptococcus pneumoniae* linking quorum sensing to competence for genetic transformation, *J Bacteriol* 181, 5004-5016.
95. Luo, P., Li, H., and Morrison, D. A. (2003) ComX is a unique link between multiple quorum sensing outputs and competence in *Streptococcus pneumoniae*, *Mol Microbiol* 50, 623-633.
96. Mair, R. W., Senadheera, D. B., and Cvitkovitch, D. G. (2012) CinA is regulated via ComX to modulate genetic transformation and cell viability in *Streptococcus mutans*, *FEMS Microbiology Letters* FEMSLE-12-01-0026, *Decision: minor revision*.
97. Aspiras, M. B., Ellen, R. P., and Cvitkovitch, D. G. (2004) ComX activity of *Streptococcus mutans* growing in biofilms, *FEMS Microbiol Lett* 238, 167-174.

98. Lemme, A., Grobe, L., Reck, M., Tomasch, J., and Wagner-Dobler, I. (2011) Subpopulation-Specific Transcriptome Analysis of Competence-Stimulating-Peptide-Induced *Streptococcus mutans*, *J Bacteriol* 193, 1863-1877.
99. Dufour D, Cordova M, Cvitkovitch DG, and CM, L. (2011) Regulation of the competence pathway as a novel role associated with a streptococcal bacteriocin, *Journal of Bacteriology* 193, 6552-6559.
100. Perry, J. A., Cvitkovitch, D. G., and Levesque, C. M. (2009) Cell death in *Streptococcus mutans* biofilms: a link between CSP and extracellular DNA, *FEMS Microbiol Lett* 299, 261-266.
101. Li, Y. H., Lau, P. C., Lee, J. H., Ellen, R. P., and Cvitkovitch, D. G. (2001) Natural genetic transformation of *Streptococcus mutans* growing in biofilms, *J Bacteriol* 183, 897-908.
102. Senadheera, D., and Cvitkovitch, D. G. (2008) Quorum sensing and biofilm formation by *Streptococcus mutans*, *Adv Exp Med Biol* 631, 178-188.
103. Syvitski, R. T., Tian, X. L., Sampara, K., Salman, A., Lee, S. F., Jakeman, D. L., and Li, Y. H. (2007) Structure-activity analysis of quorum-sensing signaling peptides from *Streptococcus mutans*, *J Bacteriol* 189, 1441-1450.
104. Li, Y. H., Hanna, M. N., Svensater, G., Ellen, R. P., and Cvitkovitch, D. G. (2001) Cell density modulates acid adaptation in *Streptococcus mutans*: implications for survival in biofilms, *J Bacteriol* 183, 6875-6884.
105. Hung, D. C., Downey, J. S., Ayala, E. A., Kreth, J., Mair, R., Senadheera, D. B., Qi, F., Cvitkovitch, D. G., Shi, W., and Goodman, S. D. (2011) Characterization of DNA binding sites of the ComE response regulator from *Streptococcus mutans*, *J Bacteriol* 193, 3642-3652.
106. Li, Y. H., Lau, P. C., Tang, N., Svensater, G., Ellen, R. P., and Cvitkovitch, D. G. (2002) Novel two-component regulatory system involved in biofilm formation and acid resistance in *Streptococcus mutans*, *J Bacteriol* 184, 6333-6342.
107. Lau, P. C., Sung, C. K., Lee, J. H., Morrison, D. A., and Cvitkovitch, D. G. (2002) PCR ligation mutagenesis in transformable streptococci: application and efficiency, *J Microbiol Methods* 49, 193-205.
108. Pirota, M., Gunn, J., Chondros, P., Grover, S., O'Malley, P., Hurley, S., and Garland, S. (2004) Effect of lactobacillus in preventing post-antibiotic vulvovaginal candidiasis: a randomised controlled trial, *BMJ* 329, 548.
109. Dani, C., Biadaioli, R., Bertini, G., Martelli, E., and Rubaltelli, F. F. (2002) Probiotics feeding in prevention of urinary tract infection, bacterial sepsis and necrotizing enterocolitis in preterm infants. A prospective double-blind study, *Biol Neonate* 82, 103-108.
110. Pena, J. A., Rogers, A. B., Ge, Z., Ng, V., Li, S. Y., Fox, J. G., and Versalovic, J. (2005) Probiotic Lactobacillus spp. diminish *Helicobacter hepaticus*-induced inflammatory bowel disease in interleukin-10-deficient mice, *Infect Immun* 73, 912-920.
111. Moayyedi, P., Ford, A. C., Talley, N. J., Cremonini, F., Foxx-Orenstein, A. E., Brandt, L. J., and Quigley, E. M. (2010) The efficacy of probiotics in the treatment of irritable bowel syndrome: a systematic review, *Gut* 59, 325-332.

112. Lebeer, S., Vanderleyden, J., and De Keersmaecker, S. C. (2008) Genes and molecules of lactobacilli supporting probiotic action, *Microbiol Mol Biol Rev* 72, 728-764, Table of Contents.
113. Lebeer, S., Vanderleyden, J., and De Keersmaecker, S. C. (2010) Host interactions of probiotic bacterial surface molecules: comparison with commensals and pathogens, *Nat Rev Microbiol* 8, 171-184.
114. Marco, M. L., Peters, T. H., Bongers, R. S., Molenaar, D., van Hemert, S., Sonnenburg, J. L., Gordon, J. I., and Kleerebezem, M. (2009) Lifestyle of *Lactobacillus plantarum* in the mouse caecum, *Environ Microbiol* 11, 2747-2757.
115. Marco, M. L., Bongers, R. S., de Vos, W. M., and Kleerebezem, M. (2007) Spatial and temporal expression of *Lactobacillus plantarum* genes in the gastrointestinal tracts of mice, *Appl Environ Microbiol* 73, 124-132.
116. Grangette, C., Nutten, S., Palumbo, E., Morath, S., Hermann, C., Dewulf, J., Pot, B., Hartung, T., Hols, P., and Mercenier, A. (2005) Enhanced antiinflammatory capacity of a *Lactobacillus plantarum* mutant synthesizing modified teichoic acids, *Proc Natl Acad Sci U S A* 102, 10321-10326.
117. Macho Fernandez, E., Valenti, V., Rockel, C., Hermann, C., Pot, B., Boneca, I. G., and Grangette, C. (2011) Anti-inflammatory capacity of selected lactobacilli in experimental colitis is driven by NOD2-mediated recognition of a specific peptidoglycan-derived muropeptide, *Gut* 60, 1050-1059.
118. Yasuda, E., Serata, M., and Sako, T. (2008) Suppressive effect on activation of macrophages by *Lactobacillus casei* strain Shirota genes determining the synthesis of cell wall-associated polysaccharides, *Appl Environ Microbiol* 74, 4746-4755.
119. van Hemert, S., Meijerink, M., Molenaar, D., Bron, P. A., de Vos, P., Kleerebezem, M., Wells, J. M., and Marco, M. L. (2010) Identification of *Lactobacillus plantarum* genes modulating the cytokine response of human peripheral blood mononuclear cells, *BMC Microbiol* 10, 293.
120. van Baarlen, P., Troost, F. J., van Hemert, S., van der Meer, C., de Vos, W. M., de Groot, P. J., Hooiveld, G. J., Brummer, R. J., and Kleerebezem, M. (2009) Differential NF-kappaB pathways induction by *Lactobacillus plantarum* in the duodenum of healthy humans correlating with immune tolerance, *Proc Natl Acad Sci U S A* 106, 2371-2376.
121. Chon, H., Choi, B., Jeong, G., Lee, E., and Lee, S. (2010) Suppression of proinflammatory cytokine production by specific metabolites of *Lactobacillus plantarum* 10hk2 via inhibiting NF-kappaB and p38 MAPK expressions, *Comp Immunol Microbiol Infect Dis* 33, e41-49.
122. Petrof, E. O., Claud, E. C., Sun, J., Abramova, T., Guo, Y., Waypa, T. S., He, S. M., Nakagawa, Y., and Chang, E. B. (2009) Bacteria-free solution derived from *Lactobacillus plantarum* inhibits multiple NF-kappaB pathways and inhibits proteasome function, *Inflamm Bowel Dis* 15, 1537-1547.
123. Feling, R. H., Buchanan, G. O., Mincer, T. J., Kauffman, C. A., Jensen, P. R., and Fenical, W. (2003) Salinosporamide A: a highly cytotoxic proteasome inhibitor

- from a novel microbial source, a marine bacterium of the new genus *salinospora*, *Angew Chem Int Ed Engl* 42, 355-357.
124. Groll, M., Schellenberg, B., Bachmann, A. S., Archer, C. R., Huber, R., Powell, T. K., Lindow, S., Kaiser, M., and Dudler, R. (2008) A plant pathogen virulence factor inhibits the eukaryotic proteasome by a novel mechanism, *Nature* 452, 755-758.
 125. Meyer, S., Kohler, N. G., and Joly, A. (1997) Cyclosporine A is an uncompetitive inhibitor of proteasome activity and prevents NF-kappaB activation, *FEBS Lett* 413, 354-358.
 126. Mucchetti, G., Locci, F., Massara, P., Vitale, R., and Neviani, E. (2002) Production of pyroglutamic acid by thermophilic lactic acid bacteria in hard-cooked mini-cheeses, *J Dairy Sci* 85, 2489-2496.
 127. Fernandez, M., and Zuniga, M. (2006) Amino acid catabolic pathways of lactic acid bacteria, *Crit Rev Microbiol* 32, 155-183.
 128. Ponnusamy, K., Choi, J. N., Kim, J., Lee, S. Y., and Lee, C. H. (2011) Microbial community and metabolomic comparison of irritable bowel syndrome faeces, *J Med Microbiol* 60, 817-827.
 129. Fuss, I. J., Neurath, M., Boirivant, M., Klein, J. S., de la Motte, C., Strong, S. A., Fiocchi, C., and Strober, W. (1996) Disparate CD4+ lamina propria (LP) lymphokine secretion profiles in inflammatory bowel disease. Crohn's disease LP cells manifest increased secretion of IFN-gamma, whereas ulcerative colitis LP cells manifest increased secretion of IL-5, *J Immunol* 157, 1261-1270.
 130. Ito, R., Shin-Ya, M., Kishida, T., Urano, A., Takada, R., Sakagami, J., Imanishi, J., Kita, M., Ueda, Y., Iwakura, Y., Kataoka, K., Okanoue, T., and Mazda, O. (2006) Interferon-gamma is causatively involved in experimental inflammatory bowel disease in mice, *Clin Exp Immunol* 146, 330-338.
 131. Kullberg, M. C., Ward, J. M., Gorelick, P. L., Caspar, P., Hieny, S., Cheever, A., Jankovic, D., and Sher, A. (1998) *Helicobacter hepaticus* triggers colitis in specific-pathogen-free interleukin-10 (IL-10)-deficient mice through an IL-12- and gamma interferon-dependent mechanism, *Infect Immun* 66, 5157-5166.
 132. Antony, S. J. (2000) Lactobacillemia: an emerging cause of infection in both the immunocompromised and the immunocompetent host, *J Natl Med Assoc* 92, 83-86.
 133. Sartor, R. B. (2001) Intestinal microflora in human and experimental inflammatory bowel disease, *Curr Opin Gastroenterol* 17, 324-330.
 134. Seksik, P., Rigottier-Gois, L., Gramet, G., Sutren, M., Pochart, P., Marteau, P., Jian, R., and Dore, J. (2003) Alterations of the dominant faecal bacterial groups in patients with Crohn's disease of the colon, *Gut* 52, 237-242.
 135. Macfarlane, G. T., Blackett, K. L., Nakayama, T., Steed, H., and Macfarlane, S. (2009) The gut microbiota in inflammatory bowel disease, *Curr Pharm Des* 15, 1528-1536.
 136. Suau, A., Bonnet, R., Sutren, M., Godon, J. J., Gibson, G. R., Collins, M. D., and Dore, J. (1999) Direct analysis of genes encoding 16S rRNA from complex

- communities reveals many novel molecular species within the human gut, *Appl Environ Microbiol* 65, 4799-4807.
137. Tannock, G. W., Munro, K., Harmsen, H. J., Welling, G. W., Smart, J., and Gopal, P. K. (2000) Analysis of the fecal microflora of human subjects consuming a probiotic product containing *Lactobacillus rhamnosus* DR20, *Appl Environ Microbiol* 66, 2578-2588.
 138. Manichanh, C., Rigottier-Gois, L., Bonnaud, E., Gloux, K., Pelletier, E., Frangeul, L., Nalin, R., Jarrin, C., Chardon, P., Marteau, P., Roca, J., and Dore, J. (2006) Reduced diversity of faecal microbiota in Crohn's disease revealed by a metagenomic approach, *Gut* 55, 205-211.
 139. Sokol, H., Seksik, P., Rigottier-Gois, L., Lay, C., Lepage, P., Podglajen, I., Marteau, P., and Dore, J. (2006) Specificities of the fecal microbiota in inflammatory bowel disease, *Inflamm Bowel Dis* 12, 106-111.
 140. Sokol, H., Pigneur, B., Watterlot, L., Lakhdari, O., Bermudez-Humaran, L. G., Gratadoux, J. J., Blugeon, S., Bridonneau, C., Furet, J. P., Corthier, G., Grangette, C., Vasquez, N., Pochart, P., Trugnan, G., Thomas, G., Blottiere, H. M., Dore, J., Marteau, P., Seksik, P., and Langella, P. (2008) *Faecalibacterium prausnitzii* is an anti-inflammatory commensal bacterium identified by gut microbiota analysis of Crohn disease patients, *Proc Natl Acad Sci U S A* 105, 16731-16736.
 141. Frank, D. N., St Amand, A. L., Feldman, R. A., Boedeker, E. C., Harpaz, N., and Pace, N. R. (2007) Molecular-phylogenetic characterization of microbial community imbalances in human inflammatory bowel diseases, *Proc Natl Acad Sci U S A* 104, 13780-13785.
 142. Martinez-Medina, M., Aldeguer, X., Gonzalez-Huix, F., Acero, D., and Garcia-Gil, L. J. (2006) Abnormal microbiota composition in the ileocolonic mucosa of Crohn's disease patients as revealed by polymerase chain reaction-denaturing gradient gel electrophoresis, *Inflamm Bowel Dis* 12, 1136-1145.
 143. Li, Q., Wang, C., Tang, C., Li, N., and Li, J. (2012) Molecular-phylogenetic characterization of the microbiota in ulcerated and non-ulcerated regions in the patients with Crohn's disease, *Plos One* 7, e34939.
 144. Ng, S. C., Benjamin, J. L., McCarthy, N. E., Hedin, C. R., Koutsoumpas, A., Plamondon, S., Price, C. L., Hart, A. L., Kamm, M. A., Forbes, A., Knight, S. C., Lindsay, J. O., Whelan, K., and Stagg, A. J. (2011) Relationship between human intestinal dendritic cells, gut microbiota, and disease activity in Crohn's disease, *Inflamm Bowel Dis* 17, 2027-2037.
 145. Kang, S., Denman, S. E., Morrison, M., Yu, Z., Dore, J., Leclerc, M., and McSweeney, C. S. (2010) Dysbiosis of fecal microbiota in Crohn's disease patients as revealed by a custom phylogenetic microarray, *Inflamm Bowel Dis* 16, 2034-2042.
 146. Sokol, H., Seksik, P., Furet, J. P., Firmesse, O., Nion-Larmurier, I., Beaugerie, L., Cosnes, J., Corthier, G., Marteau, P., and Dore, J. (2009) Low counts of *Faecalibacterium prausnitzii* in colitis microbiota, *Inflamm Bowel Dis* 15, 1183-1189.

147. Mondot, S., Kang, S., Furet, J. P., Aguirre de Carcer, D., McSweeney, C., Morrison, M., Marteau, P., Dore, J., and Leclerc, M. (2011) Highlighting new phylogenetic specificities of Crohn's disease microbiota, *Inflamm Bowel Dis* 17, 185-192.